PROJECTILE IMPACT DAMAGE IN FILAMENT WOUND CFRP TUBES

Effect of Stacking Sequence on Projectile Kinetic Energy Dissipation

A thesis presented

by

Mark Alan Will

to

The Department of Mechanical Engineering

in partial fulfilment of the requirements

for the degree of

Master of Science in Engineering

University of Cape Town

Rondebosch 7700

South Africa

[July] [2000]

Declaration

This is to certify that the work presented in this thesis is essentially my own and that no part of the thesis has been submitted for a degree at this or any other university.

M. A. Will

July 2000

Acknowledgements

I would like to express my sincere thanks to the following people and organisations for the assistance and guidance provided during my studies:

- My supervisor, Prof. G. N. Nurick, for ensuring my financial needs were satisfied and that the final product was up to standard, as well trusting me to accomplish the work without constant supervision.
- Dr Thomas Franz, my co-supervisor, for his constant willingness to provide advice and check my work.
- The staff at the Mechanical workshop, as well as the secretarial staff, for their willingness and patience in accommodating my wants and needs.
- The Materials engineering staff and students for their help and use of their equipment.
- Miles Wiehan for his assistance in modifying ABAQUS input decks.
- Somchem for their material and practical support, in particular Andrew Parsons, Michael Earl, Leon Kranhold and Eddie.

A final vote of gratitude goes to the Foundation for Research and Development (FRD), the Centre for Research in Computational and Applied Mechanics (CERECAM) and the Department of Mechanical Engineering for their financial assistance throughout my studies

Synopsis

The effect a change in laminate stacking sequence has on a its ability to dissipate projectile kinetic energy has been investigated. T800 carbon fibre filament wound tubes in an epoxy matrix are investigated, having the following lay-up; laminate A - $[-35^{\circ}/+35^{\circ}/90^{\circ}_3/-35^{\circ}/+35^{\circ}/90^{\circ}_3/-35^{\circ}/+35^{\circ}]$ and laminate B - $[90^{\circ}_6/(-35^{\circ}/+35^{\circ})_3]$. The laminates underwent projectile impact up to and beyond their ballistic limits and the significant damage mechanisms were then measured and their contribution to energy dissipation quantified. Instrumented drop tests were also performed in order to determine the normal laminate shear fracture energy release rate and energy dissipated by friction between the projectile and laminate.

The laminate stacking sequence with the best projectile kinetic energy dissipation performance has been identified and the role of the significant energy dissipation mechanisms discussed. The experimental results are compared to previous work on projectile impact on laminates and conclusions drawn as to their validity. The use of the ABAQUS finite element modelling program in such an investigation is also investigated and recommendations made.

Finite Element Modelling of a projectile impact event using ABAQUS Explicit was performed in order to assess its usefulness in such an analysis. A compliance test on both laminates was also modelled using ABAQUS Standard in order to assess the contribution of overall compliance to projectile kinetic energy dissipation.

The $[90^{\circ}_6/(-35^{\circ}/+35^{\circ})_3]$ laminate was to found have the best projectile kinetic energy dissipation performance as a result of a difference in strain energy. The significant cause for the difference in strain energy being a difference in effective local compliance and not overall compliance. The difference in effective local compliance is suggested as being due to the difference in delamination distribution, which is a result of the different stacking sequence.

The experimental results are shown to conform to previous work on flat panel laminates and finite element modelling is shown to play role in the discussion but not to be essential. In order for ABAQUS Explicit to be of significant use it is recommended that a valid user material be developed.

Table of Contents

List of Figures

List of Tables

Glossary

Symbols

A_d	Total delamination area
A_p	Total perforation area
A_{sh}	Area of shear cone
E_t & E_c	Tensile & Compressive Young's modulus
E_{nn}	Young's Modulus where nn refers to lamina (1,2,3) or global (x,y,z) axes
E_I	Kinetic energy of projectile prior to impact i.e. impact energy
E_b	Ballistic limit energy
E_d	Energy dissipated due to delamination
E_p	Energy dissipated due to perforation
E_ε	Strain energy
E_{res}	Residual energy = E_i - E_f - E_{mat}
E_f	Energy dissiapted due to friction between projectile and laminate
E_{mat}	Energy dissipated due to material failure/fracture = $E_d + E_{sh} + E_c$
E_{ck}	Energy dissipated due to matrix cracking
h	Laminate thickness
G_c,G_{IIC}	Griffith Criterion fracture toughness, Mode II fracture toughness
I_n	Interface number, n = 1 … total number of interfaces
m	Projectile mass
P_f	Friction force during perforation
R	Projectile radius
V_b	Ballistic limit velocity
V_r	Residual velocity, derived from the residual kinetic energy
V_i	Projectile impact velocity
γ_f	Through thickness shear fracture energy per unit area for laminate
ν	Poisson's ratio
τ	Shear stress
σ_t & σ_c	Tensile stress & Compressive stress
θ	Lamina fibre orientation with respect to laminate axis
ϕ	Angle of shear cone

Definitions

Ballistic limit	The kinetic energy a projectile needs to just perforate a laminate.
Bounds	Sometimes used to refer to the laminae which form an interface i.e. they are the bounds of the interface.
Distal	Rear, furthest from a point e.g. furthest lamina or interface from the impact point.
Dissipation / absorption	These two terms are used interchangeably to describe the reduction of projectile kinetic energy due to the laminate.
Extrapolate	To calculate approximately from known values, data, etc., (others which lie outside the range known)
Interpolate	Estimate from known values, etc., (others lying in the same range)
Lamina	A single layer of composite material, which when joined with other laminae form a laminate.
Line loading	Load is applied along a line as opposed to a point.
Matrix	Material which contains a secondary phase e.g. fibre reinforcement.
Shear Fracture / Perforation energy	These terms are occasionally used interchangeably, both refer to the energy dissipated due to the shear fracture cone although some texts include all damage modes in their definition of perforation energy.
"seam"	Point on filament wound tube where helical winds cross (see Figure 12).
Just Perforated	Projectile has sufficient velocity to just pierce the distal surface of the laminate
Just passed through	Projectile has sufficient velocity for the whole shank of the projectile to pass through before stopping.
Total delamination area	The sum of the area of all delaminations identified through the laminate.
CFRP	Carbon Fibre Reinforced Polymer
FEM	Finite Element Modelling
FEA	Finite Element Analysis

Chapter 1. Introduction

The thesis concentrates on the projectile energy dissipation of carbon filament wound tubes in an epoxy matrix undergoing projectile impact. The sponsoring company had a primary interest in determining which of two stacking sequences exhibited superior energy dissipation.

1.1 Foreword

The relevance of an investigation into impact damage in filament wound composite tubes is not obvious as the role filament wound products play in our lives is not readily apparent. Sports equipment such as golf clubs and fishing rods are probably the most obvious examples of such products although filament wound products perform many safety critical functions in a variety of industries.

The chemical industry relies on pipes and vessels, produced by filament winding, in order to contain and transport hazardous substances, while the defence industry makes extensive use of filament winding in order to produce ordinance such as missile bodies and rocket motors. The automotive industry has investigated the use of filament wound fuel tanks for use in natural gas powered vehicles, while the aerospace industry uses it widely in satellite launch vehicles and aircraft components such as radomes. Projectile impact in many of the aforementioned industries can result in leakage of hazardous substances due to structural failure, contents reacting violently to a projectile's kinetic energy, or failure of sub-systems. In the armaments industry the issue of insensitive munitions has become a prime consideration in their design, where products are increasingly required to be able to sustain high velocity impact without causing catastrophic failure. The tendency for a charge of high explosive or rocket fuel to detonate or burn as result of projectile impact is strongly dependent on the kinetic energy imparted to them.

Projectile impact damage in fibre reinforced composites is more complicated than in isotropic engineering materials, such as steel, in that a number of different failure mechanisms are involved. Material failure dissipates the kinetic energy of the impacting projectile but reduces the residual strength of the structure and may destroy structural integrity. Fibre reinforce materials provide the engineer with an opportunity to optimise a

laminate for a specific failure requirement and not only for load to ultimate failure, as is usually the case. A customer can specify structural integrity as a primary consideration during failure due to projectile impact in order to prevent leakage of a toxic substance. A customer could also require apparently conflicting requirements such as residual strength and projectile energy dissipation, such as in the case of a pressurised fuel tank. Fibre reinforced composites enable the structural engineer to tackle the problem at both a material and structural level.

A primary advantage of using composites is this ability to tailor them at both a material and structural level, without recourse to a specialist in materials technology, although with the accompanying disadvantage of an increasingly complex design process. Designing for load bearing and ultimate laminate failure under normal loads is well developed, as is the understanding of the various failure modes. The initiation, development and interaction of the different material modes of damage, due to projectile impact, are less commonly known and appreciated. The engineering challenge of tailoring laminates with this in mind has mainly been relegated to the armaments and aerospace industries where research and development in these fields has been strong.

1.2 Thesis aims

The primary aim of the thesis is to identify which of two different carbon fibre reinforced (CFRP) laminate stacking sequences dissipates the most projectile kinetic energy. It is achieved by conducting projectile impact tests at and around the region of the ballistic limits of the two laminates.

In order to enhance kinetic energy dissipation the incidence of energy dissipating mechanisms can be increased, the physical extent of certain mechanisms increased, or both incidence and extent increased. The relative importance of the various energy dissipating mechanisms therefore needs to be ascertained and this forms a subsequent aim of the thesis. In order to do this the measurement of the various damage modes was performed and the amount of energy dissipated by each approximated.

The scope of the work conducted is similar to that of other work, although most previous work has concerned flat panels and not tubes. The laminates tested also tended to consist of simple lay-up configurations and diverse material constituents that may also come

from a range of suppliers. The thesis aims to discuss the relevance of previous research to the particular products being tested and where possible to draw conclusions.

The thesis relies heavily on experimental work and non-destructive evaluation of the specimens, however some Finite Element Modelling (FEM) is performed in order to ascertain the suitability of utilising a FEM code for such an evaluation.

The scope of the thesis originated, as well as resource considerations, has precluded the implementation of a rigorous experimental technique. The number of test specimens were also limited due to cost considerations so that adequate conclusions as to the statistical significance of the results cannot be made. The author attempts to address these issues by relating the results to theoretical expectations and previous literature, as well as by discussing possible sources of error.

1.3 Thesis scope

The scope of the thesis has been governed by the available; time, test specimens, and experimental resources. Time constraints prevented the effective use of numerical modelling and meant that investigation relied on experimentation. The cost of specimens resulted in a fewer tests than desired and, due to the lower volume of data, reduced the ability to perform statistical analyses. Available resources, and time, resulted in an experimental set-up and method less comprehensive than other similar studies such that the residual velocity of the impacting projectile was not measured.

1.4 Thesis plan

The thesis has the following progression;

- An introduction and background to CFRP laminates and projectile impact with the aim of providing the reader with sufficient information to understand the subsequent text.

- A literature survey providing additional information.

- The experimental set up and procedures as well as the methods by which the raw results are processed are described. Possible sources of experimental error are also discussed.

- Experimental results are presented.
- The Finite Element Model and modelling approach are described.
- FEM results are presented.
- A discussion of the results with reference to the aims of thesis is presented.
- Conclusions from the discussion are consolidated.
- A number of recommendations are proposed for future work.
- A set of appendices containing raw data, results and FEM input decks conclude the thesis.

Chapter 2. Background to CFRP composite impact damage

The following is deemed sufficient to familiarise the reader with CFRP filament wound tubes in order to understand the subsequent analyses and conclusions. The reader is advised to consult a suitable text ([2], [13],[20],[22]) for a more detailed description of the subject as the following is only an introduction to the subject for the purposes of this dissertation.

2.1 Basics

CFRP laminates are constructed from a number of laminae, also known as plies, consisting of carbon fibres contained in a polymer matrix. In filament wound products the fibres are continuous, i.e. they run the full length of the structure, and are aligned in a single direction, unidirectional, for each lamina. The fibres and matrix combined offer superior material properties, depending on the nature of both constituents, than they do alone. The ability to vary the properties of the matrix, e.g. toughened or standard epoxy matrix, and fibre characteristics enables designers to tailor the properties of the lamina to their requirements.

Carbon fibres have anisotropic material properties with superior properties in the direction of the fibre than transverse to it. Polymer matrices tend to have quasi-isotropic material properties being poor in tension and stronger than fibres in compression. The combination of matrix and fibre causes unidirectional laminae to possess orthotropic properties, which can be determined experimentally or by calculation using classical laminate theory.

2.2 Unidirectional continuous fibre reinforced laminate

2.2.1 Axes

The local lamina axes are defined relative to the fibre direction (see Figure 1) where; 1 is the in-plane fibre direction, 2 is the in-plane transverse direction normal to 1, and 3 is the out-of-plane transverse direction normal to 1. The orthotropic material properties of a unidirectional lamina are specified relative to the local axis of the lamina. The orientation of each lamina, θ, is specified relative to the local axes of the laminate.

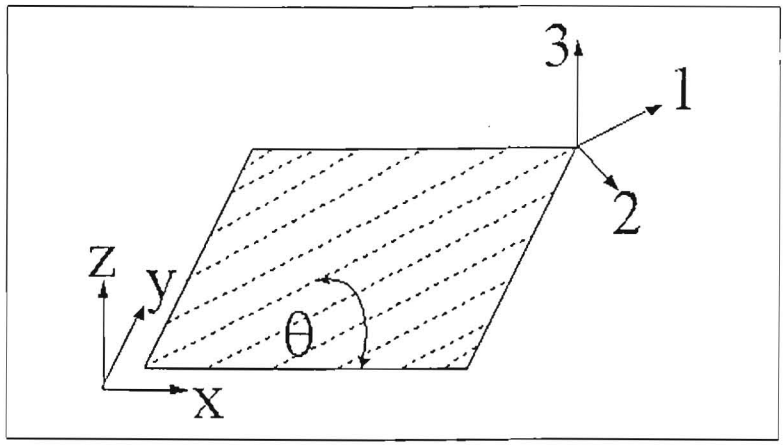

Figure 1 Laminate and lamina axes

The local axes of the laminate can be defined arbitrarily by the user or may be aligned according to some geometric feature such as an axis of symmetry. The material properties of the laminate are specified according to the local laminate axes and are typically derived from the lamina properties according to classical laminate theory. The laminate may exhibit orthotropic material properties so long as each lamina with an orientation other than 0^0 or 90^0 has a corresponding lamina with an orientation equal in magnitude, yet opposite in sense having the same material properties.

The axis system utilised in this study is based on that of the ABAQUS FEM software (see Figure 2), where material orientations in a tube are specified using the cylindrical system. The 1 axis of the lamina is in the same direction as the radial (r) direction at any point in the lamina, the 2 axis (fibre direction) and the 3 axis (transverse to the fibre) are tangential to the point on the tube. The fibre orientation is defined by a rotation (θ) counter-clockwise about the 1, or radial axis. A zero degree rotation results in the 2 axis being aligned with the polar axis (a) and the 3 axis being aligned in the hoop (h) or circumferential direction.

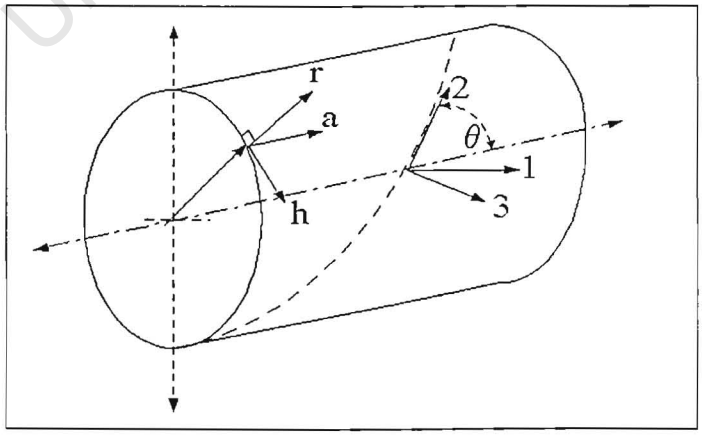

Figure 2 ABAQUS axes definition

2.2.2 *Filament winding*

The process of filament winding involves winding a filament of fibre, impregnated with polymer matrix material, around a mandrel followed by a period of curing. Curing causes the matrix to set and is typically accomplished by placing the wound form in an autoclave.

The orientations of the fibres are governed by the type of winding, i.e. polar, circumferential or helical. The specimens under investigation were produced using only helical and circumferential windings. The orientation, θ, of the helical wind is dependent on the traverse speed of the feed relative to the spindle speed while the circumferential winding always has an orientation of 90°.

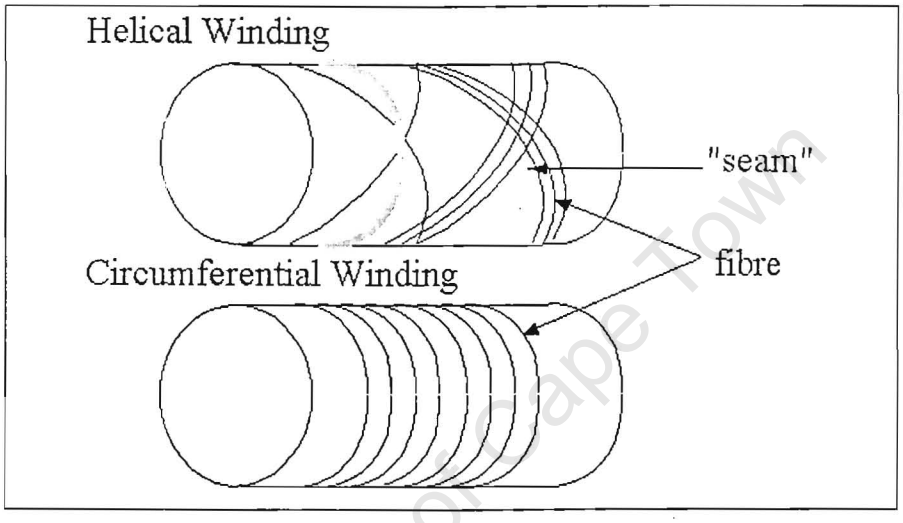

Figure 3 Filament winding

The point where the helical wind crosses over itself forms a "seam" around the tube that exhibits a characteristic zigzag pattern as successive winds overlap each other at that point (Figure 3 and Figure 12).

2.3 Failure analysis

CFRP laminates are generally thin enough to analyse using classical laminate theory, which is based on the theory of thin plates. The theory neglects out-of-plane normal stresses and assumes that deflections in the thickness direction of a plate are small compared to the thickness of the plate. Traditional CFRP laminate analysis is therefore not directly applicable to the ballistic impact of laminates.

The more common numerical approach to analysing ballistic events in CFRP laminates is to use FEA where a composite failure model is applied in what is known as a ply-discount

approach. The failure theories all relate stresses and strains to particular material failure characteristics, otherwise known as damage modes.

2.3.1 Impact damage

CFRP laminates exhibit the following significant failure modes due to ballistic impact; fibre fracture, matrix cracking and delamination. The combination of fibre in matrix also results in failure modes with a greater fracture resistance than the constituent materials on their own, such as shear failure through the thickness of a laminate. Fibre pull-out is another energy absorbing mechanism where a fibre is pulled out of the matrix dissipating energy by fracture of the interface between fibre and matrix, as well as by friction.

The damage zone may be characterised by delaminations that decrease in size from the distal side towards the impact site, giving it its characteristic fir tree shape, (see Figure 4). Through thickness fracture (also known as shear fracture) occurs immediately below the impact site and along a conical plane through the thickness of the laminate, initially as a result of Hertzian contact stresses. Matrix cracking occurs throughout the damage zone.

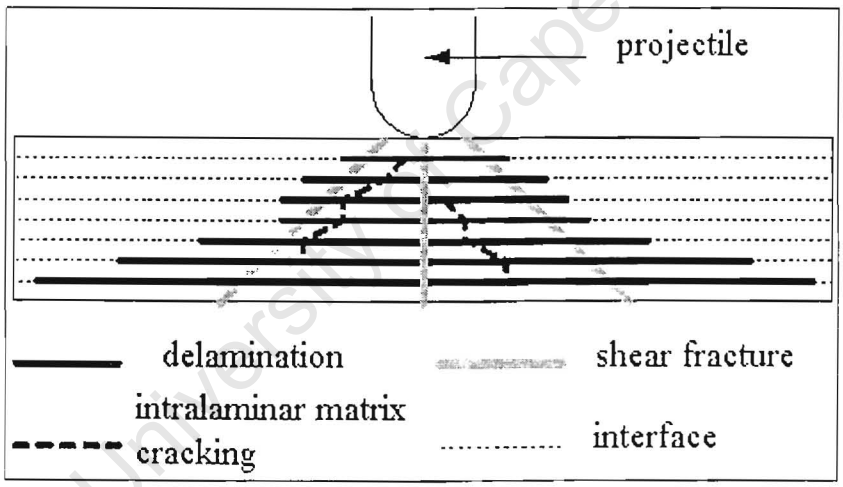

Figure 4 Impact damage

Fibre fracture and matrix cracking occur when tensile, shear or compressive loading limits, which are direction dependent, are exceeded. Particular combinations of these loads, such as combined compressive and shear loading, can also lead to failure at lower values of stress or strain.

Matrix cracks may propagate between fibres (intralamina cracking or splitting) as well as from one lamina to the next (interlamina cracking) before being arrested or deflected by a

fibre. A number of failure models use matrix cracking as a criterion for determining when and where delaminations will occur.

Delaminations differ from matrix cracking mainly in that large areas of matrix fail between adjacent laminae. Delaminations occur at lower load levels and are generally initiated at flaws within the laminate, which may occur during manufacture or as result of prior matrix cracking. The relative orientation angle of the laminae bounding a delamination determine the extent of intralamina shear stress with larger angles resulting in higher stresses. Larger intralamina shear stresses result in a greater likelihood and extent of delamination while adjacent laminae with the same orientation (no relative change in angle) should not exhibit any delamination.

Fibre pull-out energy is proportional to the length of fibre pulled out and hence its determination is extremely difficult, as it requires physical measurement or an appropriate statistical approximation.

2.3.2 Failure theories

The ability of composites to fail under mixed modes of loading and at different load levels has resulted in a number of theories, which describe a stress envelope. Theories which take into account mixed mode loading are known as interactive failure theories or criterion and can generally be categorised as either distinctive or generalised criterion. Distinctive theories, such as the maximum stress and strain theories, distinguish between different failure modes in determining the failure envelope. Generalised theories, such as that by Tsai-Wu and Tsai-Hill, differentiate between the different strengths for tension and compression but not the different failure modes. Failure criteria are generally either distinctive or generalised although the Puck criterion does incorporate both categories.

2.3.3 Fracture toughness and energy dissipation

A tough material dissipates more energy in failure and the energy it dissipates is, for linear elastic fracture mechanics (LEFM), proportional to the surface area of the crack. Griffiths [15] showed that for a net increase in crack area the dissipated energy could be given by;

$$\delta U = \delta a \cdot G_c \qquad (1)$$

Where; G_c ~ critical strain energy release, δU~ energy dissipated, δa~ crack area

G_c incorporates the energy required to initiate a crack as well as to propagate it and has been shown to be suitable for LEFM.

The energy released by matrix cracking and delamination are of the same order, 10^2 J/m^2, as failure occurs in a homogenous portion of the composite and as a result is easily determined. The energy released due to fibre failure alone is significantly less than when it fails in a composite, as the combination of fibre in matrix inhibits crack growth significantly. In projectile impact fibre failure tends to be localised, occuring along the shear fracture surface, i.e. Hertzian crack, through the thickness of the laminate, (see Figure 5) . The G_c value quoted for the shear fracture surface is obtained from quasi-static punch tests and are of the order of 10^3 to 10^4J/m^2.

[3]

Figure 5 Hertzian crack (glass)

2.4 Laminate finite element modelling

The FEM code used is ABAQUS Explicit and Standard, the non-linear and linear options of the general purpose code, and the accompanying manuals [1] provide additional information on the modelling process and theory. The non-linear option (ABAQUS Explicit) is used to model projectile impact as it takes into account the inertial effects that are significant in such impact events and non-linear deformation.

2.4.1 Elements

Composites can be modelled using shell, brick or continuum elements although shell and brick elements are only suitable for plane strain or stress problems. Normal projectile impact on CFRP laminates precludes the use of shell and brick elements for the meaningful analysis of impact damage. The use of brick elements is not possible as ABAQUS Explicit does not

enable the orientations of the material property directions to be specified. 3D eight node reduced integration continuum elements are the most suitable elements as;

1. material orientations can be specified
2. more appropriate values of stress through the thickness and at the interfaces of the laminae are provided

2.4.2 Model

The geometric model, element definition, contact definition and mesh generation were initially produced using CAE, the ABAQUS pre-processor, although further mesh refinement was undertaken manually.

The model represents the upper quarter of a tube, in order to save simulation time, and as such does not fully represent the experiment. The smaller model should, however, reproduce the same trends as a full model.

Adjacent laminae of the same material and orientation are modelled by a set of 3D continuum elements. The thickness of the element set being the same as the total thickness of the laminae which it represents. Each named set of elements can be assigned different material properties and orientations (Figure 2).

The impactor is simulated as a rigid surface as it exhibits no appreciable deformation.

Contact between the impactor and laminate is specified as penalty contact, which reduces computational cost by allowing small amounts of initial over contact. The laminate contact surface is specified as the slave surface and the projectile as the master surface.

The boundary conditions applied were those necessary to; achieve a quarter symmetric model, reflect physical boundary conditions, and to ensure the projectile contacted the laminate perpendicularly.

2.4.3 Implementing failure

ABAQUS does not have a composite failure model for continuum elements and in order to implement one in Explicit the user would have to produce a user material. ABAQUS Explicit allows for a user material with the feature VMAT, which would require implementing composite failure models according to the ply discount approach. The user material would be based on an accepted theory, such as Tsai-Hill, which does not directly model material

failure, rather it simulates it by degrading the appropriate material properties. The current set of numerical tests do not implement a user material as it is not a requirement of this work.

2.5 Projectile impact

The sequence of events during a projectile impact event cannot practically be described by a single theory due to the varied failure modes. Damage is caused by stress waves, Hertzian contact and localised response.

2.5.1 Stress waves

Elementary stress wave theory states that in a linear elastic rod a tensile or compressive disturbance propagates with a velocity given by;

$$c = \left(E/\rho\right)^{\frac{1}{2}} \qquad (2)$$

where c is also known as the through thickness speed of sound.

The time taken to travel through the thickness of the laminate is given by;

$$t = h/c$$

where h is the laminate thickness.

2.5.2 Localised response

The dynamic plastic response of clamped beams [20] to light projectile impact is localised as there is insufficient kinetic energy to propagate the plastic hinges to the boundary (Figure 6). The transverse displacement profile for light strikers is logarithmic as opposed to linear for heavy strikers.

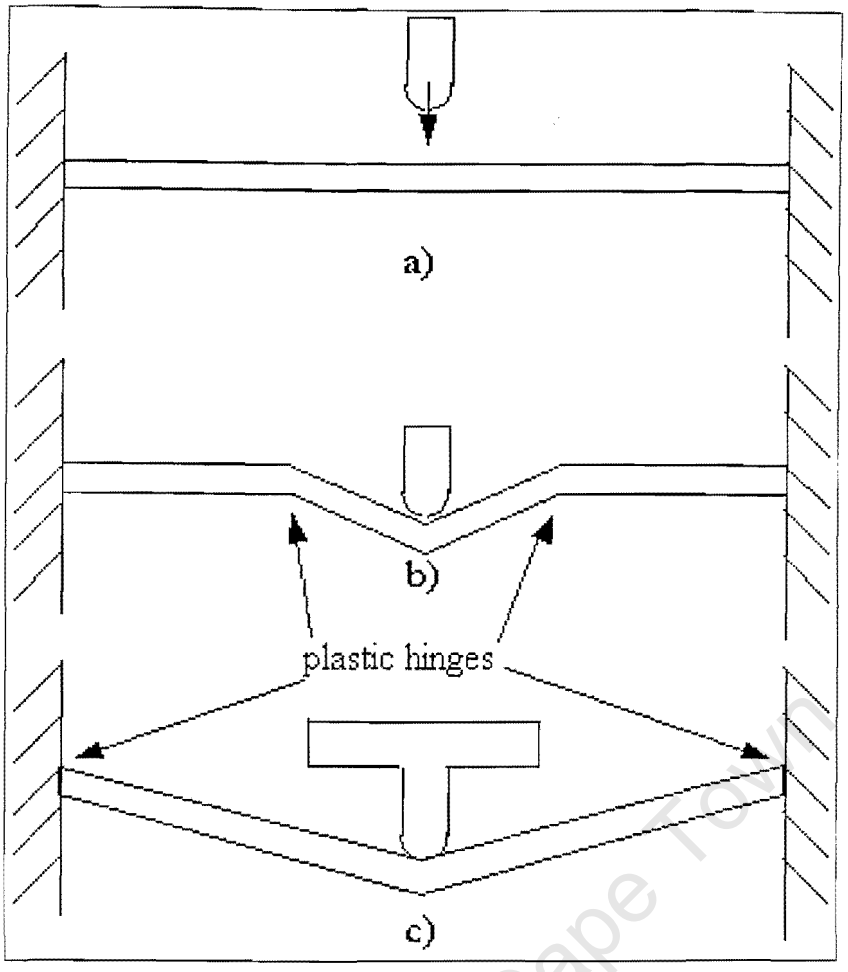

[20]

Figure 6 a) light projectile impact b) localised dynamic response c) static response

Light projectile impact is considered to occur when the mass of the beam is significantly heavier than the projectile.

2.5.3 Hertzian contact

The Hertzian contact theory was derived from experimental observations of fracture due to contact between curved surfaces. The theory has proven to be particularly reliable for impact between brittle materials, i.e. linear elastic fracture, and as such is applicable in CFRP laminate investigations.

The theory describes a drop-shaped region (see Figure 7) below the contact area where all three principal stresses are compressive and proportional to the radii and geometry of the curved surfaces.

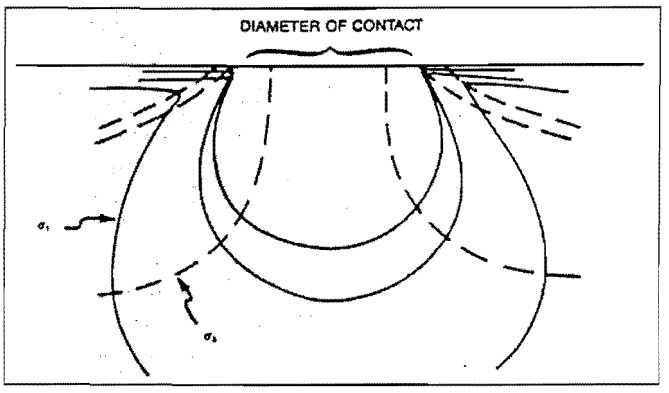

[3]

Figure 7: Hertzian stress field

The maximum compressive stress, σ_c, or maximum pressure normal to the surface is given by;

$$\sigma_c = \frac{3 \cdot P}{2 \cdot \pi \cdot a \cdot b} \qquad (3)$$

where; P = contact load, a & b = axes of ellipsoid contact area

Chapter 3. Literature survey

3.1 Introduction

The theory on impact damage is consolidated around basic features, such as the distribution of damage through the laminate and the influence of dissimilar laminae orientations on delamination. The many variables involved in composite materials and impact events has meant that much of the research has been isolated to specific problems, i.e. a particular composite undergoing a particular event. The following chapter attempts to coherently present the findings and observations found in research literature, relevant to the thesis.

3.2 Experimental approach

Literature does not provide a standard set up for the ballistic testing of tubes as replication of in service conditions appears to have been a priority.

Highsmith et al. [16] investigated the effect of impact damage on strength in filament wound composite tubes by placing the tubes, unfastened, in a cradle. The cradle was lined with an elastomeric material in order to relieve stress concentrations at the edges of the supports.

Evans and Alderson [12] investigated low velocity impact damage in filament wound tubes utilising two support conditions likely to be encountered during normal service life. The tubes were floor-supported along their length and in half-circumference end-cradles. The results, particularly of the latter support condition, indicated a degree of equivalence between static and impact tests.

Mines et al. [21] investigated high velocity perforation of flat polymer composite laminates and reported that the boundaries were chosen so as to avoid the local damage interacting with them. The panel was clamped along all of its edges such that each boundary was 100mm from the impact point, which was considered sufficient for static tests and for a 5.84g projectile travelling at 571m/s.

3.3 Non-destructive testing

The X-raying of CFRP laminates relies on the judgement of the person interpreting the images and the clarity of the damage in the image. The clarity of damage is enhanced by introducing a dense material into the damage site.

Highsmith et al. [16] obtained normal and oblique views of damage utilising X-rays and by enhancing the image of the damage site by saturating it with a high density dye. The dye consisted of the following solution; 60g ZnI (densifying material), 10mL water, 10mL isopropyl alcohol (reduce viscosity), and 10mL Kodak "Photo-Flo" (wetting agent). A small dam of putty was built around the impact site, filled with the dye and left to soak for a minimum of 4hrs. The damage site is rendered more opaque to the X-rays by the denser material.

3.4 Impact damage

The extent and type of damage is governed by; target stiffness, boundary conditions, impactor geometry, ply stacking sequence [18], impactor velocity, and material strain-rate sensitivity.

3.4.1 Impact velocity

The analysis of impact damage is heavily dependant on the impact velocity as it is not only an indication of a laminates performance but also determines the response of the laminate.

The velocity at which a projectile of particular mass and geometry just perforates a structure (ballistic limit) is a useful measure of a laminates ability to resist impact damage and is the most important factor in designing protective structures [19]. Jenq et al. [19] showed that the ballistic limit in glass reinforced epoxy laminates does not vary significantly with increasing impact energy.

High velocity impact (>20m/s) results in a stress wave that initiates and propagates damage throughout the laminate. The stress wave emanates from the impact site and propagates at the through thickness speed of sound [10]. The initial compressive stress wave causes critical matrix cracking before reflecting off the back surface as a tensile stress wave. The tensile stress wave initiates and propagates delaminations from the critical matrix cracks.

Cantwell and Morton [2] investigated high velocity impact perforation in CRFPs and used a truncated cone to approximate the surface of through thickness laminate shear. The approximation was stated to produce the same trends observed in experiments. The apex started at the impact site with a diameter equal to that of the projectile and has a 45° half angle so that the area of the shear zone is given by;

$$A = \sqrt{2} \cdot \pi \cdot t(t + r) \qquad (4)$$

where, r - radius of projectile

Cantwell and Morton [5] state that impact loading by a light projectile at high velocity induces a very localised form of target response resulting in much of the incident energy being dissipated in a very small volume. The areal geometry of the target is stated to be less important at high rates of strain.

Low velocity impact, also known as quasi-static loading, results in global deflection of a thin laminate, while high velocity impact results in a highly localised response. Low velocity impact for carbon fibre reinforced epoxy laminates is stated by Davies et al. [10] to occur below $20m.s^{-1}$. It is also stated that for impact velocities in excess of $20m.s^{-1}$ (high velocity impact) stress waves must be considered when investigating damage in carbon fibre reinforced epoxy composites.

The relevance of low velocity impact (<20m/s) damage in composite laminates to high velocity impact is limited, however some aspects, such as delamination shape, are common to both. The available literature provides insight into the causes of particular delamination shapes and the prevalence of particular shapes.

Highsmith et al.. [16] on filament-wound composite structures, using toughened and normal matrices, considered low velocity impact damage (1.84m/s to 2.81m/s). The damage has been described in terms of an overall delamination area consisting of two lobes ("peanut" shaped) that intersect at the impact site that for the toughened matrix were found to cluster near the line of 90° fibre failure. The reduction in delamination toward the impact site is attributed to stress relief as a result of fibre fracture below the impact site. Asymmetry of the delamination lobes was attributed to stress relief as a result of fibre fracture in the smaller lobe region. The authors described fibre fracture within the interior helical layers, at locations removed from the impact site, that are attributed to compressive loading during springback after initial displacement due to impact. In the toughened matrix specimens fibre fracture also occurred in the exterior 90° direction fibres. Damage area was generally found to be smaller for the toughened matrices and in both matrix systems damage area increased with impact velocity.

Choi et al.. [8] utilised line-loading low velocity impact to investigate the onset of damage, i.e. critical matrix cracks, in laminate plates of varying lay-ups and thicknesses. The triggering of total laminate failure was ascribed to surface fibre failure, although this only occurred for sharp-nosed impactors and line loading at high velocities. Surface fibre damage

occurred earlier than internal damage if the surface ply group was too thin, resulting in premature failure. Location of the critical matrix cracks shifted from the mid-plane to the back surface as the 90° plies were more evenly distributed through the laminate, although the cracks still occurred in the 90° plies. The inclination of the critical cracks also changed from an angle of 45° to near perpendicular to the loading direction. The initial failure for lay-ups with all the 90 ° plies in the centre was dominated by the interlaminar shear stress/strength ratio, which was reduced as the plies were more evenly distributed. The authors concluded that failure was due to a combination of interlaminar shear stress and transverse tensile stress and that both are critically important for initiating impact damage.

Choi and Chang [9] considered point loading low velocity impact damage in graphite reinforced epoxy laminates ($[+45_4/-45_8/+45_4]$ lay-up), following on from previous work on line loading impact, for a variety of impact velocities and masses. The authors concluded, from the line loading impact results, that intralamina cracking or critical cracking is the initial damage mode, which propagates into the nearby interface of dissimilar materials (see Figure 8) and initiates delamination along the interface and away from the location of impact. The damage morphology of the point-loaded specimens at low impact energy (1.7J at 4.15m.s^{-1}) consisted of short matrix cracks parallel to the +45° plies. Delamination at the last interface between +45 ° and -45° plies, occurred at higher velocities (5.89 m.s^{-1}) while at even higher velocities (9.02m/s) a second, smaller delamination occurred at the first interface. The delamination shape was described as "peanut" shaped with the major axis aligned with the +45° plies. The delamination at the last interface always governed the overall size of damage. A $[0_3/90_3/0_3/90_3/0_3]$ laminate was also considered with the only significant difference being that the major axis of the delaminations being oriented along the 0° axis. The authors postulated that point loading impact damage therefore followed that of line loading damage.

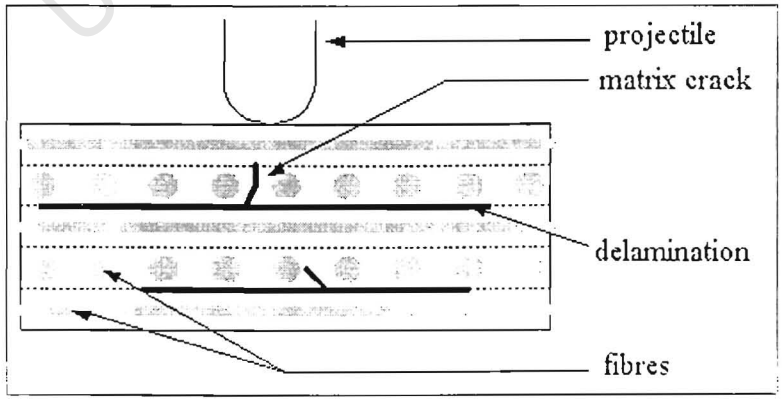

Figure 8 Delamination initiation & propagation

Hitchen and Kemp [17] considered low velocity impact damage in carbon fibre reinforced epoxy laminates with an impact mass of 2kg, at 2.5m.s^{-1} (6.25J), and 6 different lay-ups of 0 and 45° ply variations. The authors found that damage morphology consisted of a crush zone at the impact site that sustained considerable fibre damage. In addition to delamination, splitting was observed that tended to be most extensive in the plies furthest from the impact site. Delaminations initiated at almost every dissimilar ply interface and tended to be oriented parallel to the lower ply (furthest from the impact site) bounding the delamination. The total delamination area was found to be smaller for panels that had 45° surface plies. The delamination shapes are described as circular, diamond, elongated and "peanut" (also known as waisted) shaped (Figure 31). The latter shape is associated with a combination of delamination and fibre fracture in the lower ply and the energy absorbed by this medium may reduce lateral delamination growth.

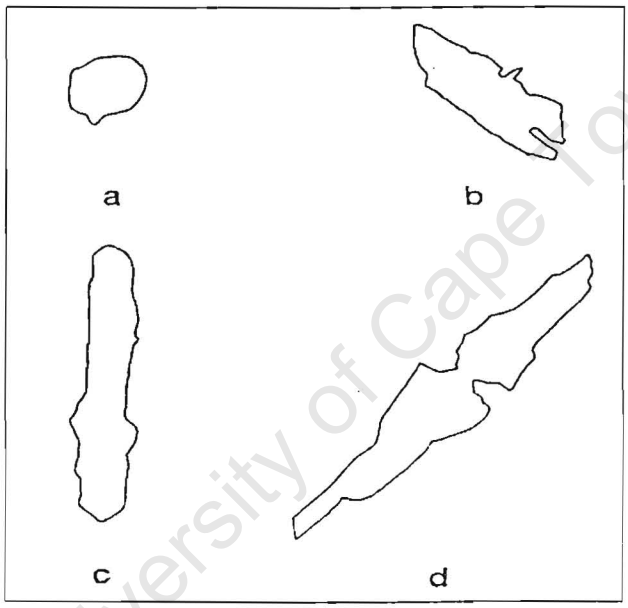

[17]

Figure 9 Delamination shapes a) circular b) diamond c) elongated d) peanut or waisted

3.4.2 Total delamination area

The total delamination area through an impacted laminate is determined by summing the delamination area at each interface. Determining the actual area at each interface requires the use of a de-ply technique* or ultrasonic C-scanning.

* Specimens are impregnated with a gold solution, baked in an autoclave and then laminae are separated. Delaminations are defined by gold residue.

Mines et al. [21] while investigating ballistic perforation of laminates, visually measured the delamination areas immediately below the impacted and distal surfaces. The delamination areas at the remaining interfaces were then calculated by a linear interpolation between the measured areas.

Cantwell and Morton [5] show (Figure 10) that Delamination area increases steadily with impact energy and that delamination in multi-angle composites is more likely to occur at interfaces where the mismatch in bending stiffness is greatest i.e. where difference in laminae orientations is greatest.

Kitchen and Hemp's [17] results (Figure 11) with regard to delamination distribution through the laminate do not show a linear relationship as delamination area increases rapidly in interfaces furthest from the impact site.

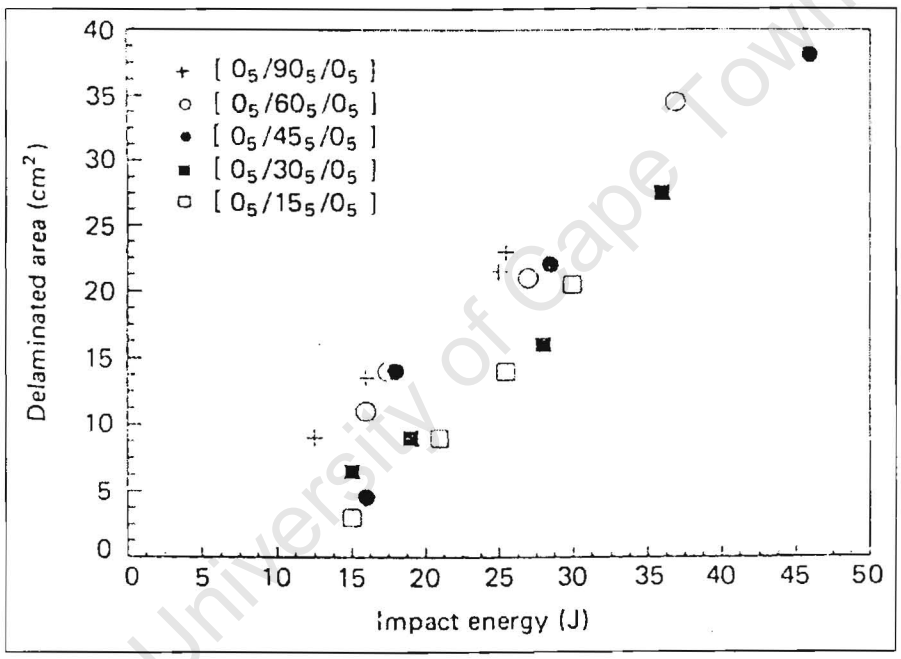

[5]

Figure 10 Delamination versus impact energy

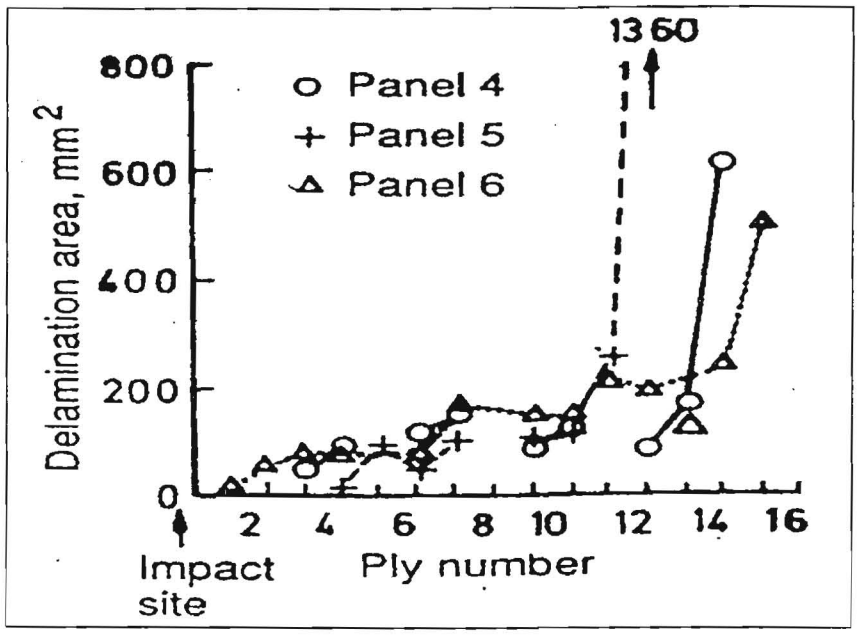

[17]

Figure 11 Delamination area versus ply number

3.4.3 Energy dissipation

An energy balance consideration [21] of a projectile impact event shows that the initial projectile kinetic energy is equal to the sum of the kinetic energy post impact and the energy dissipated by material failure and straining.

Belingardi et al. [4] found that fibre reinforced epoxy laminates could be assumed to have a linear elastic relationship up until brittle fracture. Since very little plastic deformation occurs it can be assumed that projectile kinetic energy dissipation is due to material fracture and elastic strain energy.

Cantwell and Morton [5] state that manufacturers have sought to improve the energy dissipated due to strain by reducing the cross section of T300 carbon fibres from 7-8μm to approximately 5μm in later generation fibres. It is suggested that because damage in high velocity impact events is localised a reduction in fibre diameter may not be beneficial in dissipating impact energy. At high strain rates the structure is said to behave in a local mode and the strain energy absorbing of the fibres and structure is less important. *Strain energy is still concluded to be one of the most significant energy absorbing parameters in determining the impact response of a composite structure.*

Cantwell and Morton [5] state that at high velocity impact local energy absorbing mechanisms such as fibre pull-out and fracture become dominant. Delamination and splitting

have a similar energy absorption ability, however both are an order of magnitude less than the energy absorption ability of fibre fracture and fibre pull-out [5]. Chamis et al. [7] identified flexure and interlaminar shear deformation as dominant energy absorption mechanisms for low velocity impact events†.

Mines et al. [21] investigated high velocity projectile impact on glass fibre reinforced epoxy laminates and proposed tnat energy absorption is dominated by shear effects. The total energy absorbed was suggested to be approximately equal to the local perforation energy (E_{sh}), delamination energy (E_{dl}) and friction energy (E_f). It was assumed that energy absorbed due to the deflection of the panel is negligible. Energy absorbed by delamination is assumed to be dominated by the mode I (through thickness shear failure) fracture toughness, which for graphite reinforced epoxy laminates is essentially strain rate insensitive. Static load-deflection curves were used to determine the friction energy component for both static and dynamic perforation cases. The overall perforation energy was given by;

$$E_p = E_f + E_{sh} + E_{dl} \qquad (5)$$

where; $E_f = P_f \times x$

x ~ length of projectile passed through laminate, P_f ~ friction force

3.4.4 Effect of ply stacking sequence

Hitchen and Kemp [17] show that the stacking sequence can affect the number of dissimilar faces i.e. interfaces between laminae with dissimilar orientations. The maximum energy absorbed (approximately 6.6J) by delamination is found to be relatively constant irrespective of the number of dissimilar interfaces increase whereas the energy required to initiate delamination increases.

Choi et al. [8] investigated impact damage in graphite reinforced epoxy laminates and observed that the inclination of intralamina cracks were dependant on the configuration of the laminate. The more evenly dispersed the stacking sequence ($[0_3,90_2,0_3,90_2,0_3,90_2,0_3]$ compared to $[0_6,90_6,0_6]$) the higher the initial impact damage for a blunt nosed impactor.

Hull and Shi [18] reviewed damage mechanism characterisation and suggested that transverse shear stresses were involved with the inclination of intralamina cracks. A clear connection between the intralamina cracks and delaminations is also stated. Since both transverse shear

†Results based on Izod test i.e. low to medium velocity test.

stresses and delaminations are known [17] to be related to ply stacking sequence it can be further suggested that the inclination of intralamina cracks also depends on the stacking sequence.

Cantwell and Morton [5] state that the fibre stacking sequence determines both the elastic energy absorbing capability as well as the failure mode of a composite

3.5 Impactor

3.5.1 Effect of projectile geometry

The shape of the projectile head, otherwise known as the tup, has a significant effect on impact damage and perforation energy. The standard tup shapes are flat, conical, and hemispherical.

Mines et al. [21] utilised the standard tup shapes while studying high velocity perforation of laminates. The authors found that for full perforation some intense shear areas for the hemispherical tup could be seen, where energy absorption due to shear (E_{sh}) was given by;

$$E_{sh} = A_{sh} \cdot \gamma_f \qquad (6)$$

where; $A_{sh} = \pi.D.h$, D is the impactor diameter and h the laminate thickness

It was also observed that there was an increase in overall perforation energy, i.e. energy absorption, for flat tups, however, there was a decrease in static perforation energy for hemispherical tups. Static and quasi-static tests showed that cone and hemispherical tups produce the lowest impact forces and flat tups the lowest values of displacement and energies.

3.5.2 Impact incidence

The angle at which an impacting projectile contacts a laminate (incidence) determines initial contact stresses and the path it travels through the laminate. The incidence may therefore affect initial failure and overall energy dissipation.

Goldsmith [14] in a review on projectile impact states that normal impact demands that the velocity vector of the projectile be coincident with its axis of symmetry, as well as that of the target surface normal. Oblique impact occurs frequently for long-rod projectiles as a result of

natural flight path deviations i.e. effects of trajectory, drag etc. . Long rods are projectiles with a length: diameter ratio in excess of 10. Oblique impact results in asymmetric loading, which may add or cancel the effect induced by obliquity. In the absence of any directional changes of an oblique projectile the only difference in a perforation phenomenon would be the path length through the target, i.e. laminate thickness. The ballistic limit has been found to increase by about 30% when bending stresses, due to oblique impact, cause the projectile to fracture.

3.6 Material properties

3.6.1 Strain-rate properties

The strain-rate properties of CFRP laminates are difficult to obtain experimentally, however previous work has shown them to be relatively insensitive to strain-rate.

Qian et al. [24] investigated low to high velocity (4.5m/s to 25m/s) impact response in CFRP plates and utilised standard material properties in the analysis. The numerical results showed good agreement with the experimental results, indicating that material strain rate sensitivity had no significant effect on the outcome.

Dee et al. [11] considered the high strain rate mechanical properties of a graphite reinforced epoxy matrix torospherical shell, which was considered to be quasi-isotropic. The in-plane ultimate tensile strength was found to be strain rate insensitive while the ultimate strain and elastic modulus relatively insensitive. The out of plane tensile properties were also found to be strain rate insensitive. The compressive strength was found to be strain rate sensitive with the in-plane high strain rate value being 29.4% higher while the out of plane value was found to be 28.3% lower than the corresponding quasi static value.

3.6.2 Fracture energy

Phillips and Harris [22] discussed the strength, toughness and fatigue properties of polymer composites and state that values of G_c for matrix cracking and G_{IIC} for delamination are of the same order, approximately 400 J/m^2. Values for through thickness shear failure are generally two orders or more higher for CFRPs being of the order of 20-30kJ/m^2.

Abrate [2] in a text on impact of composites quotes values, for CFRPs, of 37.5 kJ/m^2 for γ_{fn} and 500 kJ/m^2 for G_c.

Cantwell [6] investigated high velocity impact on unidirectional and woven Grafil XA-S carbon fibre reinforced Ciba Geigy BSL 914C epoxy resin. Transverse fracture testing yielded a γ_f value of 30kJ/m^2 for the plain unidirectional material.

Cantwell and Morton [5] reviewed the impact resistance of composite materials and quoted the following fracture energy release rate values for CFRPs; matrix splitting - 0.1-1kJ/m^2, delamination - 0.1kJ/m^2, and transverse fibre fracture - 20kJ/m^2.

Hitchen and Kemp [17] investigated impact on CFRP (T800H/924C) laminates and suggest that G_{IIc} for this material lies between 300 and 580J/m^2.

The consensus of literature is that delamination and matrix cracking have energy release rates in the range 300 J/m^2 to 600J/m^2 and for through thickness shear failure the range is between 20kJ/m^2 and 40kJ/m^2.

Chapter 4. Experimental set-up and procedure

4.1 Specimens

The specimens were provided in the form of five 1.7 metre long tubes of which four were of one stacking sequence (A laminate) and one of another sequence (B laminate). The number of tubes and type of sequences was determined by the cost of producing the specimens. The single B laminate tube resulted in a low number test specimens and limited the ability to draw conclusions from the results.

4.1.1 Lay-up

The filament wound lay-up has been approximated to a laminate of unidirectional laminae, where a single helical winding is equivalent to two identical orthotropic laminae of the same magnitude of orientation yet of a positive and a negative sense. The difference between the actual wound laminate and the approximation being that the "seam" (Figure 12 a)) is neglected in the approximation (Figure 12 b)) as it forms a very small portion of the laminate. The "seam" is the point where successive helical winds cross each other such that they are interwoven at that point and should affect delamination.

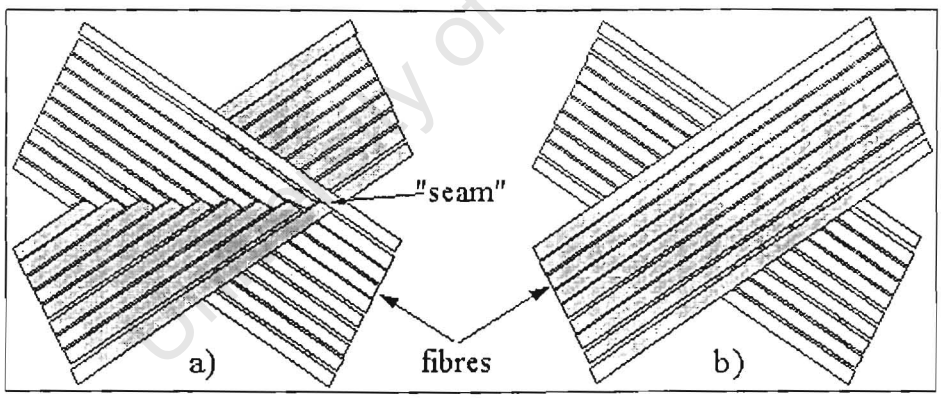

Figure 12 a) filament wound; b) laminate approximation

Delamination shape was affected in the few cases where impact occurred off the seam, however, the total area was not affected (see section 5.1.5 Area sizes).

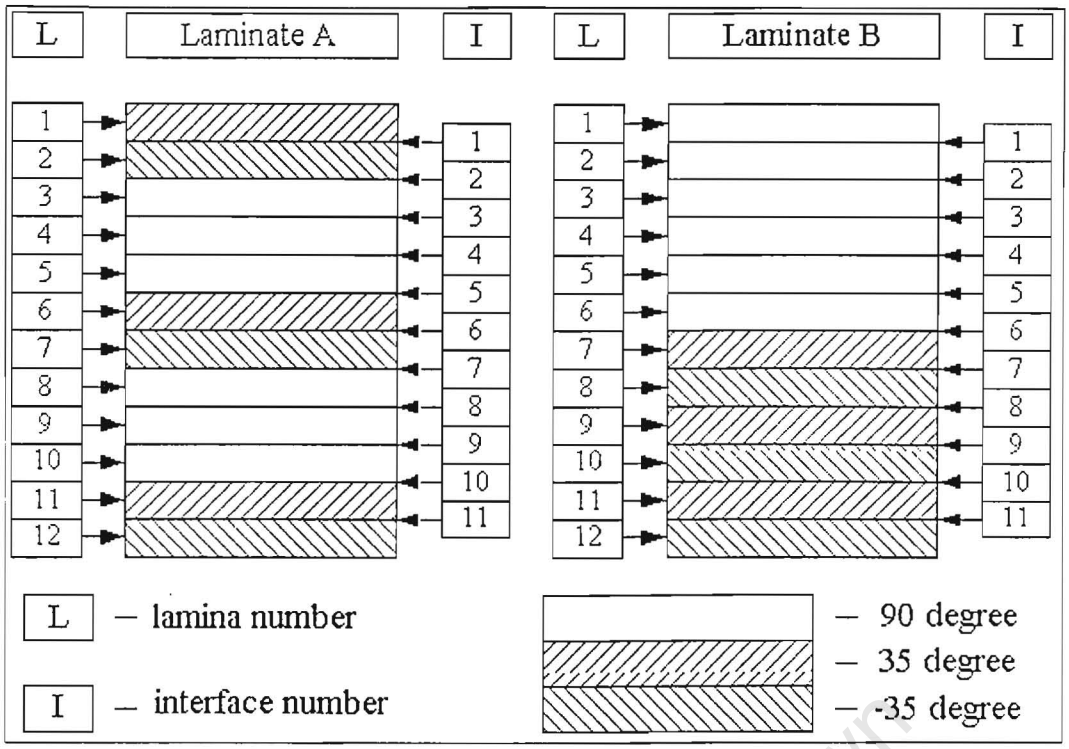

Figure 13 Laminate and interface numbers

Laminate A (see Figure 13) has 3 interfaces with a 70° difference in ply orientations located at interfaces; 1, 6 and 11 as well as 4 interfaces with a 55° difference located at interfaces; 2, 5, 7 and 10. Laminate B has 5 interfaces with a 70° difference in ply orientations located at interfaces; 7 to 11 as well as a single interface with a 55° difference located at interface 6.

The following is the conventional means of specifying the approximate laminate sequence and orientations;

A - $[-35^{\circ}/+35^{\circ}/90^{\circ}_3/-35^{\circ}/+35^{\circ}/90^{\circ}_3/-35^{\circ}/+35^{\circ}]$

B - $[90^{\circ}_6/(-35^{\circ}/+35^{\circ})_3]$

(subscript indicates a repeated lamina)

4.1.2 Dimensions

The tubes have a 140.5mm outer diameter and a 2.5mm wall thickness. Measurement of the lamina thickness, using scanned images, showed that each 35° and -35° lamina was approximately 0.15mm thick and each 90° lamina was 0.267mm thick.

The tubes were cut to lengths suitable for testing according to the following criteria;

1. Tubes should fit in the clamp i.e. minimum length of 300mm.
2. Tubes should be long enough so that the boundary edge (clamp) should not interfere with the damage site.
3. Tube free edges should be cut outside of the seam i.e. minimum length of 300mm (see Figure 14).

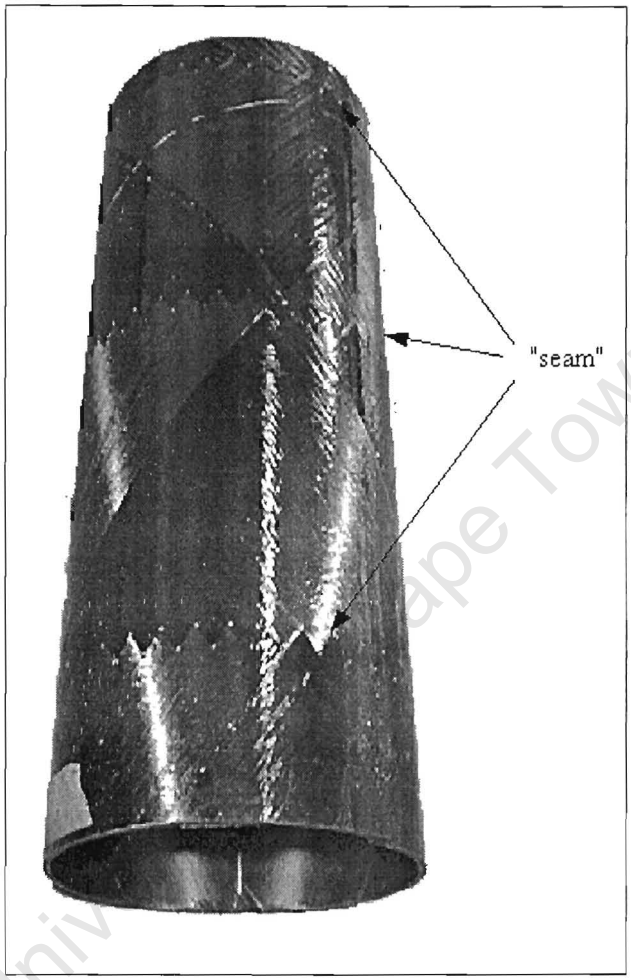

Figure 14 Specimen

Mines et al. [21] considered that a flat panel of dimension 200mm x 200mm was the minimum size necessary to prevent local damage interacting with the boundary. The current specimen is stiffer by virtue of material properties and geometry so that should be even more localised. A minimum specimen length of 300mm was expected to be more than long enough to prevent damage interacting with the boundary. The length also ensures that the impact location will occur between "seams" that will serve to prevent delaminations reaching the clamp i.e. boundary. The damage at and above the ballistic limit was larger than estimated,

however it was not large enough to reach the "seams" and interact with the boundary, so validating the original assumption.

The tubes were cut to size by band saw on the outside of the seam. The cutting tended to induce delaminations at the free edges, however the "seam" prevented the propagation of these small delaminations into the impact site.

4.1.3 Residual stress

Laminates all have a certain amount of residual stress mainly due to the effects of curing. A number of A laminate tubes were cut in half longitudinally and all contracted a similar amount across their diameters (from 140.5mm to 137mm), as a result of residual stress. The fact that they all contracted a similar amount is indication that there is no significant variation of residual stress among the A laminate specimens. The B laminate tubes, due to their scarcity, were not cut in half and so the extent of their residual stress has not been assessed.

The two lay-ups both underwent the same production process, i.e. same fibre/matrix volume ratio, and same curing cycle so that the difference in lay-up would be the significant cause of any residual stress difference. Determining the effect of staking sequence on residual stress would be beyond the scope of the thesis and is suggested for follow-up work.

4.1.4 Material properties

A rigorous analysis of laminated composites typically requires that physical testing for material properties be performed. The reasons for this being that composite material properties have been known to vary considerably, typically as a result of the manufacturing process or the variability of the fibre properties.

In order to obtain the true material properties of an orthotropic lamina a flat laminate composed of a number of laminae of the same orientation and fibre volume ratio is required. The lack of such a laminate and the lack of adequate facilities precluded the physical testing for material properties.

The fibre and matrix material properties were obtained from the sponsoring company and their manufacturer's websites [25]. Some material constants could not be obtained from the company or manufacturers in which case a value from a similar material was substituted.

Laminate material properties used in the finite element analysis were calculated using a commercial laminate analysis software.

Material properties[‡]:

- Matrix [26]: E = 2.9Gpa [23], ν = 0.35, G = 1.25Gpa, ρ = 1.25g/cm^3
- Fibre [25]: E_{11} = 294Gpa, E_{22} = 2.83Gpa, G12 = 50Gpa, ν_{12} = 0.23, ρ = 1.81g/cm^3
- 90° lamina: Vf = 0.6 [23], E_{11} = 177.6GPa, E_{22} = 2.845GPa, G_{12} = 4.438GPa, $G_{13} = G_{12}$, G_{23} = 3.012GPa, ν_{12} = 0.278, $\nu_{13} = \nu_{12}$, ν_{23} = 0.528
- 35° lamina: Vf = 0.65 [23], E_{11} = 192.1GPa, E_{22} = 2.843GPa, G_{12} = 5.088GPa, $G_{13} = G_{12}$, G_{23} = 3.003GPa, ν_{12} = 0.272, $\nu_{13} = \nu_{12}$, ν_{23} = 0.527

The laminate in-plane properties are the same such that;

E_{11} = 33.11GPa, E_{22} = 117.44GPa, ν_{12} = 0.118, G_{12} = 18.431

The bending stiffness of the two laminae, determined by the software, are different and so imply a different compliance.

High strain-rate material properties are even more difficult to obtain than standard material properties. The material properties for carbon/epoxy laminates do not exhibit significant variation with strain rate [24] and many researchers assume no change.

4.2 Impactor

Mild steel was found to be a satisfactory material for the impactor as no discernible plastic deformation or fragmentation occurred.

4.2.1 Gas gun projectile

Body: 8mm diameter, 19mm long

Head: hemisphere, 8mm diameter

Material: mild steel

Mass: 10.15grams +/-0.02grams

[‡] Material properties without a source reference were calculated using laminate analysis software.

The projectiles were cut to length on a band saw and then machined on a CNC lathe in order to produce a consistently shaped hemispherical head.

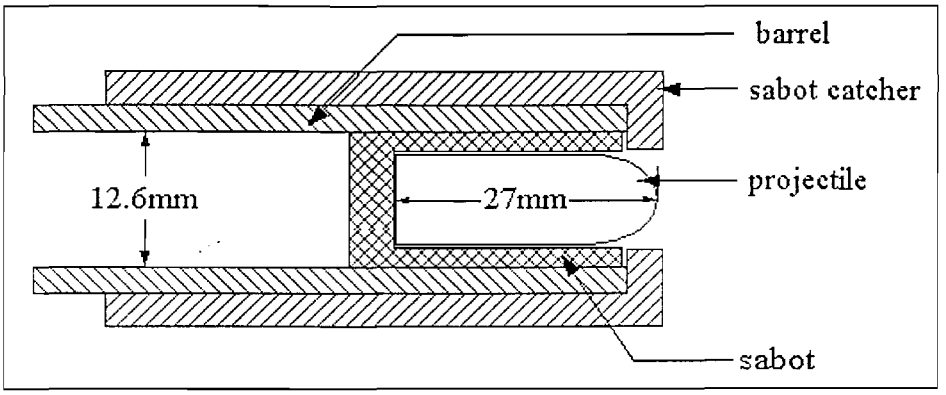

Figure 15 Projectile and sabot

The projectile was placed within a Perspex sabot for firing, which was machined from oversized 12mm diameter Perspex rod. The Perspex sabot was caught by a steel catcher placed over the end of the barrel (see Figure 15).

4.2.2 Drop tester tup

Body: 8mm diameter

Head: hemisphere, 8mm diameter

Material: mild steel

Mass: 3.192kg

The mass of the drop tester tup was determined by considering the velocities that could be achieved with the available drop height and by attempting to obtain impact energies similar to those achieved in the ballistic tests.

4.3 Apparatus

4.3.1 Clamp

The following is a summary of the clamp design and operation.

Design requirement

The clamp should;

1. Maintain contact with the specimen around its entire circumference.
2. Produce the same clamping stresses in each specimen.
3. Prevent the specimen from moving globally.
4. Have sufficient span so that the boundary does not to interact with the damage site.
5. Present the specimen to the projectile such that the projectile impacts normally to the surface.
6. Clamp should be mountable on the gas gun I-beam (Figure 17) and the drop tester mounting table (Figure 20).

Operation

1. Slide specimen into clamping plates and align the desired impact point with the barrel exit.
2. Tighten clamping bolts until the split is 1.5mm apart[§,**].

[§] 1.5mm was found, by trial and error, to be sufficient to hold the specimen firmly such that it could not be dislodged manually.

[**] Where specimens have been too large to achieve this the author attempted to achieve a similar tightening torque by feel, in hindsight a torque wrench should have been used for every specimen.

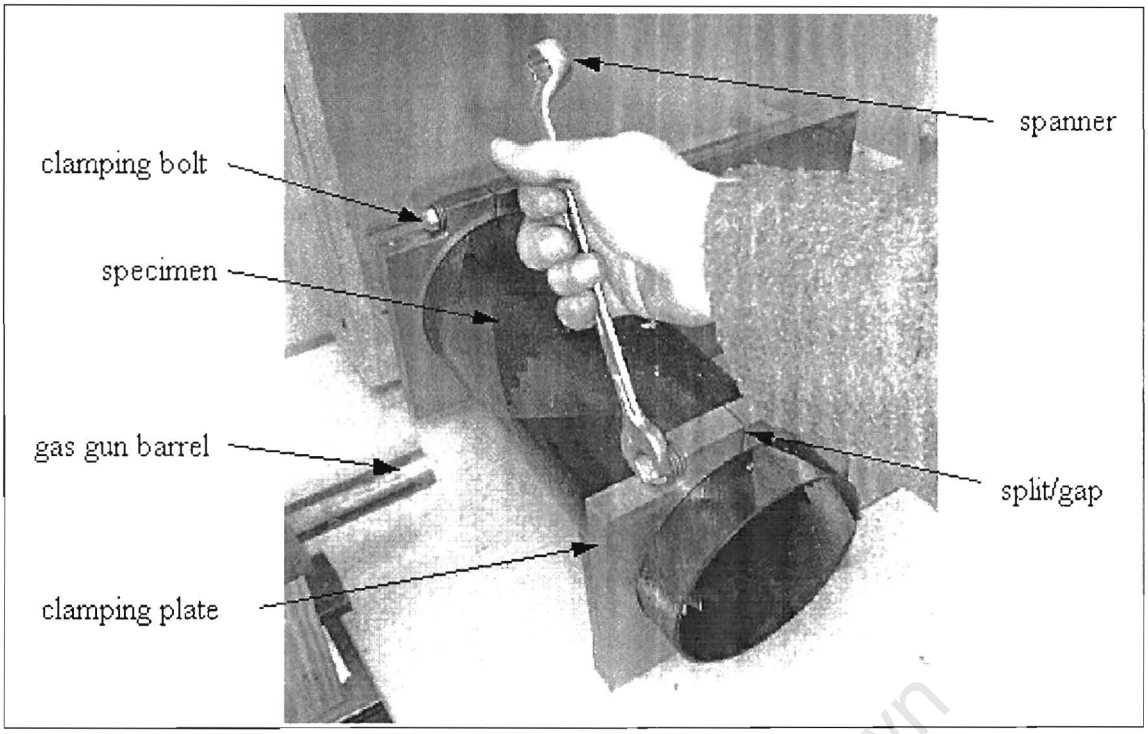

Figure 16 Clamp

4.3.2 Gas gun

Description (Figure 17)

The gas gun equipment consists of a;

1. barrel
2. main cylinder
3. firing valve (Figure 18)
4. firing solenoid
5. pressure controls
6. nitrogen gas bottle
7. velocity sensor
8. sabot catcher (Figure 15 & Figure 19)

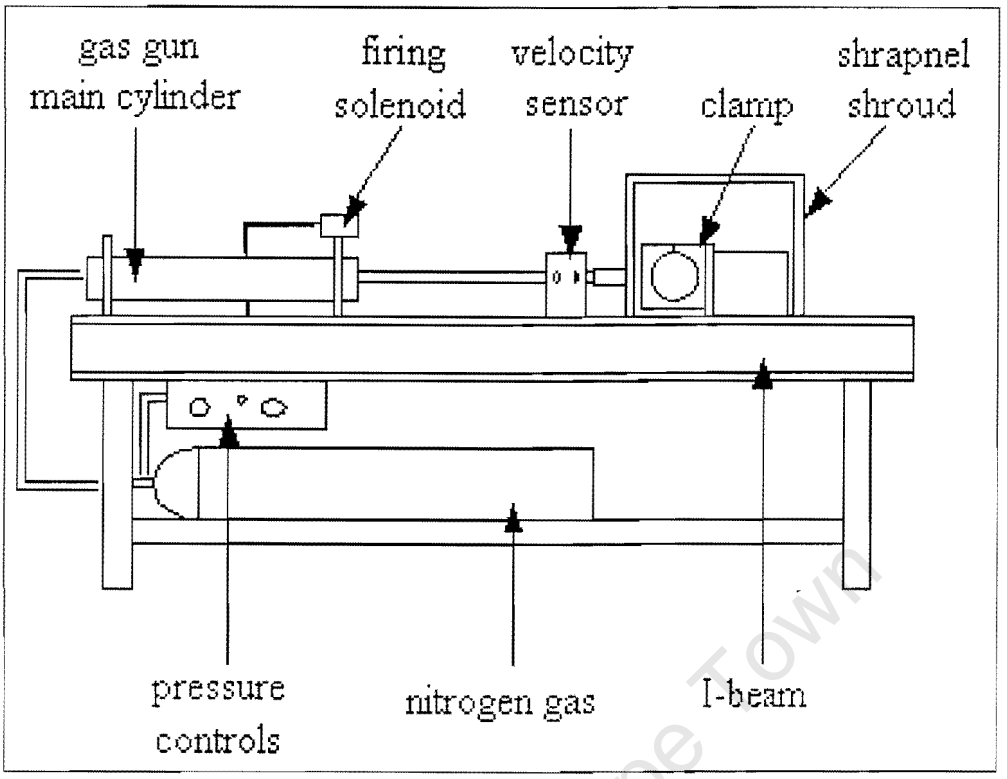

Figure 17 Gas gun set-up

Operation

1. Pressurise the main cylinder and firing valve, always maintaining a firing valve pressure greater than the main cylinder but not exceeding a 2bar difference, until the desired main cylinder pressure has been achieved.

2. Depress solenoid button to fire.

The firing solenoid (Figure 18) vents pressure on one side of the firing valve shuttle (P2) causing it to move from its seat at the base of the barrel. The pressure in the main cylinder is then able to escape down the barrel propelling the sabot and projectile. The solenoid is triggered by a button mounted remotely from the gas gun to ensure the operator is not near the gas gun during operation.

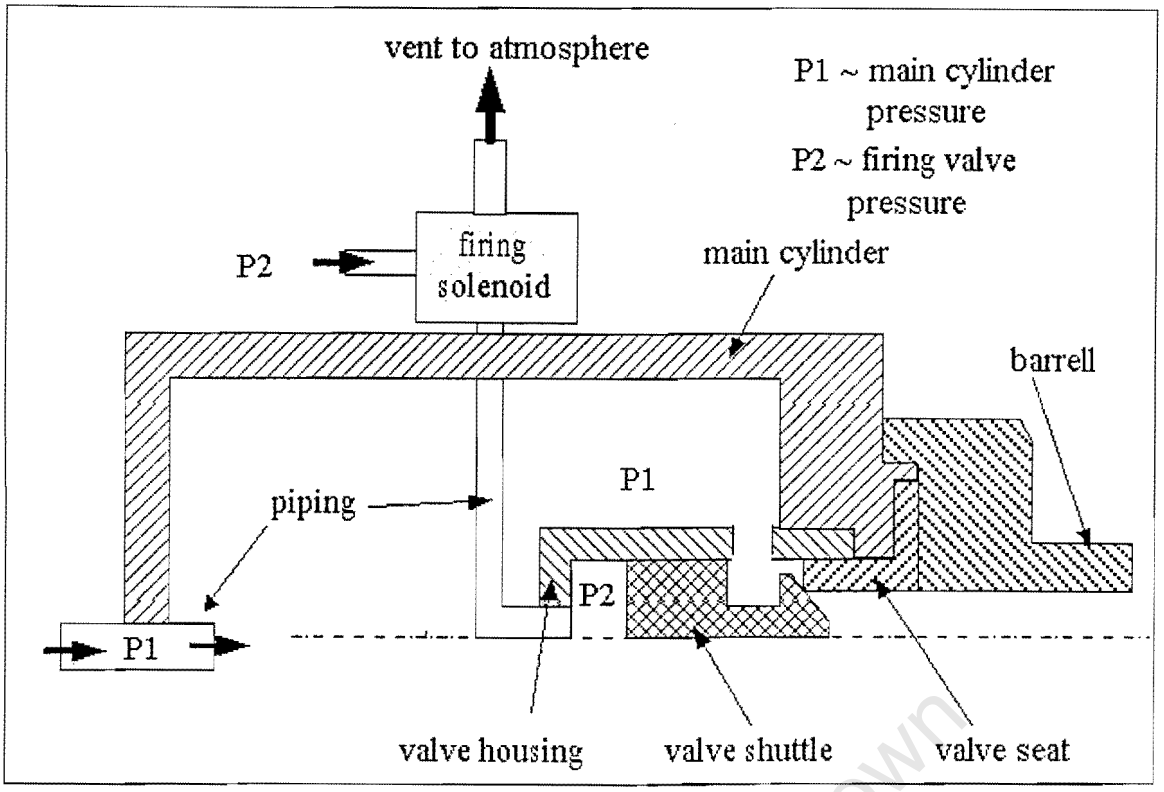

Figure 18 Firing valve

The velocity sensor consists of two pairs of infrared sensors, one an emitter and the other a receptor, connected in tandem and mounted in a wooden housing over the suppresser of the barrel. The infrared sensors are connected to a timer so that when the projectile interrupts each infrared beam the timer measures the time it takes to travel between the two. The distance between the two pairs of sensors is 50mm, which when divided by the measured time provides the velocity of the projectile in the last portion of the barrel.

The shrapnel shroud (Figure 19) is an essential safety feature, which is lowered over the target in order to trap the projectile and fragments.

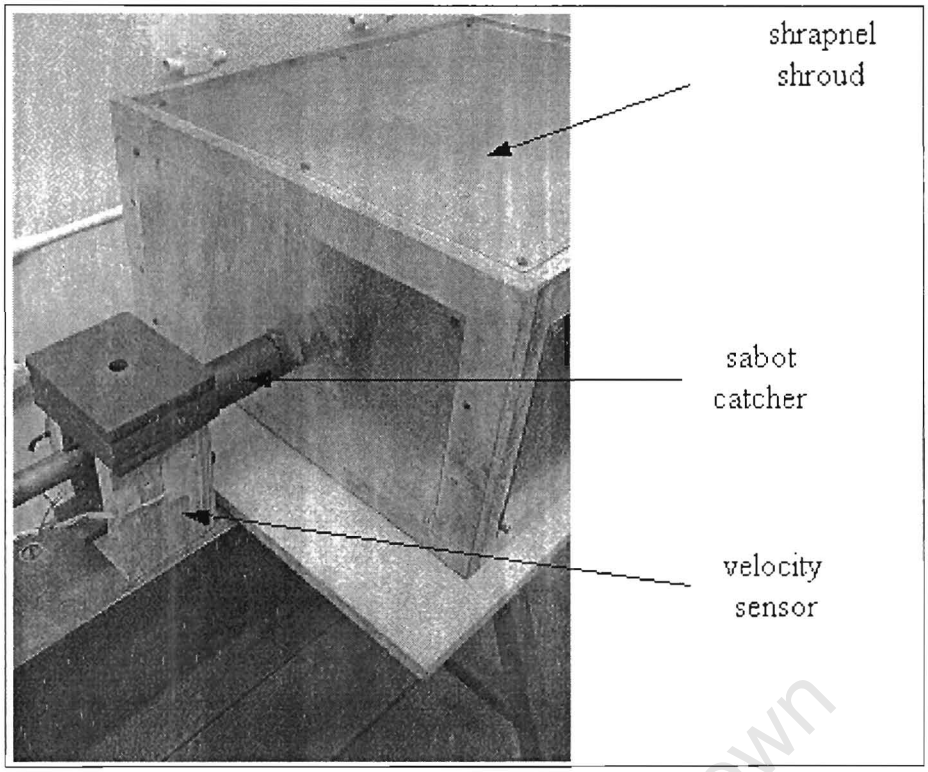

Figure 19 Shrapnel shroud

4.3.3 Drop tester

Description (Figure 20)

The drop tester equipment consists of a;

1. Computer
2. Mounting table
3. Velocity sensor
4. Track
5. Tup & load cell
6. Mass
7. Release mechanism
8. Cantilever

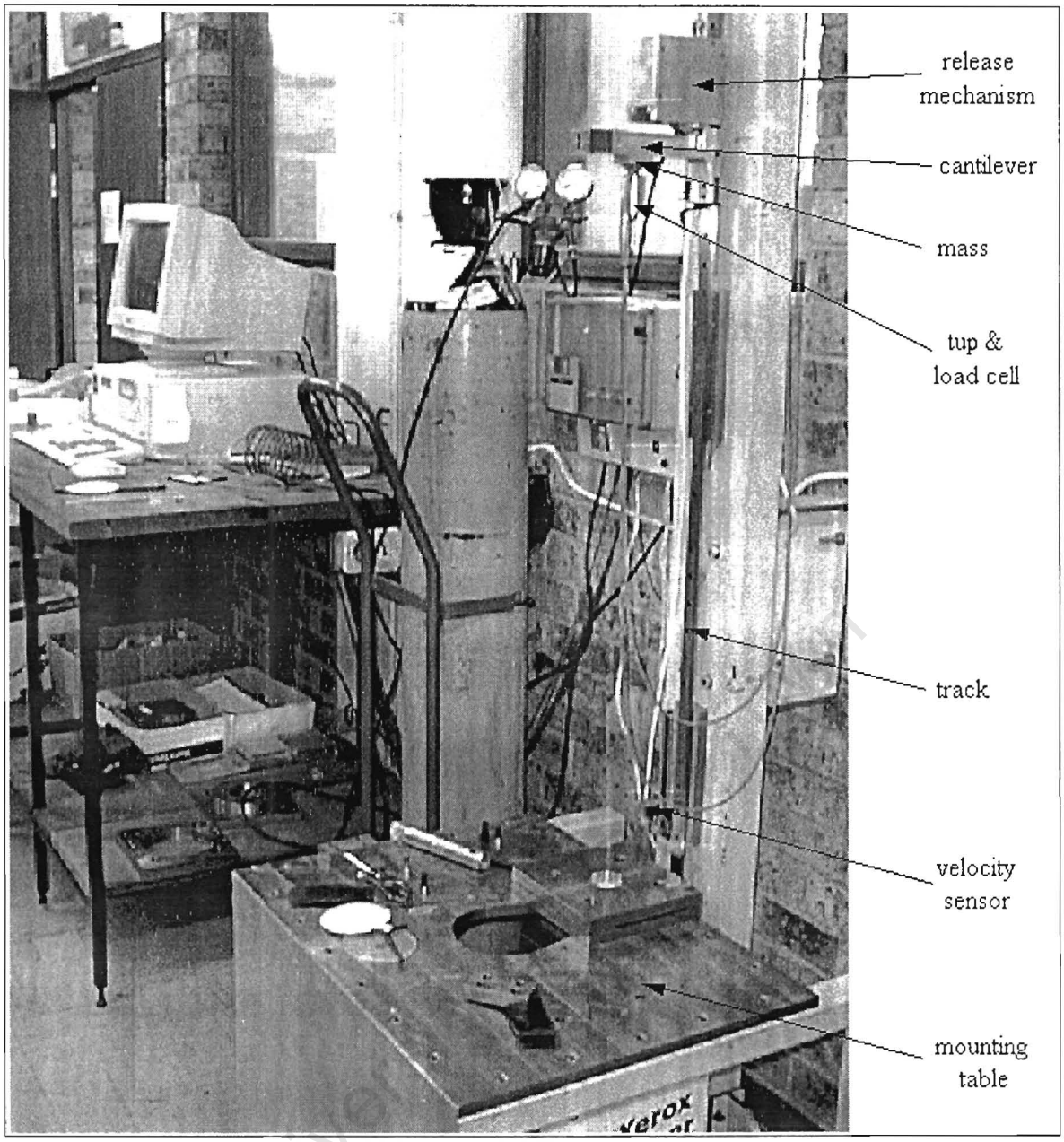

Figure 20 Drop tester

Operation

1. Switch computer on start drop test program.

2. The mass, tup and load cell are mounted on the cantilever and connected to the release mechanism.

3. The specimen clamp is bolted to the mounting table.

4. Release mechanism is then raised to the required drop height.

5. Release cantilever.

6. Copy program data and transfer into text editor before commencing next drop test.

Output

The program provides output in the following forms:

- Force history vs. displacement
- Force history vs. time
- Energy vs. displacement

4.4 Gas gun test

Loading the projectile

1. Weigh projectile.

2. Ensure projectile fits snugly in the sabot without sticking.

3. Ensure sabot fits snugly in the barrel without sticking.

4. Place projectile in sabot.

5. Place sabot with the projectile in the barrel.

6. Push to the base of the barrel with ramrod.

7. Ensure ramrod has gone the required depth to ensure no other objects remain in the barrel.

Gas gun preparation

1. Pressurise the main cylinder and firing valve until desired main cylinder pressure has been achieved.

2. Perform 2-3 test firings without a specimen to ensure required velocity is being achieved.

Test

1. Load projectile
2. Place sabot catcher on the end of the barrel.
3. Place specimen in clamp (see Figure 16)
4. Place shroud over specimen and ensure hole matches with barrel end.
5. Check main cylinder pressure.
6. Ensure velocity timer has been zeroed.
7. Press solenoid trigger button.

Test program

The aim of the test program was to induce impact damage over a range of velocities from a velocity sufficient to induce below visual inspection damage to above the ballistic limit.

The program for the gas gun test on A laminate specimens consisted of 2 phases;

Phase 1 -Determining the ballistic limit

Due to the limited number of specimens available this phase was conducted on half pipe specimens. The reduction in structural stiffness was assumed not to significantly affect the ballistic limit to that of a full tube section, as the damage was localised.

Phase 2 -Performing the tests

The tests are to range from impact velocities sufficient to induce internal laminate damage, otherwise known as below visual inspection damage (BVID), up to velocities beyond the ballistic limit.

The test program could only be applied in full to the gas gun tests on the A laminate specimens, as there were insufficient B laminate specimens for ballistic testing.

The approach taken for the gas gun test on the B laminate specimens was to perform the first test in the region of the ballistic limit of the A laminate specimen. The subsequent impact velocities depended on whether the impact is pre-ballistic or post-ballistic limit.

4.5 Drop test

Procedure

1. Select and weigh the mass ingots.
2. Attach mass and tup to cantilever.
3. Attach specimen clamp to the mounting table.
4. Turn on drop tester and initialise the program.
5. Test (see Drop tester)

The approach taken for the drop test was to match the lowest impact energy of the gas gun test and determine the subsequent impact velocities depending on whether the impact resulted in perforation or not i.e. pre or post-ballistic limit. A total of four tests were performed where 2 resulted in perforation and the other 2 did not. The results of particular interest are those from the perforated specimens where the force vs displacement plots for the tup enable values for shear perforation energy to be determined and hence values for work done per unit crack area. The force due to friction can also be obtained from the plot enabling calculation of energy dissipated due to friction [21].

4.6 X-ray non-destructive testing

The specimens were X-rayed tangentially, i.e. through the thickness, of the impact site and another taken radially to the impact site, after damage site enhancement had taken place.

4.6.1 Damage site enhancement

X-ray images are formed by relative changes in material density of the object being X-rayed, which allow varying amounts of X-rays through to the film. If there is not a sufficient difference in density of the target object then no image will form on the film. The delaminations within a damaged laminate do not offer a sufficient change in density to produce adequate images for analysis and so it is necessary to increase the density of the damaged area in order to enhance the image.

The density of the damage site is increased by impregnating the site with a denser material, which is introduced in the form of a solution. The solution used [16] was a zinc iodide solution with the following composition; 60mg ZnI_2, 10ml iso-propynol, 10ml Kodak Photo-flow (a wetting agent), and 10ml distilled water. The ZnI_2 is the densifying material while the water and iso-propynol are the dissolving solution that carries the ZnI_2 through the damage site. The Kodak Photo-flow serves to ensure that the solution flows and dries evenly.

4.6.2 Tangential image

The tangential image was obtained by placing the specimen on the X-ray film with the impact site lying normal to the X-ray film. The X-rays therefore pass tangentially through the impact site producing an image of the longitudinal cross section of the impact site. The image is taken before damage enhancement, as the densifying material would obscure the cross sectional image. **The images show the distribution of delaminations, through thickness shear fracture, and intra-laminar matrix cracking.**

The relative change of density through the thickness is more apparent tangentially than radially so that useful images are obtained without damage site enhancement.

4.6.3 Radial image

The radial image is obtained, after the damage site has been enhanced, by placing film on the inside of the tube and following the curvature of the tube. The image taken is sufficiently accurate so that there is no need to perform additional image manipulation to account for curvature. **The images show the delamination shapes and sizes, the distal delamination in particular.**

4.6.4 Processing X-ray images

Scanning

Scanned images of the X-rays were obtained on a standard desktop scanner that had been modified by the addition of backlighting. The dimensions of the scanned area were noted for each image so that suitable scaling in subsequent processing could take place.

Image manipulation

Two programs were investigated for use in enhancing the images to enable easier interpretation.

The two programs investigated were Adobe Photoshop Pro®, a general-purpose image manipulation program, and Osiris, a freeware X-ray image manipulation program for the medical community. Adobe Photoshop Pro® offered a superior levels-adjusting function, which enables selective contrasting to be obtained. Osiris provides a good histogram equalisation function, which reduces the noise in an image by "smoothing" the greyscale changes by fitting a histogram to the discontinuous greyscale gradient at the pixel level. The effect of histogram equalisation is to clarify the image thus making interpretation easier.

The use of both level adjusting and histogram equalisation (Adobe Photoshop Pro® and Osiris) on a single image was not necessarily beneficial in clarifying the image. The use of either function (program) had to be selective.

4.7 Image interpretation

Image interpretation relied on the use of the digital images and X-ray viewing table (light box). The digital images had the advantages of being able to selectively enhance aspects of an image and to highlight identified features on the image without ruining it permanently. Viewing the actual X-ray on a light box had the advantage of clarity, which was generally used in conjunction with the digital image in identifying and confirming features.

4.7.1 Identifying delaminations

Delamination boundaries in the radial images are characterised by a continuous band of lighter and darker regions (Figure 21), which may simply be a relative difference in light intensity rather than a distinct contrast in light intensity.

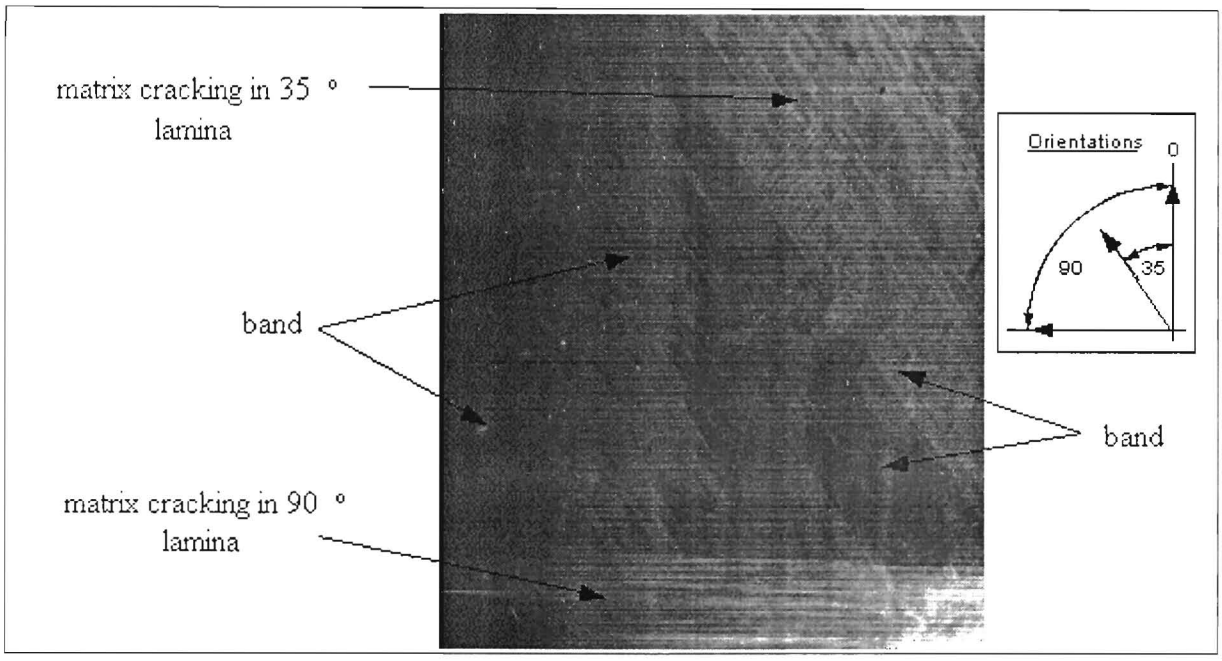

Figure 21 Section of a radial X-ray

The reason for this banding is that the densifying material (ZnI_2) flows more easily and evenly around the perimeter of a delamination. A delamination with adjacent delaminations will find portions of the adjacent laminae impinging (Figure 22) on the flow of the densifying solution in the central region.

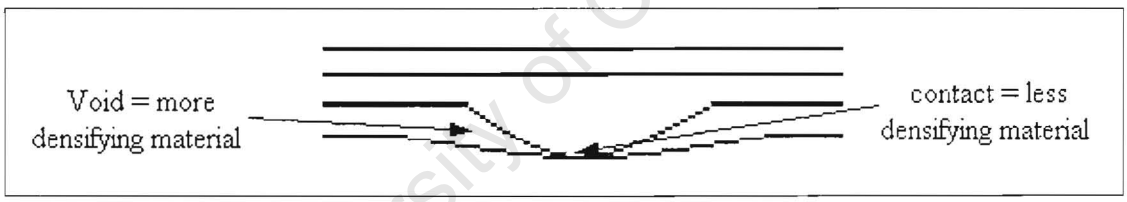

Figure 22 Void formation due to delaminations

Delaminations in the tangential images are identifiable as continuous dark regions or cracks of less dense material that run along the thickness (see Figure 23). The cracks are best identified using a combination of scanned images and the actual X-rays on a light box. The actual images have the advantage of clarity, i.e. no pixelation, and the scanned images enable easy magnification of regions of interest as well as the ability to mark and measure the images without permanently defacing them.

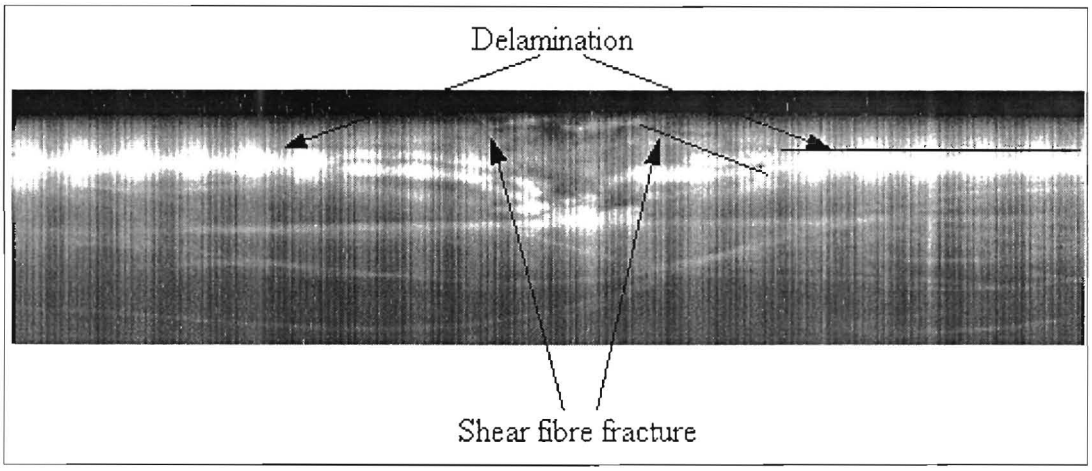

Figure 23 Tangential X-ray

The tangential X-rays yield measurements on the relative delamination length along the polar axis and are not indicative of delamination length about the circumference.

4.7.2 Identifying matrix cracking and fibre fracture

Matrix cracking and fibre fracture are characterised by distinct bright lines in the radial X-ray images. Matrix cracks tend to run along and between the fibres so that the lines due to matrix cracking are almost all aligned with the direction of the fibre orientation of the lamina in which they lie. Fibre fracture is identifiable by lines running across the direction of fibre orientation.

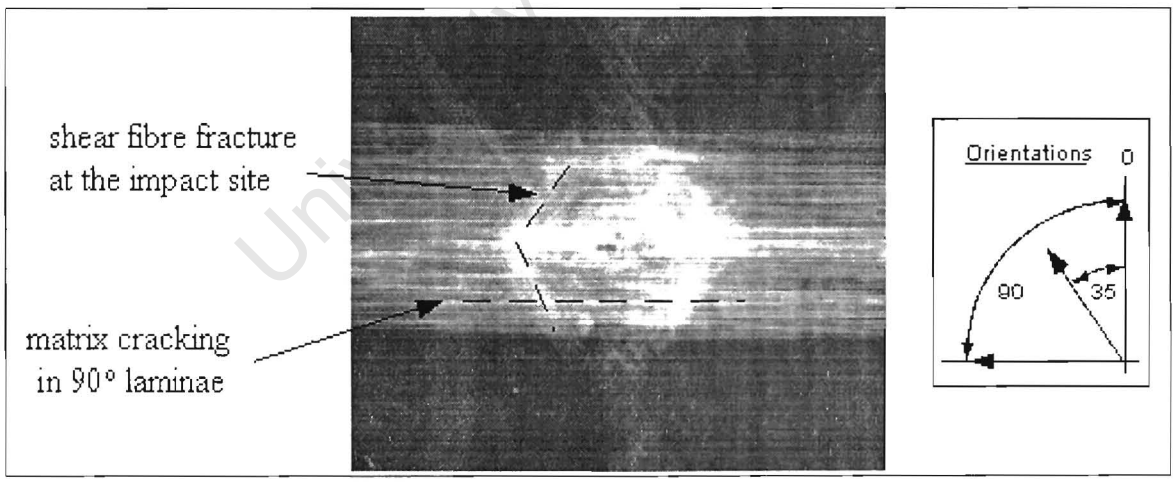

Figure 24 Cracking and Fibre Fracture

4.8 Axial images

A couple of images from both Laminate A and B were sectioned transversely through the impact site (see Figure 25) and scanned. The images are able to provide information on delamination propagation in the 90° orientation.

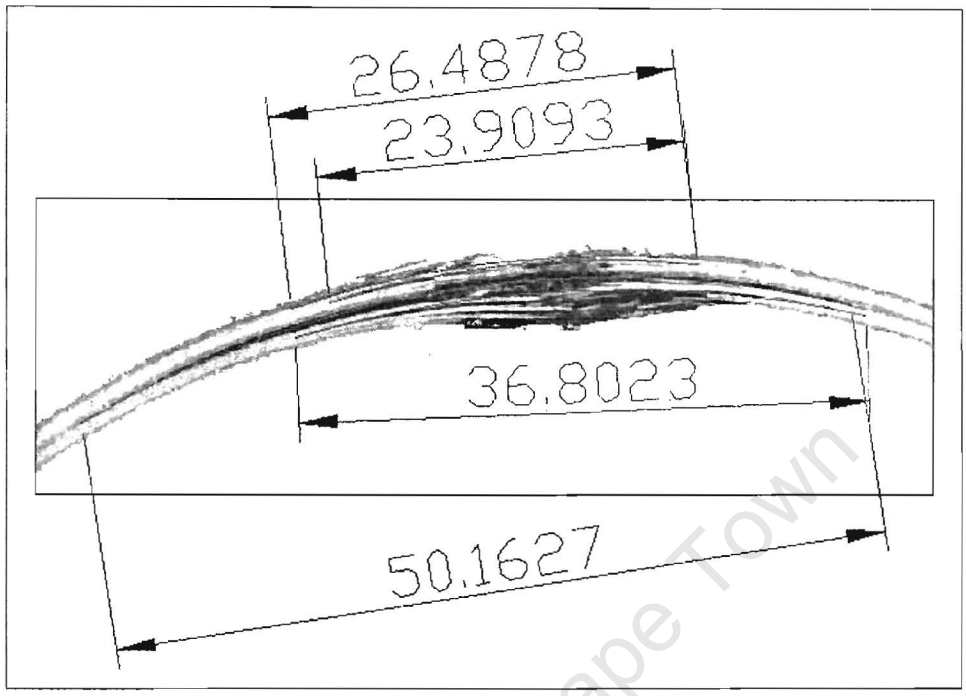

Figure 25 AutoCAD Measurement of an Axial Image

The number of specimens sectioned and scanned were limited because the process is destructive and there are only four B laminate specimens. The results from the images were used to reinforce interpretations from the Tangential and Radial X-ray images.

4.9 Measurements

Measurements have been obtained from the X-rays by importing the digital image into AutoCAD and scaling them to the correct size. The image then serves as a template upon which the various features can be marked and measured.

4.9.1 Delaminations

The tangential X-rays provide information that enables the size distribution (Figure 26) of the delaminations to be determined. The delamination half-lengths are measured, as are the interfacial locations through the thickness of the laminate.

Correction factor

The correction factor accounts for inaccuracies induced by scaling and all the measurements are multiplied by the factor. The thickness of the laminate in the digital image of the tangential X-ray is first measured and then the correction factor calculated. The correction factor is determined according to the following function;

Correction factor = Manufacturer's specified thickness / Measured thickness

Measured lengths

The impact point is marked with a centre line from which the delaminations are also marked and measured thus providing a measure of the half-length of the delamination. The damage is symmetric about the impact site so that the half-length is sufficient for describing the full-length distribution through the thickness.

The half-length measured is not taken to be the maximum length of a particular delamination, as this would require the maximum length of a delamination to lie on or near the line passing longitudinally through the impact site. The delamination shapes are generally uniform so that although the length measurements may not be directly attributable to a geometric characteristic, i.e. maximum length or area, they are useful in that they are able to provide trends describing the change in delamination size with interfacial location.

Interfacial location

The depth of each delamination is measured from the impact surface of the laminate, as the upper surface suffers little or no deformation. The measurements are then multiplied by the correction factor before being compared to the ideal location of the interfaces (Table 1) and are assigned the interface location number to which they are closest. The lamina thickness for the -/+35° windings is approximately 0.15mm and for the 90° windings is 0.267mm.

Table 1 Interface depth location

Laminate A	Interface	Depth
Orientations of adjacent laminae		(cm)
35 & -35	1	0.015
-35 & 90	2	0.030
90 & 90	3	0.057
90 & 90	4	0.083
90 & 35	5	0.110
35 & -35	6	0.125
-35 & 90	7	0.140
90 & 90	8	0.167
90 & 90	9	0.193
90 & 35	10	0.220
35 & -35	11	0.235

Laminate B	Interface	Depth
Orientations of adjacent laminae		(cm)
90 & 90	1	0.027
90 & 90	2	0.053
90 & 90	3	0.080
90 & 90	4	0.107
90 & 90	5	0.133
90 & 35	6	0.160
35 & -35	7	0.175
-35 & 35	8	0.190
35 & -35	9	0.205
-35 & 35	10	0.220
35 & -35	11	0.235

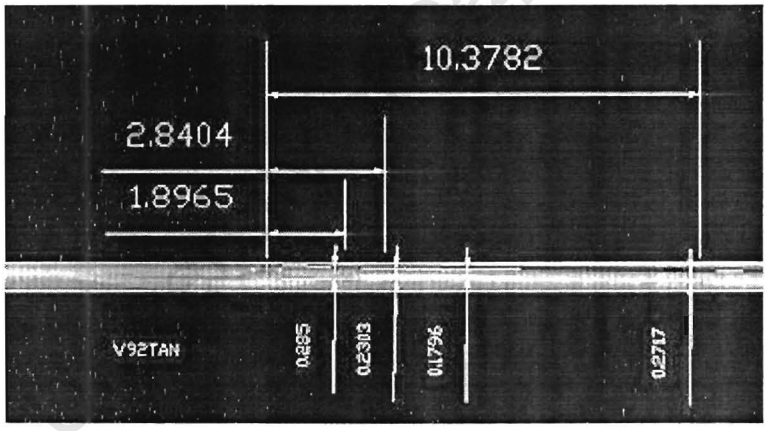

Figure 26 AutoCAD measurement of tangential X-rays

Area

The delamination areas are determined by importing the radial X-ray images into AutoCAD and marking the delamination boundaries (Figure 27). AutoCAD is able to provide the area of a closed polyline. The closed boundaries of all the delaminations could not be identified, as other features obscured them. The existence and general size of these delaminations could be observed although their areas could not be determined accurately with confidence. The

distal delamination area was clearly observable, as was the maximum delamination area at the 90° laminae interfaces.

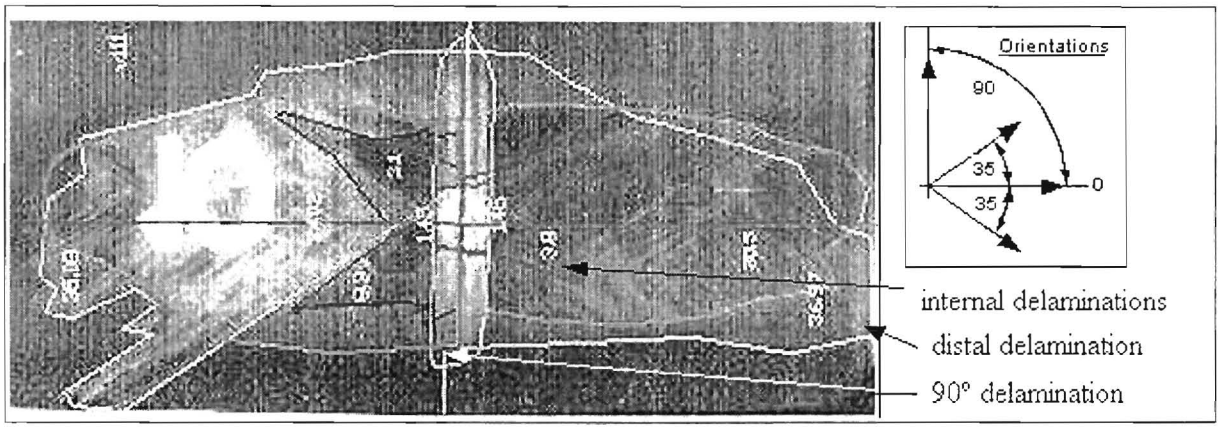

Figure 27 AutoCAD measurement of radial X-rays

4.9.2 Shear and fibre fracture

The extent of through thickness shear fracture is determined by the examination of both the tangential and radial X-rays. The tangential X-rays are useful in determining the extent of shear fracture and the radial X-rays for showing additional fibre fracture.

Shear fracture in tangential X-rays (Figure 23) are characterised by dark lines running across the direction of fibre travel, which correspond to the sides of the shear cone described previously. Fibre fracture not located at the impact site should be visible in the radial X-rays as bright lines running transverse to the fibre directions due to the X-ray dye. Fibre fracture was not readily visible in the radial X-rays (Figure 24), other than at the impact site (accounted for by shear fracture), and so it was concluded that its contribution to overall damage is relatively insignificant.

4.9.3 Matrix cracking

Matrix cracking was measured from the radial X-rays where it appears as long bright lines running in the fibre direction. The overall damage is essentially symmetric so that only half of a region was physically measured at a time.

4.10 Results conversion procedure

The basis of the analysis of experimental results lies in relating observable damage to the energy dissipated. The observed damage needs to be characterised into the standard damage modes and the extent of each damage mode quantified. The amount of energy dissipated can be determined by applying the energy release rates for each damage mode.

The most significant energy dissipating damage modes observed in the x-rays are delamination, shear fracture and matrix cracking.

4.10.1 Delamination

The extent of delamination is commonly determined by extrapolating a measured area, taken from a radial X-ray image of the damage site, through the laminate. Mines et al. [21] were able to measure two delaminations at known interfaces through the laminate and then applied a linear interpolation between them.

In this study the only delamination area that can be measured with confidence and their interface location ascertained is the large delamination at the distal interface (I_{11}) and so an interpolation between two delaminations cannot be done with confidence. The extrapolation of a single measured delamination area to estimate the delamination areas at the remaining interfaces could only be performed on the basis of a known trend. A trend could be ascertained from the tangential X-rays, which provided a measure of the change in delamination lengths as well as their probable interfacial location.

The current extrapolation of delamination areas has been based on the trend functions fitted to the measured delamination lengths versus interface location.

Delamination distribution trend

The most appropriate trend that described the distribution of measured delamination lengths was a power function and not linear, which raised some doubt as to the validity of utilising a linear interpolation in such studies. The reason for this non-linearity may be due to the similarity described for the response of beams to impact by light projectiles. Jones [20] describes the normal transverse displacement response of a beam due to light projectile impact, as a logarithmic function.

Damage is partially a function of global strain, i.e. beam displacement, so that non-linear straining along the beam can reasonably be assumed to result in a non-linear distribution of damage through the beam. The power function that provided the closest fitting trends was of the following form;

$$y=c.x^{b} \qquad (7)$$

c and b are constants

y ~ delamination length, x ~ interface number

A laminate gas gun test

The observed delaminations are all located in the middle and lower half of the laminate at interfaces bounded by -35 and +35° laminae, i.e. I_5, I_6 and I_{11} (Figure 28). Delaminations are not apparent in the lower half at interfaces bounded by 90° laminae i.e. at I_7 to I_{10}.

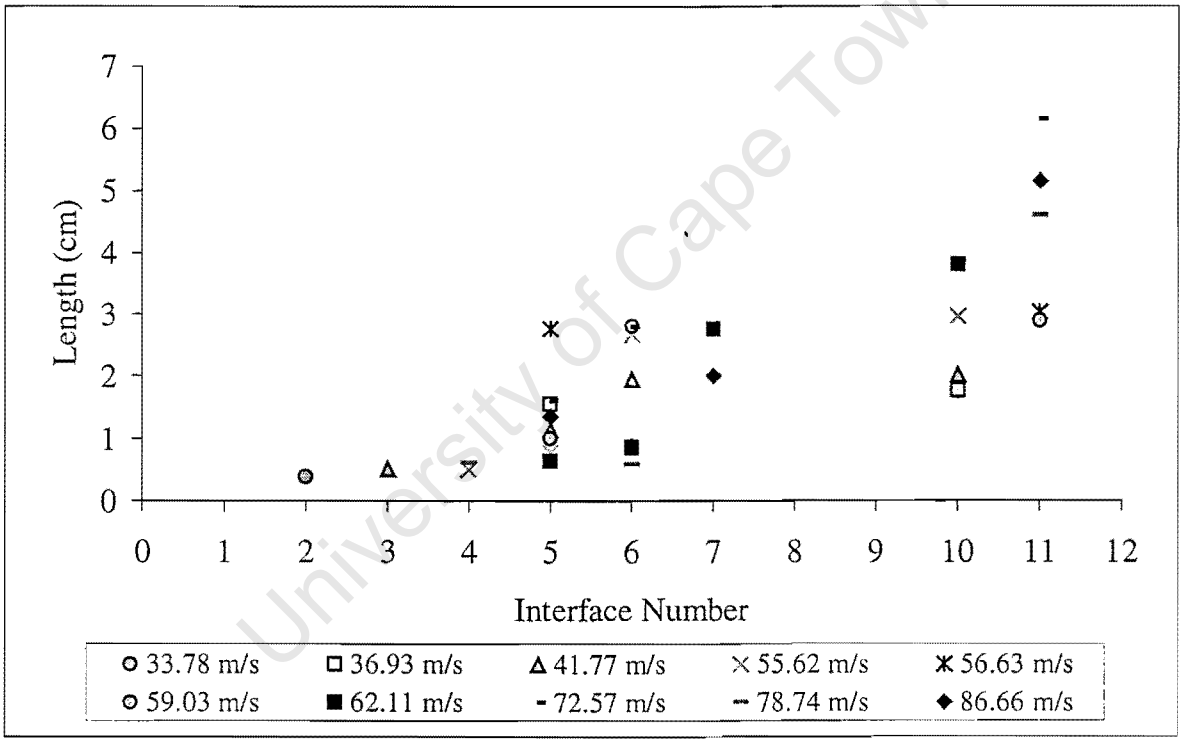

Figure 28 Laminate A: Delamination length distribution

A few specimens yielded too few length measurements to fit trends to and in such cases the trend from the specimen with the closest impact velocity has been used. Table 2 provides the trends and correlations used in the analysis for the respective velocities.

Table 2 Laminate A: Trends and correlations

Velocity	Trend	Correlation	Reference
(m/s)	$y=c.x^b$		
33.78 & 36.93	$y = 0.192x^{0.92}$	0.98	Figure 57
41.77	$y = 0.163x^{1.19}$	0.84	Figure 58
55.62 & 56.63	$y = 0.0397x^{1.98}$	0.75	Figure 59
59.03 & 62.11	$y = 0.0089x^{2.7}$	0.85	Figure 60
72.57	$y = 0.1355x^{1.61}$	0.96	Figure 61
78.74	$y = 0.0243x^{2.14}$	0.82	Figure 62
86.66	$y = 0.0798x^{1.72}$	0.98	Figure 63

B laminate gas gun test

The same approach used for determining the A laminate specimen trends has been used for the B laminate specimens with Table 3 showing the trends and correlations used. The best fitting trend was a power function and exhibited correlation values ranging from 0.78 to 0.97, although the relatively high values may be due to the limited number of data points against which some of the trends were fitted.

Table 3 Laminate B: Trends and correlations

Velocity	Trend	Correlation	Reference
(m/s)	$y=c.x^b$		
76.69	$y = 0.0203x^{2.58}$	0.97	Figure 64
92.42	$y = 0.0151x^{2.54}$	0.78	Figure 65
111.61	$y = 0.0163x^{2.5}$	0.85	Figure 66
138	$y = 0.0032x^{3.22}$	0.97	Figure 67

The delaminations are all located in the lower half of the laminate at all the interfaces bounded by -35 and +35° laminae, i.e. I_7 to I_{11}, see Figure 29. Delaminations are not apparent in the upper half at interfaces bounded by 90° laminae.

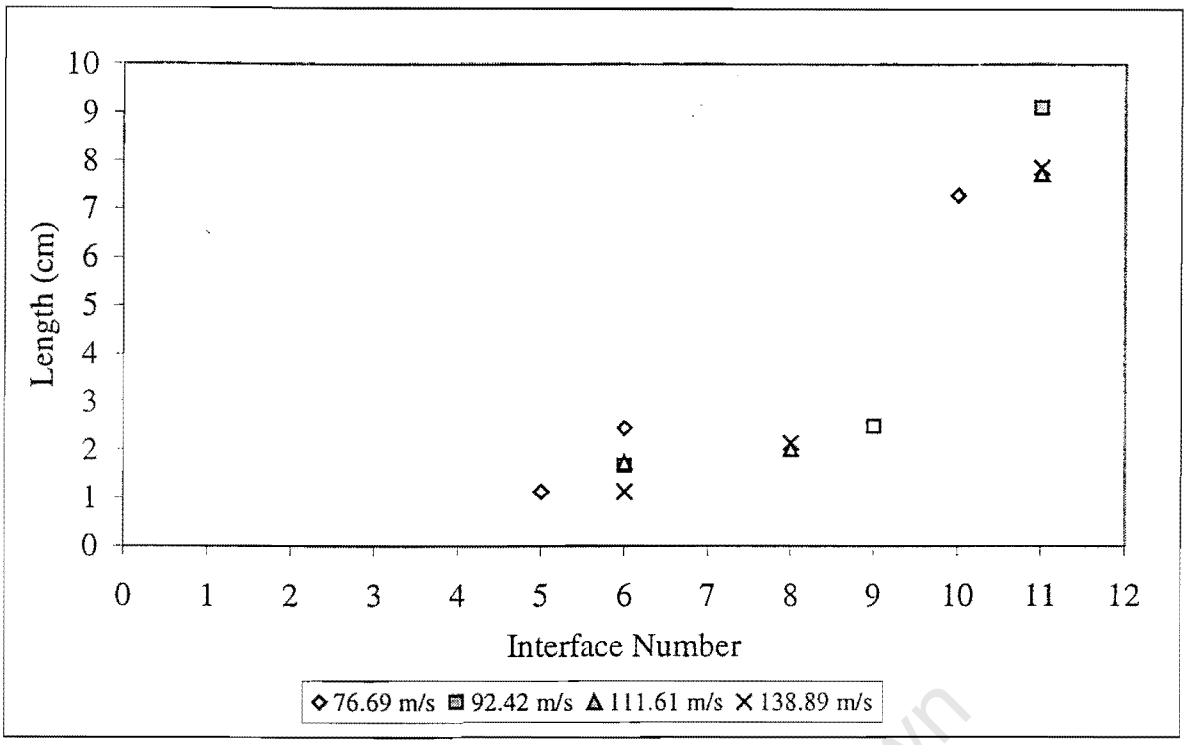

Figure 29 Laminate B: Delamination length distribution

Delamination ratios

The delamination ratio was determined by dividing the calculated lengths, f(x), by the distal delamination length, f(11), for each specimen. The calculated lengths are determined according to each test specimen's trend function.

The reason for using the distal delamination as the reference value is because in the radial X-ray images the distal delaminations are clearest and so their measurements can be used with the greatest confidence as a reference. The I_{11} length for the A laminate specimens, from the tangential X-rays, also showed the strongest correlation with impact energy suggesting that of all the measurements they could be used with the greatest confidence. Table 4 lists the measured distal delamination lengths and their correlation with impact energy.

Table 4 List of distal delamination lengths and impact energies

Impact Energy	Interface No.	Delamination Length
(J)		(cm)
5.792	10.000	1.751
6.921	10.000	1.764
8.864	10.000	2.020
15.698	10.000	2.964
16.273	11.000	3.030
17.685	11.000	2.887
19.617	10.000	3.800
26.726	11.000	6.142
31.465	11.000	4.602
37.921	11.000	5.152
Correlation of delamination length with impact energy		0.897

The B laminate specimen length results at the distal delamination showed no strong correlation with impact energy, rather it appeared to be relatively constant.

Delamination areas at -35° and +35° laminae interfaces

The form of the extrapolation using trend functions is;

$$A_x = A_{11}.f(x)/f(11) \qquad (8)$$

where, f(x) ~ delamination length trend at interface number x.

f(x) is a power law unique for each specimen except where those specimens yielded too few experimental measurements to fit a trend. The trend from the specimen with the closest impact velocity has been used in cases where a trend could not be adequately determined.

In the tangential X-rays of the A laminate specimens no delaminations are readily visible at the interfaces bound by 90° laminae and this is even more evident in the plots of lengths versus interface number (Figure 28 & Figure 29). Lower transverse shear stresses are a result of reduced differences in orientation angle, which are significant in inhibiting delaminations.

Delamination areas at 90° laminae interfaces

A laminate specimens

The tangential X-rays show no delaminations occurring at the 90° laminae interfaces, however the radial X-rays show at least one delamination aligned in the 90° direction. The radial X-rays did not show evidence of multiple delaminations in the 90° laminae implying that there was either a single delamination or two delaminations of similar size and shape, one obscuring the other. The axial images show some delamination occurring at I_2 and I_7, with the major axis of the delamination being in the 90° direction. The delamination at I_2 is approximately 50% shorter than that at I_7, suggesting that the I_7 delamination corresponds to the 90° delamination observed in the radial X-rays.

The total delamination area due to 90° delaminations was therefore approximated as 1.5 times the area of the 90° delamination measured in the radial X-rays.

B laminate specimens

The radial X-rays do not show any apparent delamination in the 90° layers (see section 5.1.6) although matrix cracking was evident, so that it has been assumed that any unobservable delaminations are too small to make any appreciable contribution to energy dissipation.

4.10.2 Shear fracture

The energy dissipation due to shearing of fibres and matrix requires the determination of a shear fracture area and a value for the fracture energy per unit area (γ). The lateral area of a fustrum is an accepted approximation [2] where the area is given by the following function;

$$A_{sh} = 2 \cdot \pi \cdot r \cdot h + \pi \cdot h^2 \cdot \tan(\phi) \qquad (8)$$

where, r ~ radius of projectile, h ~ thickness of laminate & ϕ ~ angle of cone, fustrum

The angle of the fustrum has previously [2] been taken to be 45°, however for the current work it has been measured at approximately 73° for the A laminate and 51° for the B laminate (see section 5.3 Shear fracture). The reason for these values being that in those specimens where penetration or significant fibre fracture has taken place, distinct oblique fractures with such inclinations could be observed in the tangential X-rays.

The value of work done per unit crack area is an order higher than that of delamination and matrix cracking usually being in the region of 20 - 40 kJ/m^2 (see section 3.4.3). The energy consumed in perforation from the drop tests was of the order of 3 to 3.4J, which is a work per

unit crack area of 21 to 25kJ/m^2. The energy value for shear fracture (E_{sh}) is obtained from the area, below the the plot of tup force vs displacement (Figure 30), characterised by a sudden decrease in tup force.

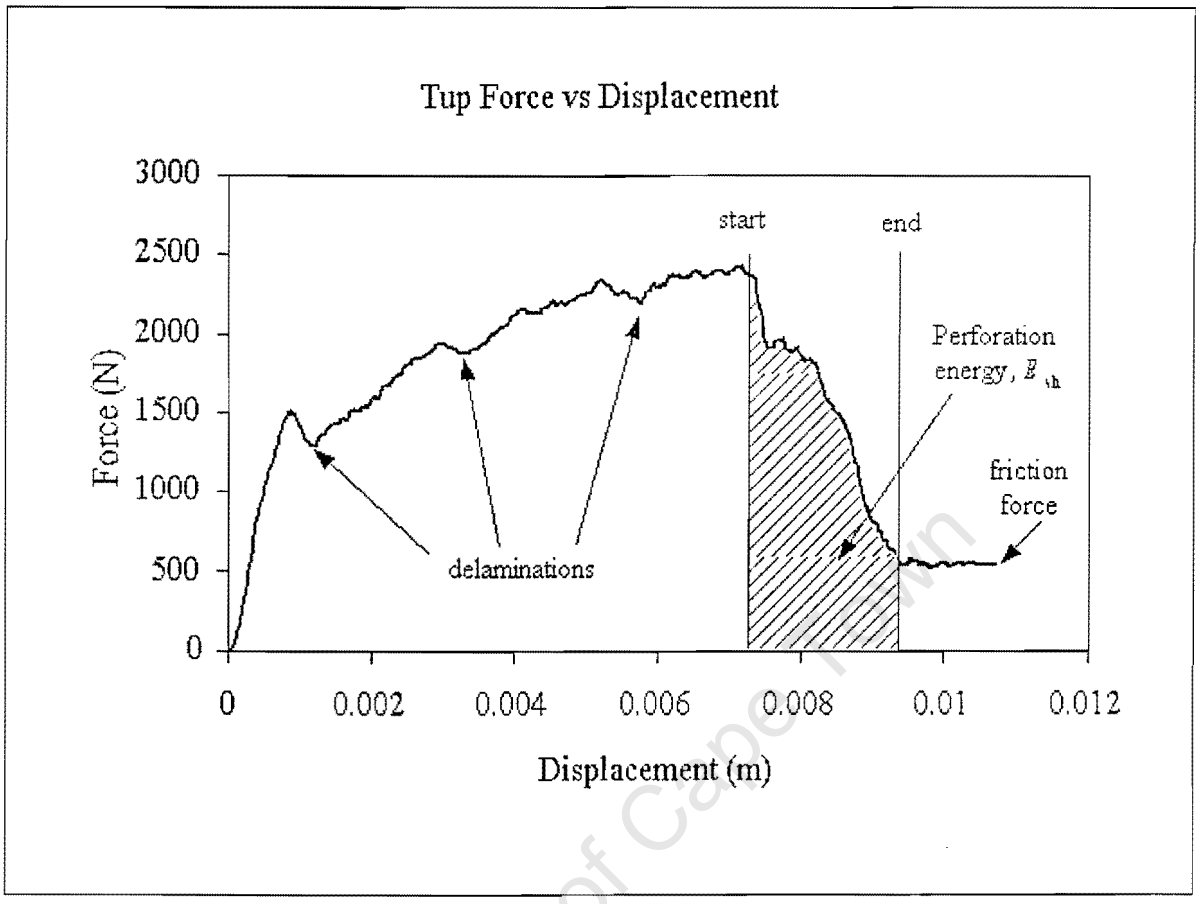

Figure 30 Drop tester result for perforated specimen.

4.10.3 Matrix cracking

Matrix cracking is observed to be most severe in the 90° laminae of the B laminate specimens where it can be seen with the naked eye in the surface lamina. Matrix cracking also occurs in the -35° and +35° laminae within the delamination areas, although to a much smaller extent.

The determination of the total area of matrix cracking has been accomplished using the following procedure;

1. Consider a half of the maximum delamination area

2. Measure the lengths of the cracks.

3. Sum the lengths of the cracks and multiply by the average thickness of a lamina (0.2083mm).

The assumptions of symmetric damage and single ply crack depth would appear to be reasonable as subsequent analysis (see section 5.2) shows a strong correlation between total cracking and impact energy, as would be expected.

The value of work done per unit crack area is of the same order as that of delamination ($500J/m^2$).

4.11 Experimental error

The scope of the thesis has meant that aspects of the experimental method may introduce some error. The most probable sources of experimental error are;

- boundary conditions
- impact incidence
- impact velocity readings
- systematic error

4.11.1 Boundary conditions

The points of concern regarding the boundary conditions centre around whether;

1. damage interacts with the boundary,
2. clamping force is sufficient to prevent significant global displacement at the boundary,
3. clamping force is consistent for all tests.

The first concern is dealt with in the section regarding the experimental set-up where it is shown that the damage does not interact with the boundary.

Global displacement at the boundary would result in energy dissipation due to friction between the specimen and clamp. It was considered by placing reference marks on the

specimens a short distance from the clamp and measuring them before and after each test. No measurable change in the reference mark position occurred.

The consistency of the clamping force is ensured by closing the clamping plate gap (see Figure 16) to a set distance of 1.5mm. A couple of specimens had radii slightly larger than 140.5mm and in such cases the torque consistency was achieved by feel. A torque wrench should have been used to ensure torque consistency, however torque judged by feel, although not exact, should be reasonably accurate. It is therefore assumed that any error introduced is likely to be too small to effect the overall conclusions of the investigation.

4.11.2 Impact incidence

The point and incidence of impact was assessed by conducting a series of firing tests on plywood targets placed at the point of impact for the specimens and a cross marked at the point of the impact. The obliquity of the projectile i.e. amount of deviation from normal impact, was assessed by the hole it made in the plywood target. Oblique impact would result in an elliptical hole in the plywood while normal impact would result in a round hole. Normal impact on the tube specimens also requires that it occur at the centreline of the tube so that deviation from the target point is also crucial.

The tests showed that at the impact plane the projectile impacted the plywood essentially normally, however it occasionally deviated horizontally a small amount (less than 1mm). The lateral deviation could be an error due to measurement or due to the sabot being slightly off centre in the barrel. The sabot is slightly under size so that a small amount of movement is possible within the barrel. The impact is normal and since the deviation is horizontal and not vertical the impact will be normal to the tube.

The normal impact is also an indication that no contact occurred between the sabot catcher and projectile as this would have caused the projectile to tumble.

The projectiles that perforated the laminate did not break so that the conclusions regarding energy dissipation and ballistic limit should, according to Goldsmith [14], still be valid.

4.11.3 Impact velocity

The velocity of the projectile is measured in the last portion of the barrel such that energy losses may occur between the point of measurement and that of impact. Possible energy

losses may occur due to; separation from the sabot, contact between the projectile and sabot catcher, and projectile drag once it has left the muzzle.

The sabot was machined from Perspex rod, which has a relatively low coefficient of friction, and had a cavity diameter such that the projectile did not rattle, yet could separate from the sabot easily. The energy loss due to separation, i.e. friction, is considered to be negligible as the low coefficient combined with minimal constraining force means almost no friction.

Energy loss due to drag acting on the projectile between exiting the muzzle and impacting the target is also assumed to be negligible as the flight path is only 5cm.

4.11.4 Systematic - operator consistent error

Measurements that rely on the observations and judgements of personnel are prone to errors of habit, i.e. operator systematic error. An example of where such error may occur is the measurement of the delamination area on the radial X-rays, which require the person to choose the area's boundary. The boundary will lie within the broad tide mark (see Figure 21) and the point chosen in the tide mark is prone to the preference or habit of the individual. The measured systematic error is an indication of consistent deviation between the measurements of one personal as opposed to another set of measurements from the same samples.

Systematic error is determined by having additional personnel repeat the measurements for a small sample and compare the deviation in the results.

Tangential X-ray measurements

The range of systematic error for the A laminate specimens, determined for a small sample, was found to be between 10 and 14% less than those used in the analysis. Laminate B specimens exhibited errors of between 1 and 14% less than those used in the analysis. The maximum error of 14% results in a maximum error in corresponding shear cone fracture energy of 41% less than that used in the analysis and maximum error to total energy dissipated due to material failure of 10% less.

Radial X-ray measurements

Radial X-ray measurements of A laminate specimens exhibited systematic error with a range of 12 to 15% less than those used in the analysis. A single reading, which resulted in a 33% error, was ignored as it was found that the comparative measurement was made using

incorrect features in the X-ray. Laminate B radial X-ray measurements exhibited a range of 8 to 13% less. The maximum error of 15% results in a maximum error in corresponding delamination fracture energy of 15% less than that used in the analysis and maximum error to total energy dissipated due to material failure of 13% less.

Tangential and radial X-ray measurements

The combined errors of tangential and radial X-ray measurements result in a maximum deviation to the total energy values of 23% less than those used in the analysis. The maximum error was determined using maximum measured deviations and not the mean deviation so that the actual systematic error is likely to be less than 23%. The comparative measurements were all less than the authors suggesting that even if the maximum error case were true error it would not affect the final observations

4.11.5 Scaling

Images imported into AutoCAD were smaller and needed to be scaled, although their aspect ratios were preserved. Scaling to the correct size was achieved by noting the scanned size as indicated by the scanning software and scaling the AutoCAD image until it was the same again. The process of scaling was verified by initially including a line of known length next to the X-ray and checking its length in AutoCAD after scaling was completed. The only error introduced by scaling would be due to numerical round off by the software, however it is reasonable to assume that it is small enough to ignore.

Chapter 5. Experimental results

This chapter presents observations in regard to significant aspects of the experimental results while the analysis is contained in the following chapter. A comprehensive listing of the results is contained in APPENDIX A and the images upon which they are based can be found in APPENDIX B.

5.1 Delaminations

The process of identifying and measuring delaminations are described in section 4.7) Image interpretation of chapter Chapter 4) Experimental set-up and procedure.

5.1.1 Tangential X-ray measurements: Laminate A

Delamination interfacial locations (refer to Figure 28)

The majority of delaminations identified in the tangential X-rays are found to lie on interfaces bound by +/-35° laminae (interfaces 6 & 11) and at interfaces with a 90° upper lamina and 35° lower lamina (interfaces 5 & 10). The delaminations were found to increase in length from the impacted surface towards the last, or distal, interface.

In the lower half of the laminate no delaminations were readily visible at interfaces bound by 90° laminae (interfaces 7 to 9). In the upper half of the laminate thickness short cracks were visible at the 2nd, 3rd and 4th interfaces. The cracks are not considered delaminations as they bound by 90° laminae and their lengths are short enough to be consistent with inter-laminae matrix cracking.

Length distribution through the laminate

In order to obtain the overall delamination area it was necessary to determine the area of the delaminations at each interface. The procedure, as described in chapter Chapter 4) Experimental set-up and procedure, used trends fitted to the plots of length versus interface number in order to extrapolate the area of the delamination at the distal interface to the remaining interfaces likely to have delaminations. The best trend is found to follow a power law. The correlation of trends with measured lengths (Table 2) ranges between 0.75 and 0.98 although the low number of data points are probably responsible for such high values.

5.1.2 Tangential X-ray measurements: Laminate B

Delamination interfacial locations

(refer to Figure 29)

The delaminations identified in the tangential X-rays are found to only lie on interfaces bound by +/-35° laminae (interfaces 6 to 11) and to increase in length from the impacted surface towards the distal interface. Delaminations were not readily observed at interfaces bound by two 90° laminae (interfaces 1 to 5), in the upper portion of the laminate although material failure or cracking is observed in the upper laminae.

Length distribution through the laminate

The best trends describing delamination length distribution (Table 3) through the laminate were found to have strong correlations (0.78 to 0.97) to power laws although the high correlation values are in part due to the low number of data points. The delamination data used in determining the trend are all bound by +/-35° laminae so that the length distribution is not effected by interspersed 90° laminae.

5.1.3 Axial images: Laminate A

Axial measurements and observations (Table 10) show separations occurring in the upper half of the laminate at interfaces bound by 90° laminae. The most significant separation observed occurred at interface 7 where it has a 35° upper and 90° lower lamina. A similar separation is also visible at interface 2, also with a 35° upper and 90° lower lamina though it is approximately 50% shorter. The 7 and 2 interfaces have laminae with dissimilar orientations suggesting that the observed separations may well be delaminations. Separations also occur at interfaces 3 and 8, with lengths 50% and 70% that of interface 7, although these are bound by 90° laminae only.

The delaminations, at interfaces bound by +/-35° laminae or a lower 35° lamina (interfaces 5,6, 10 and 11), observed in the tangential X-rays were not readily observed in the axial images.

5.1.4 Axial images: Laminate B

The images reveal separations between the laminae at interfaces 2 to 6 with that at interface 6 being the longest and most distinctive. Interface 6 is bound by an upper 90° and lower 35° lamina. The delaminations in the lower half, i.e. those bound by +/-35° laminae only and observed in the tangential X-rays, were not evident.

5.1.5 Radial X-ray measurements: Laminate A

A number of delamination areas were measured from the radial X-rays, however only the delamination at the distal interface was used for the extrapolation.

Area shapes

The shape of the delaminations depend on the laminae bounding an interface and the impact velocity (energy).

Figure 31 depicts some of the delamination shapes observed in the X-rays. The shapes carry the following descriptions;

a) Oblong, elongated

b) Peanut-shaped or waisted

c) Cross-shaped

d) Elliptical, oval or circular

e) Asymmetric

The oblong shaped delamination was found in all the A laminate specimens and was oriented in the 90° direction. The peanut-shaped delamination was most distinctive in specimens impacted at velocities below 59m/s as was the oval delamination. The peanut-shaped delaminations are most prevalent in the A laminate specimens, however the cross-shaped delaminations are not readily discernible. The arms of the crosses are oriented in the +35° and -35° directions. The elliptical or oval shape is associated with the distal delaminations as it is usually the largest. The delamination is seen at impact velocities greater than 56m/s to extend further along strips oriented in the +/-35° directions. The elliptical shape probably exhibits some necking around the impact site, however this is

not always seen due to the other delaminations obscuring the view. The asymmetric shape is found to occur in those specimens where impact occurred off the seam at velocities close to or above the ballistic limit. The flattened side of the asymmetric shape corresponds to the seam closest to the impact site (see APPENDIX B, 72.57m/s (26.73J) impact specimen).

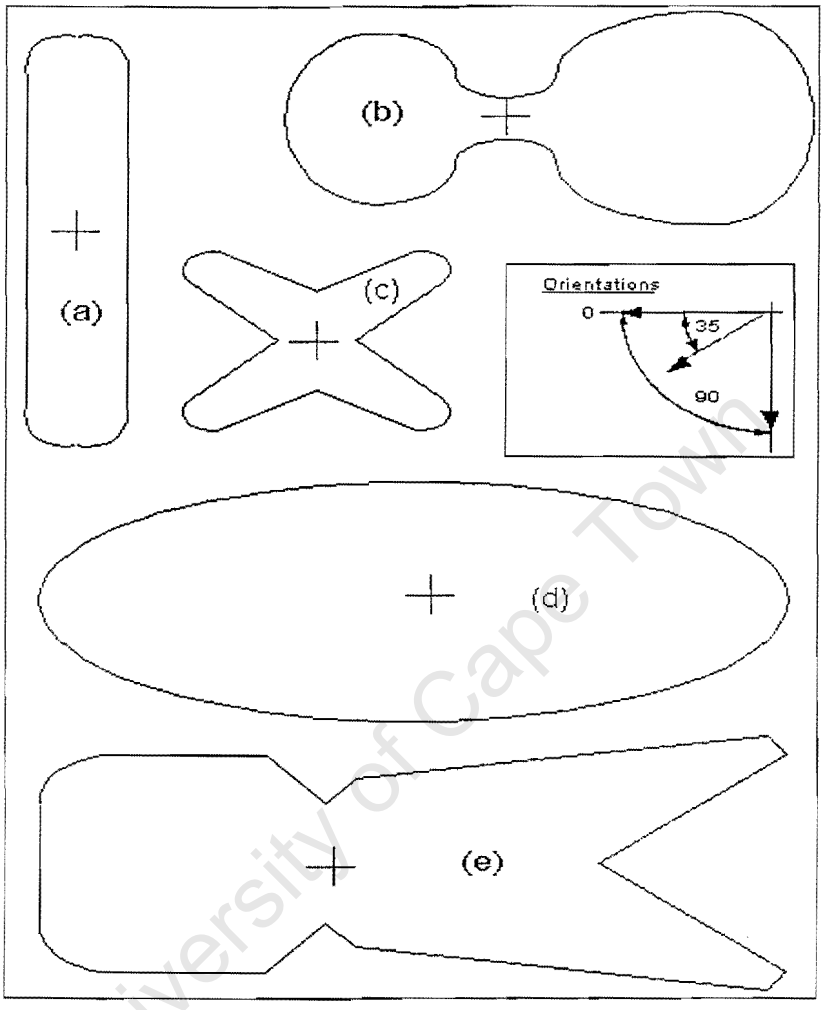

Figure 31 Delamination shapes:
a) oblong or elongated, b) peanut shaped or waisted, c) cross shaped,
d) elliptical, oval or circular e) asymmetric

Area sizes

The distal delamination area measured on the radial X-rays increases linearly with impact energy (Figure 32), having a correlation of 0.97, up to the ballistic limit. The number of data points for post ballistic limit are too few to draw any conclusions other than that delamination size is no longer as dependent on impact energy post-ballistic limit as pre-ballistic limit.

The total delamination area also increases linearly with impact energy prior to the ballistic limit albeit with a lower correlation of 0.88 (see Figure 33). The number of data points post ballistic limit are insufficient to determine a trend for delamination growth with increasing impact energy.

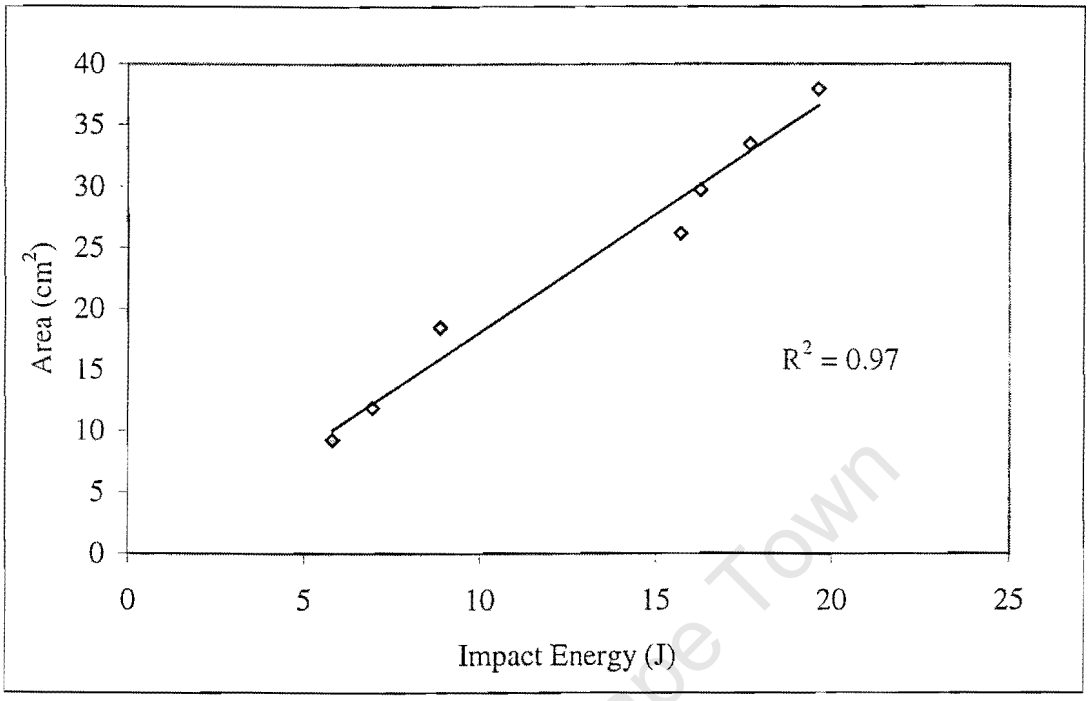

Figure 32 Laminate A: Pre-ballistic limit distal delamination area

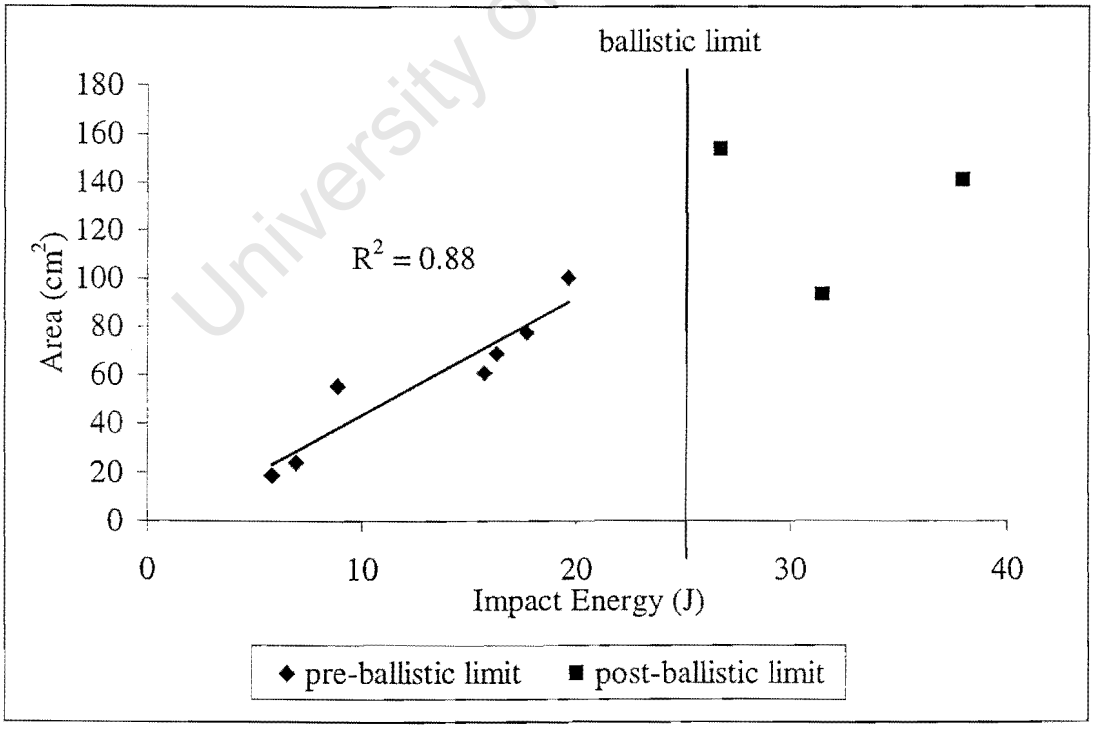

Figure 33 Laminate A: Total delamination area

The test at 41.77m/s (8.86J) exhibited a distinct oval-shaped delamination at the rear interface that had a length of about 5.3cm and width of 4.3cm and is included for later use in the discussion.

5.1.6 Radial X-ray measurements: Laminate B

Area shapes

(see APPENDIX B)

The radial X-rays of B laminate specimens exhibit more and clearer delamination shapes than in A laminate, such that more of them could be measured other than just the distal delamination.

The cross-shaped delaminations (see (c) Figure 31) are distinctly visible in the radial X-rays and are the most common type. The distal delamination shapes tended to be a combination of elliptical and cross-shaped delaminations. The oblong-shaped delamination, which was prevalent in the A laminate specimens, was not visible at all in the B specimens.

Area sizes

The total delamination area does not show a strong correlation with impact energy (Figure 34). The total delamination area for the specimen impacted at 76.69m/s (29.76J) is larger than the others impacted at much higher velocities. The reason for this anomaly is not clear and is treated with caution. The subsequent tests, pre and post-ballistic limit, all exhibit delamination areas of a similar magnitude having an average size of 205cm^2.

The low number of tests precluded any meaningful comparison of distal delamination to impact energy.

t Test

The ability to measure more delaminations in the B laminates in the radial X-rays provide the opportunity of testing the validity of the extrapolation procedure by performing a t test. A t test essentially compares the mean of a sample of data to that of another sample and returns a probability of them belonging to the same population. A low t test value

indicates that the measured and extrapolated values do not compare well and so there would be cause for concern.

The two data sets compared were the delaminations measured from the radial X-rays and the delaminations extrapolated from the distal delamination. The lowest t test probability value of 0.27 is for the test at 76.69m/s (29.76J) while the remaining 3 tests had probilities ranging from 0.71 to 0.81.

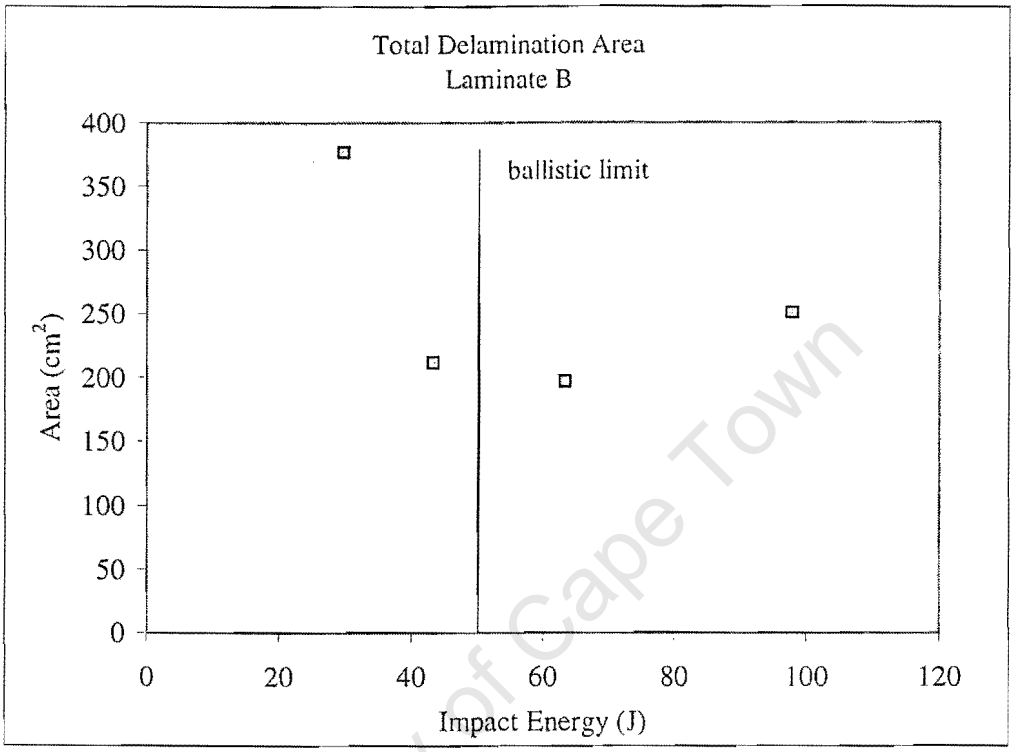

Figure 34 Laminate B Delamination Areas

5.2 Matrix cracking

The determination of the extent of matrix cracking appears to be rather primitive as it assumes the following;

1. the majority of cracks are visible in the X-rays.

2. X-ray visible cracks occur in a single lamina i.e. a crack does not pass through more than one lamina at a time.

5.2.1 *Radial X-ray measurements: Laminate A*

Matrix cracking shows a strong linear correlation of 0.94 with impact energy (see Figure 35), however the extent of matrix cracking could not be measured from the X-rays for the specimens impacted at 41.77m/s (8.86J) and 86.66m/s (37.92J). The images for these tests were of poor quality due to the developing machine malfunctioning and hence the trend was used to determine values for cracking area at 41.77m/s (8.86J) and at 86.66m/s (37.92J).

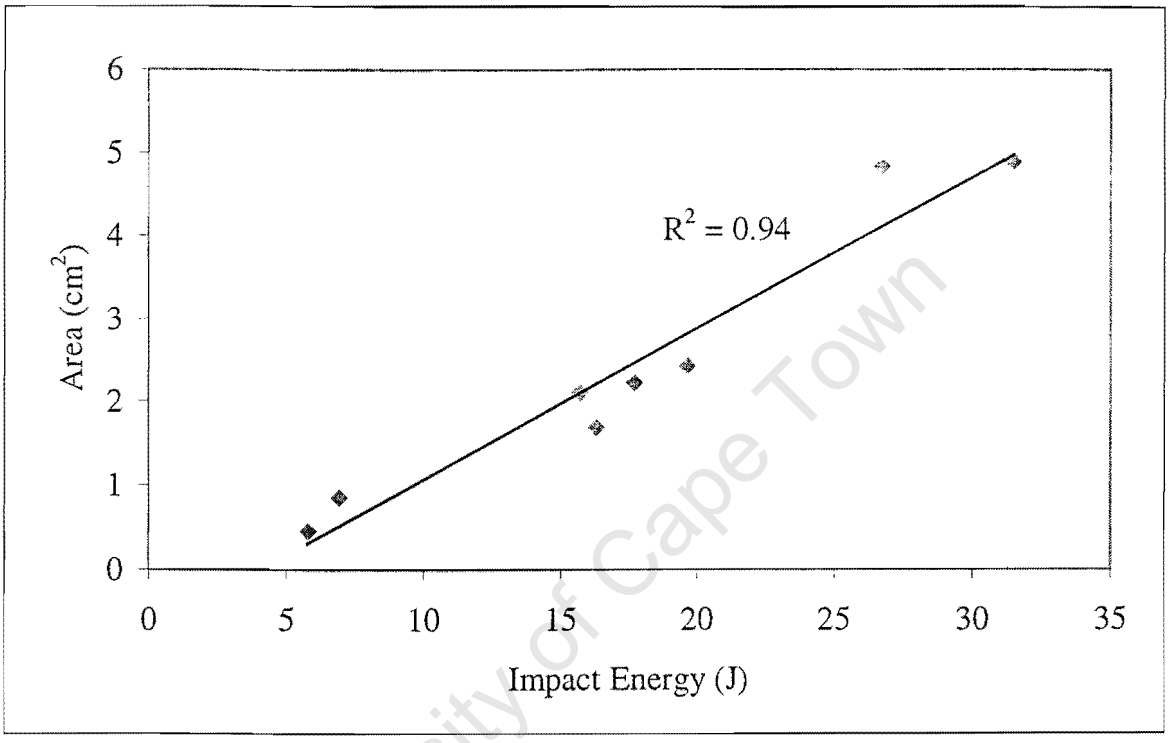

Figure 35 Laminate A: Matrix cracking area

5.2.2 *Radial X-ray measurements: Laminate B*

The extent of matrix cracking does not show a strong correlation with impact energy (see Figure 36), with the data being scattered in a band of 5 cm^2 and 7.5 cm^2. The matrix cracking in the first layer (90° orientation) of the B laminate was visible to the naked eye.

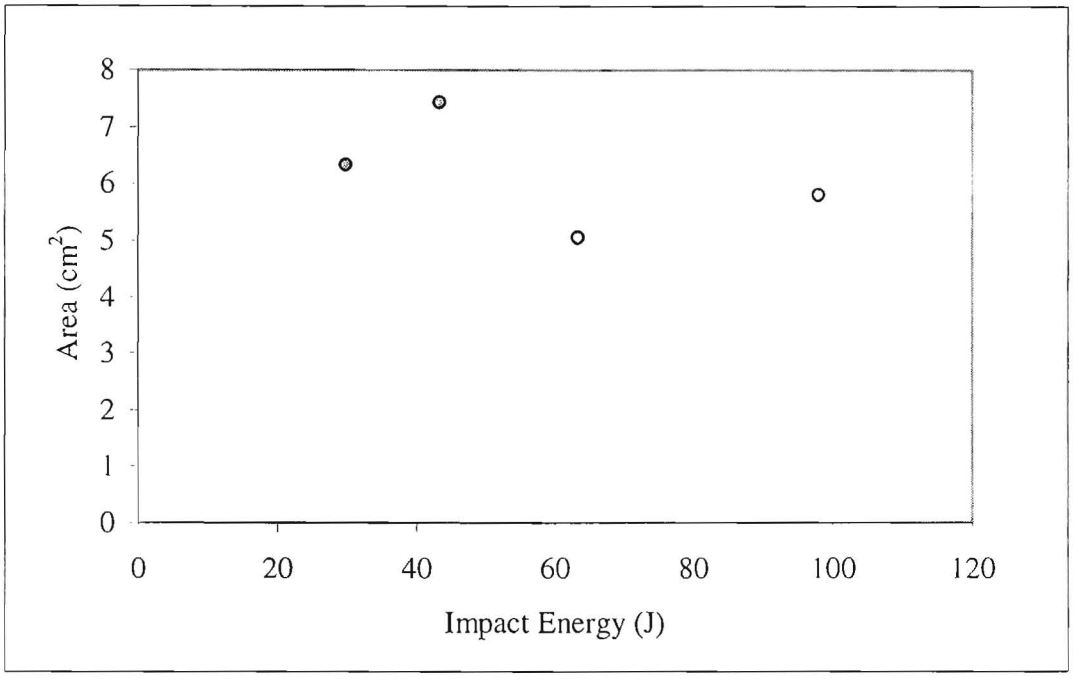

Figure 36 Laminate B: Matrix cracking area

5.3 Shear fracture

In specimens just prior to the ballistic limit and in all specimens post ballistic limit a series of cracks (Figure 37) were observed, in the tangential X-rays, to run through the thickness of the laminate that had consistent inclinations. In post-ballistic specimens, in particular, fibre fracture was found to occur along these cracks and so these distinct cracks were concluded to be the surface of the shear cone described in section 2.3.1.

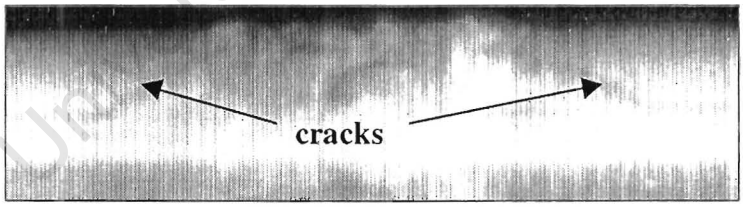

Figure 37 Tangentential X-ray showing shear fracture cracks

5.3.1 Tangential X-ray measurements: Laminate A

The angle of the shear cone was observed to be on average 73 degrees with a standard deviation of 0.97 and a 95 % confidence of it being within 0.85 degrees or 1.2% of the average. The laminate did not shear entirely as no distinctive plug was formed, however extensive fibre breakage and matrix damage was still evident.

The shear cone is first visible in the specimen impacted at 59.03m/s (17.69J) but only reaches a depth of 1.25mm or half the laminate thickness. The depth of the cone increases with impact velocity but displays no strong correlation with impact energy.

The fracture area used in determining the dissipated energy includes, for those specimens which were fully penetrated, the area of laminate fractured immediately below the impactor. Such fibre fracture at velocities below the ballistic limit was not assumed as it was not readily visible or quantifiable in the specimens, although it would be reasonable to assume that some fracture took place.

5.3.2 Tangential X-ray measurements: Laminate B

The angle of the shear cone was observed to be on average 52 degrees with a standard deviation of 3.24 and a 95 % confidence of it being within 3.17 degrees or 6.1% of the average. The laminate again did not shear entirely as no distinctive plug was formed, however extensive fibre breakage and matrix damage was still evident.

The specimen impacted at 76.69m/s (29.76J) exhibited shear fracture which reached a depth of 1.95mm or approximately 75% of the laminate thickness. The depth of the cone increased with impact velocity but again displayed no strong correlation with either impact velocity, energy or momentum.

The fracture area used in determining the dissipated energy included the area of laminate fractured immediately below the impactor. Such fibre fracture at velocities below the ballistic limit was not assumed as it was once again not readily visible or quantifiable in the specimens, although it would be reasonable to assume that some fracture took place.

5.4 Ballistic limit

5.4.1 Laminate A

The ballistic limit for lamina A is estimated to be in the region of 70m/s (24.87J) for the following reasons;

- a projectile lodged in a half specimen at 71.15m/s (25.69J) and in a full specimen at 72.57m/s (26.73J).

- no projectile penetrated below the 70m/s and all above either lodged in the specimen or passed through.

The ballistic limit is defined as that velocity where the projectile just penetrates the laminate and since the two projectiles that lodged were more than slightly through indicates that the limit is slightly less than their velocities.

In the case of the test at 86.66m/s (37.92J) the projectile impacted the opposite side of the inner tube after passing through the laminate. The projectile left a mark on the convex surface slightly lower than the perforation hole but still on its line of flight. The downward deviation is an indication of a deflection or change of trajectory. A small slightly oval delamination was also produced which was visible to the eye but was not X-rayed. The length and width of the delamination are approximately 5.5cm and 4cm respectively.

5.4.2 Laminate B

The ballistic limit for laminate B is assumed to be in the region of 95m/s for the following reasons;

- The depth of the shear cone at 92.42m/s (43.35J) is about 2.11mm or 84% of the laminate depth, which means that the laminate was almost penetrated totally.

- projectiles with greater velocities passed through the specimen and those with velocities less did not penetrate at all

5.5 Energy dissipation

The main energy dissipation categories considered here are material failure, strain and friction.

The energy dissipated due to material failure is further considered in terms of the different failure mechanisms and their contributions relative to total energy dissipated by material failure as well as relative to impact energy. The crack energy release rates used in determining the energy dissipated by material failure were obtained from literature (see section 4.1.4) and a single instrumented drop test (Figure 30).

The total energy dissipated due to material failure and friction is always less than the impact energy. The balance of the projectile kinetic energy is dissipated as strain energy or retained as a residual velocity. The strain energy in this study can only be approximated in the region of the ballistic limit where the impact, residual and dissipated energy due to material failure are known.

The energy due to friction is assumed not to be dependent on the stacking sequence since the number and orientations of laminae in both laminates is the same. The projectile experiences the same material in both laminates and both laminates have the same in-plane properties so that in-plane forces exerted on the projectile will be similar. Two drop tests which resulted in perforation were performed on A laminate, however due to instrument failure only one set of results was available (see Figure 30). The friction force is indicated by the point where the graph levels out at a constant value as a result of the tup experiencing a constant friction force as it slides through the laminate.

The friction force in the case of the current laminates and tup or projectile is approximately 550N. The energy dissipated due to friction is therefore given by the friction force times the distance over which it acts. The energy dissipated due to friction for a laminate 2.5mm thick and just perforated (ballistic limit) is therefore approximately 1.37J and for a projectile 27mm long and having passed through the laminate entirely it is approximately 14.8J.

5.5.1 Laminate A

Figure 38 illustrates the various energy dissipation mechanisms in relation to impact velocity and is included for general reference by the reader. Figure 40 shows the proportion of impact energy that each energy dissipation mechanism accounts for. Figure 41 shows the proportion of total material failure energy accounted for by each damage mechanism. Figure 39 is the same as Figure 38 except material failure energy is considered as a whole in order to emphasise its role in energy dissipation.

The dissipated energy due to material failure shows a strong correlation (0.93) with impact energy up to the ballistic limit after which it exhibits some scatter within a band of 10 to 14J, about an average of 13.2J.

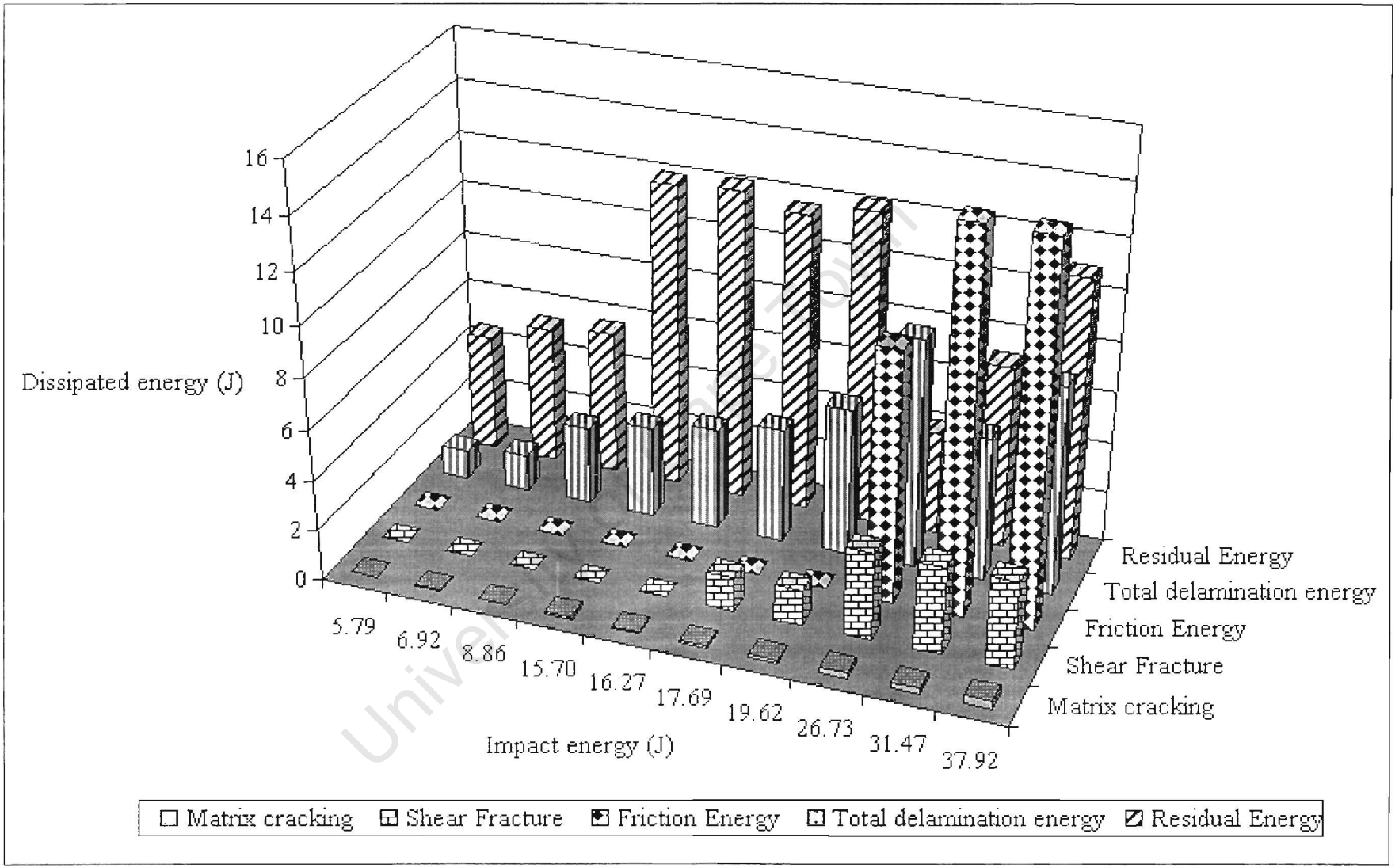

Figure 38 Laminate A: Energy dissipation mechanisms and their contributions

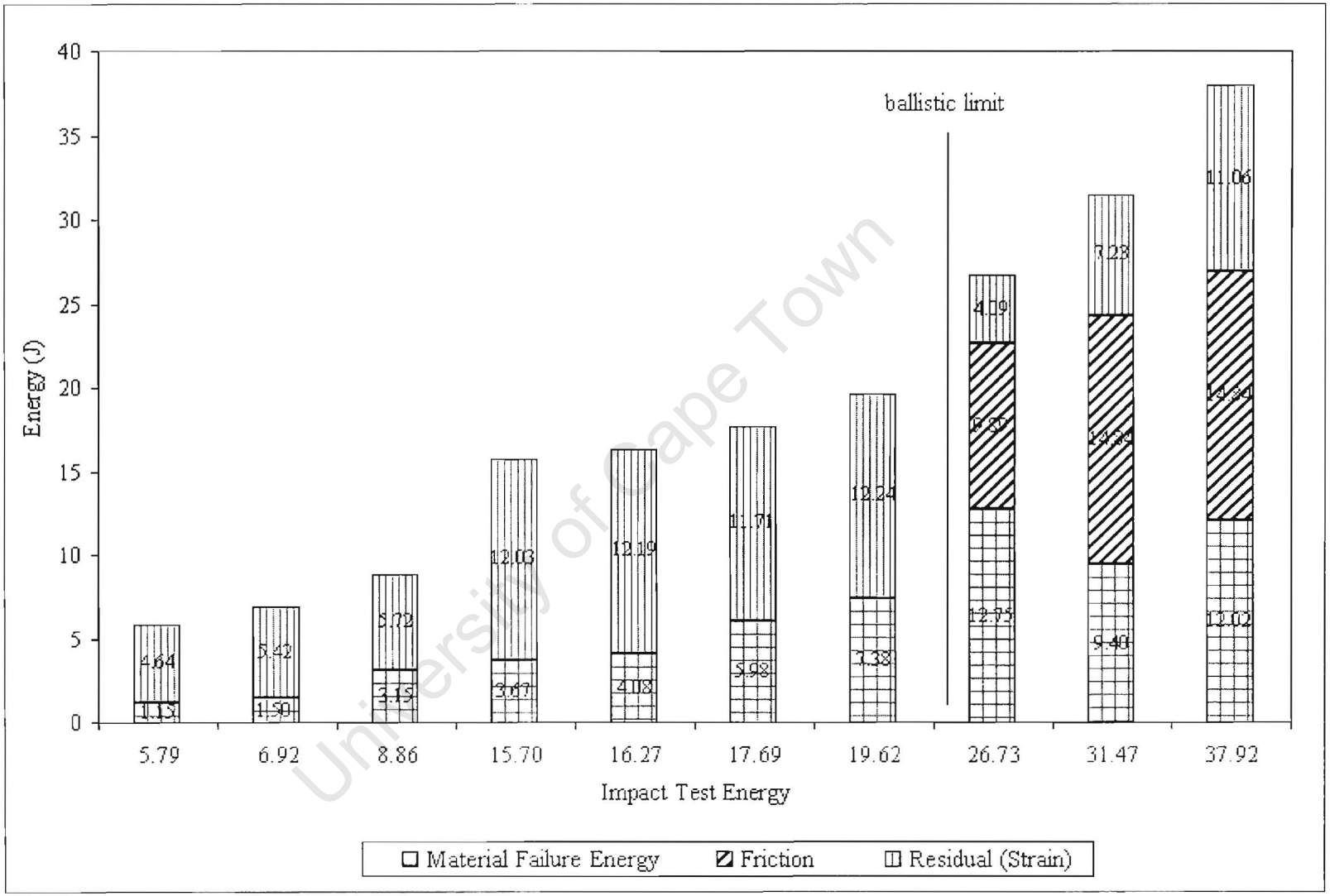

Figure 39 Laminate A: Material failure, friction and residual energy

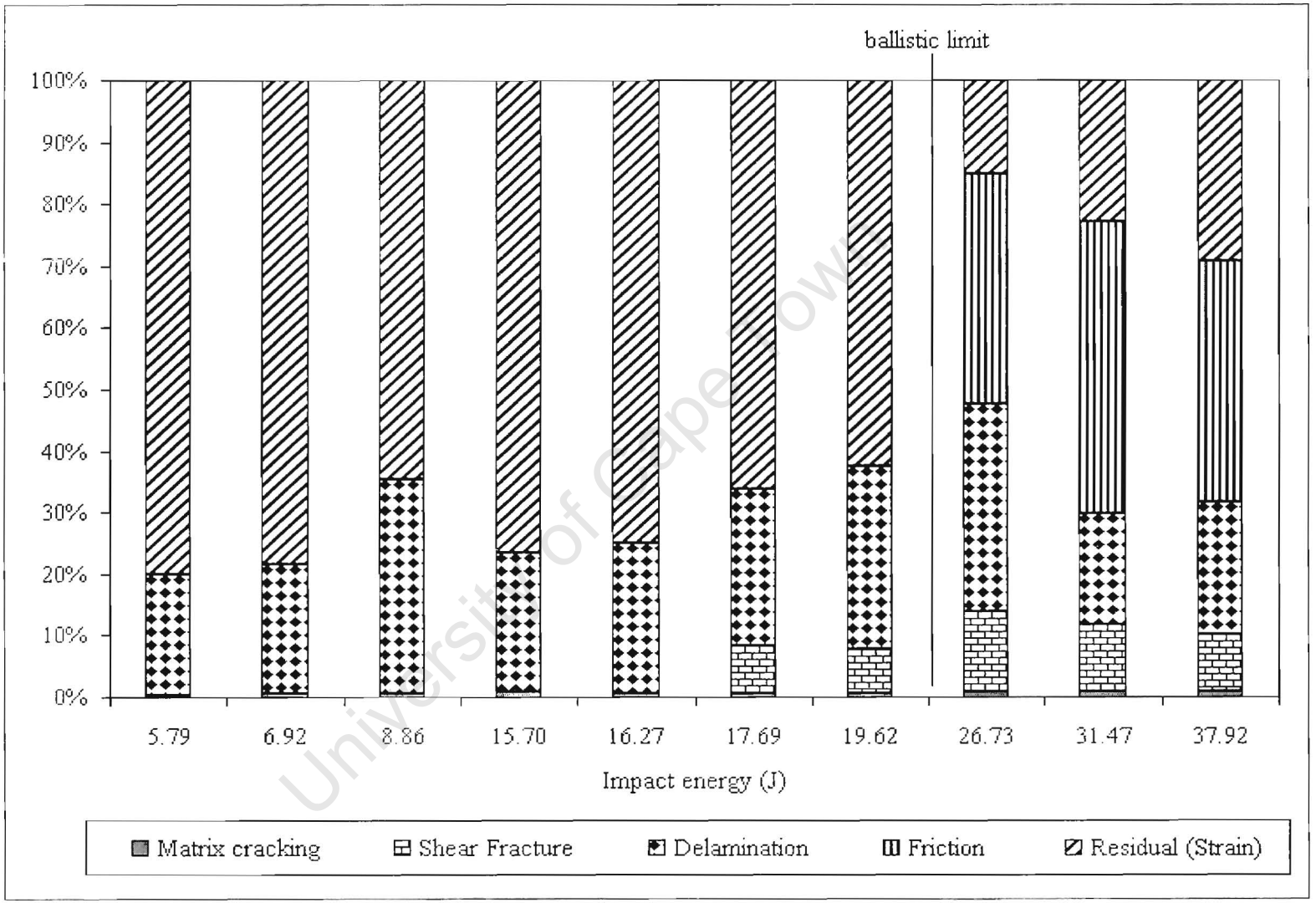

Figure 40 Laminate A: Percentage mechanism contribution to impact energy dissipation

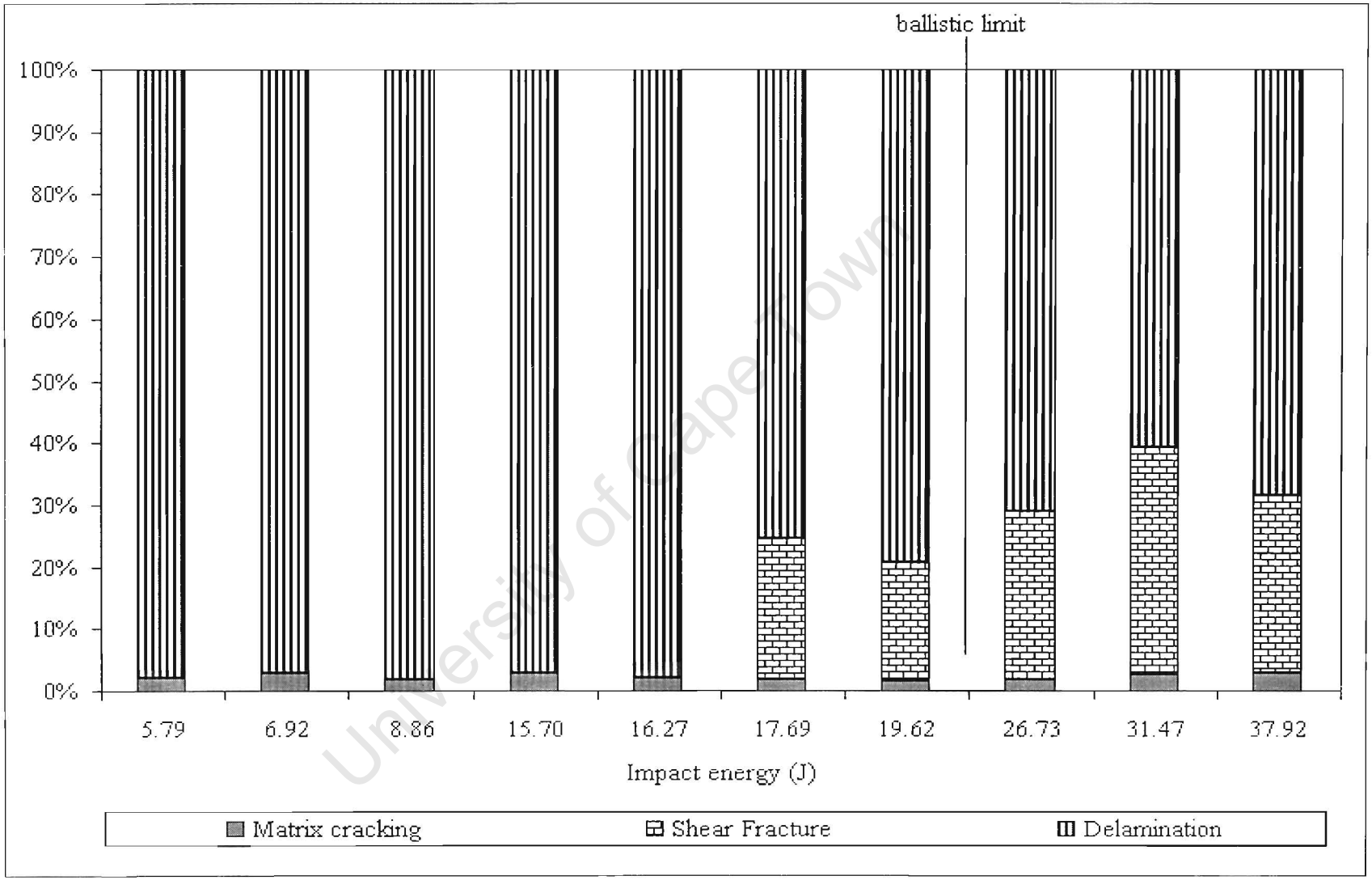

Figure 41 Laminate A: Percentage mechanism contribution to energy dissipated due to material failure

Friction

The friction energy dissipated by the 72.57m/s (26.73J) test (Figure 39) on the A laminate was approximately 9.89J since the length that passed through the laminate was approximately 15.5mm. The energy dissipated by friction accounts for 13.6% of the impact energy (Figure 40), approximately the same as that of delamination.

Friction energy of 1.37J at the ballistic limit should only account for approximately 5.5% of the impact energy dissipated as only about 2.5mm of the projectile passes through.

Delamination

For specimens where no shear fracture occurs at velocities below the ballistic limit, delamination accounts for approximately 98% of energy dissipation due to material failure (Figure 41) and post-ballistic limit it accounts for 60 to 70% (Figure 41). The number of data points limit are too few to draw conclusions as to the development of delaminations post- ballistic.

In relation to the proportion of impact energy (Figure 40) dissipated delamination energy increases slightly from 20% to just below 40% with impact energy pre-ballistic limit. Post-ballistic limit delamination decreases from 30% to 20% , although with only 3 data points a trend cannot be concluded.

Matrix cracking

Matrix cracking accounts for between 1.5% and 2.6% of the energy dissipated due to material failure (Figure 41). The level of matrix cracking appears to be fairly constant in relation to the other material damage. The contribution of matrix cracking relative to impact energy is almost negligible, lying in the region of 0.3% (Figure 40).

Shear fracture

Post ballistic limit, i.e. once the shear cone is through the entire thickness, shear fracture accounts for approximately 30% of energy dissipated due to material failure (Figure 41), although with only 3 data points the level of confidence cannot be established. In relation to the impact energy it accounts for approximately 4.4% (Figure 40).

Shear fracture accounts for approximately 14% (3.46J) of the impact energy at the ballistic limit.

Strain energy

The test closest to the ballistic limit is that impacted at 72.57m/s (26.73J) where the projectile was lodged in the laminate i.e. residual kinetic energy is zero. The energy dissipated due to material failure was determined to be approximately 13.35J (Figure 39) and the energy dissipated due to friction between the projectile and laminate is approximately 9.89J. The strain energy is therefore 3.81J, which accounts for about 14% of the impact energy.

Assuming that material failure is likely to be similar to that of the specimen impacted at 72.57m/s (26.73J) for a specimen impacted at the ballistic limit (approx. 70m/s) the strain energy would be approximately equal to;

Impact energy (24.87J) - Material dissipation energy (12.75J) - friction energy (1.37J)

$$= 10.75J$$

Strain energy is therefore responsible for approximately 43% of the energy dissipated at the ballistic limit and is approximately 84% that of the energy dissipated by material failure.

The strain energy cannot be ascertained for the other tests as this would require knowledge of the residual velocity of the projectile.

5.5.2 Laminate B

Figure 42 illustrates the various energy dissipation mechanisms in relation to impact velocity and is included for general reference by the reader. Figure 44 shows the proportion of impact energy accounted for by each energy dissipation mechanism. Figure 45 shows the proportion of total material failure energy that is accounted for by each damage mechanism. Figure 43 is the same as Figure 42 except material failure energy is considered as a whole in order to emphasise its role in energy dissipation.

The energy dissipated due to material failure does not exhibit a strong correlation with impact energy rather it appears to settle in a band of 10 to 15J with an average of approximately 12.5J.

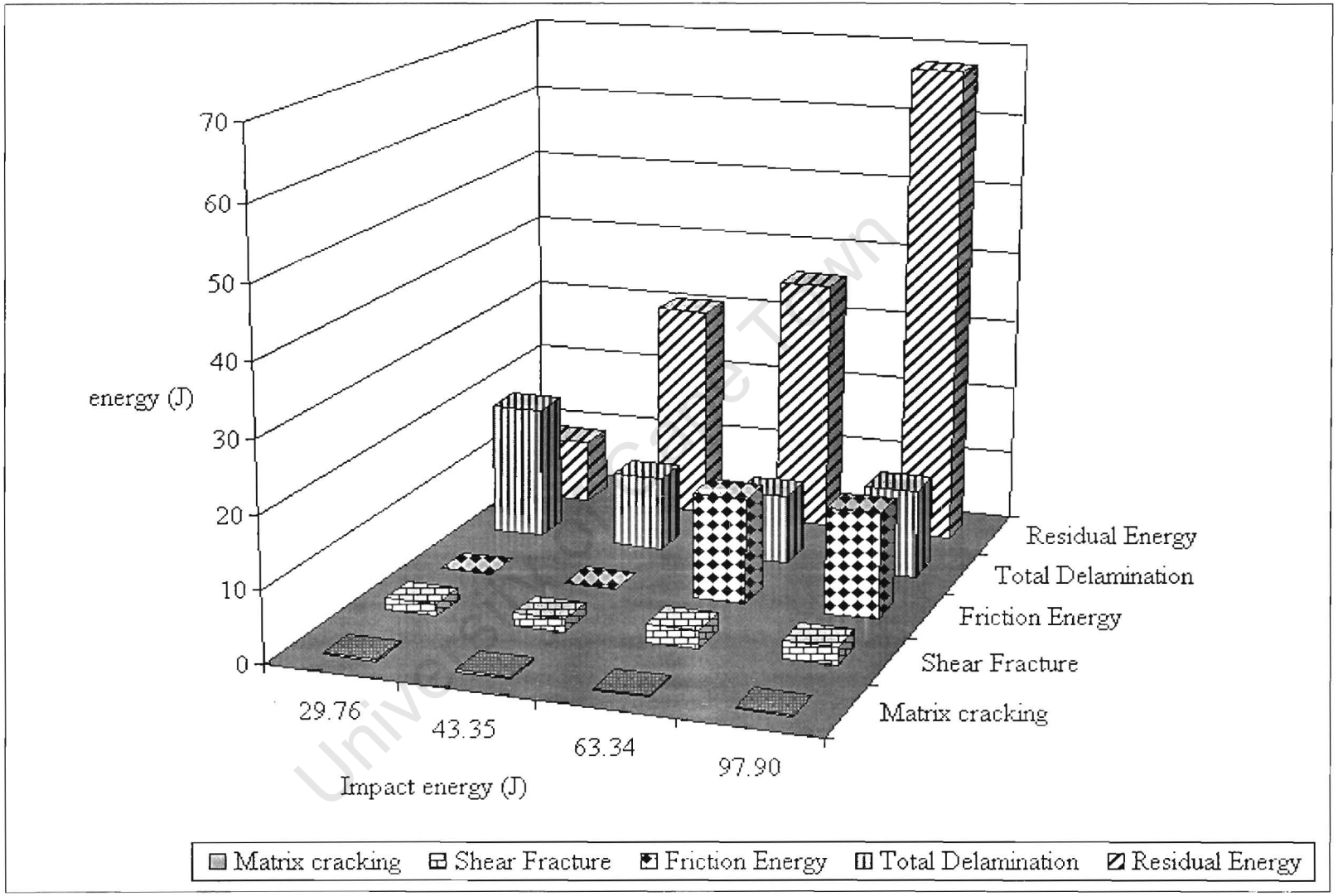

Figure 42 Laminate B: Energy dissipation mechanisms and their contributions

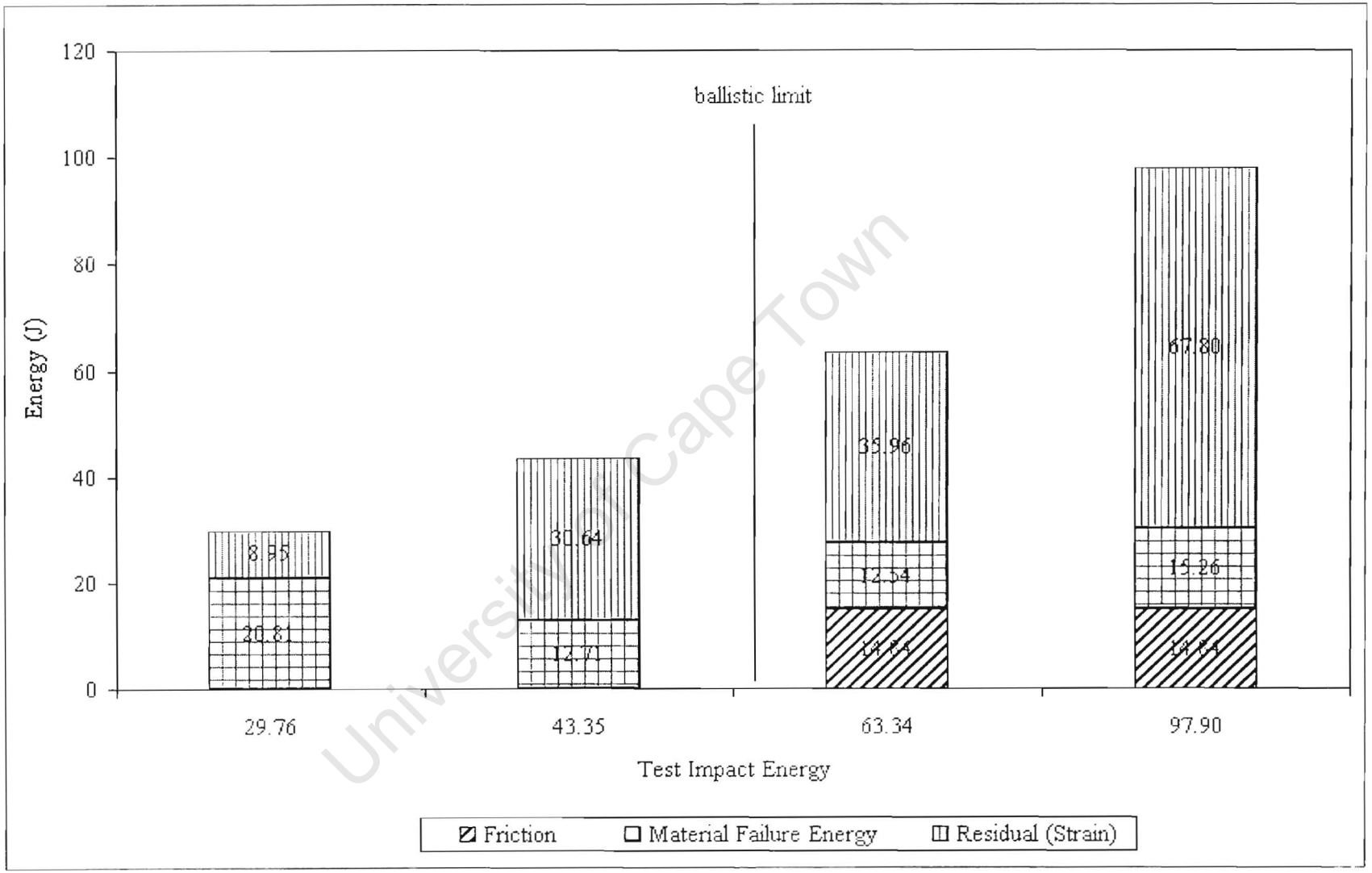

Figure 43 Laminate B: Material failure, friction and residual energy

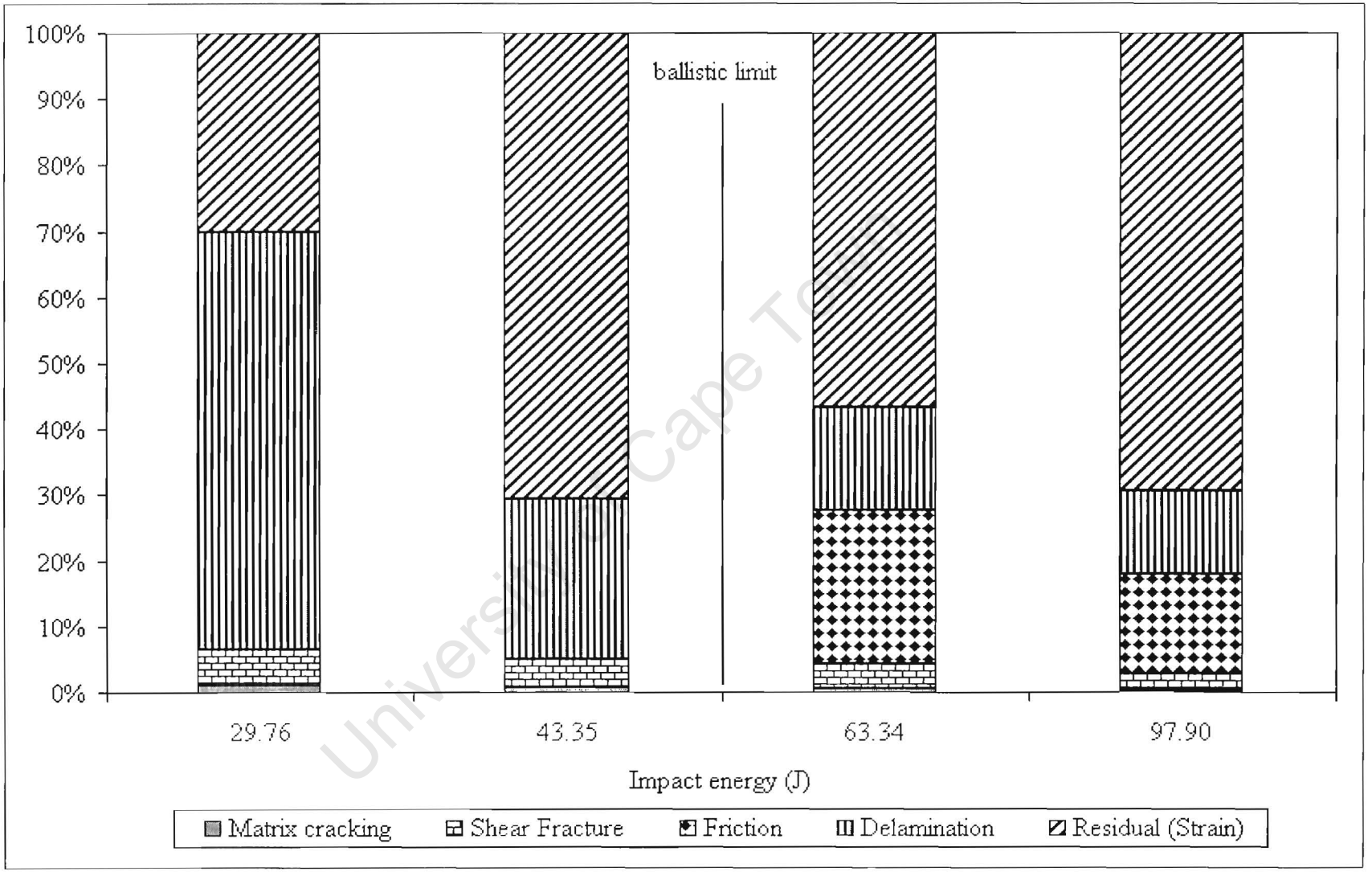

Figure 44Laminate B: Percentage mechanism contribution to impact energy dissipation

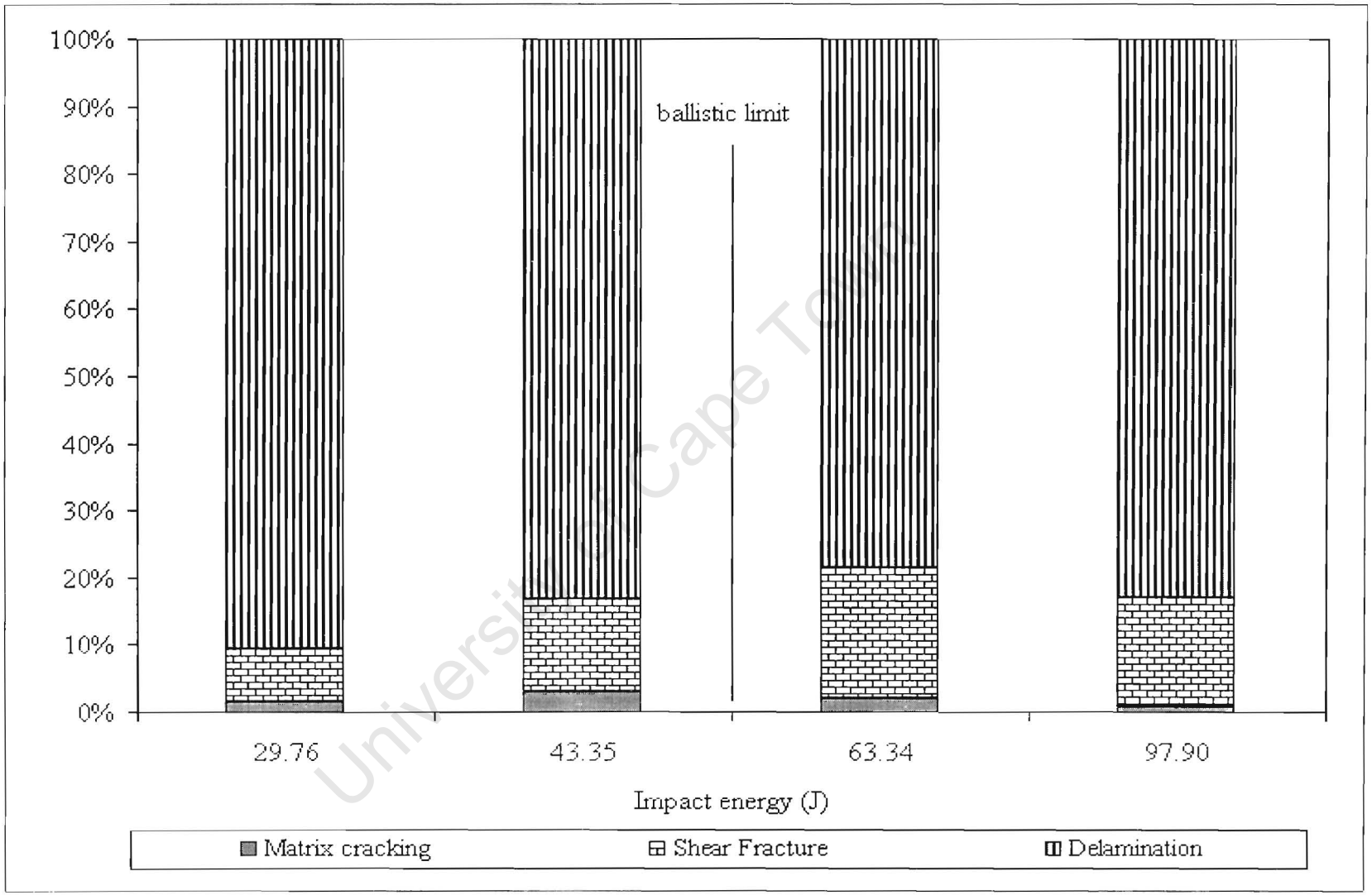

Figure 45 Laminate B: Percentage mechanism contribution to energy dissipated due to material failure

Delamination

The tests prior to the ballistic limit experienced some shear fracture so that delamination at 76.69m/s (29.76J) accounted for 90% of energy dissipation due to material failure (Figure 45). Post-ballistic limit delaminations account for 70 to 80%, although with only 2 data points pre and post ballistic limit a relationship to impact energy could not be ascertained.

In relation to the total impact energy (Figure 44) delamination accounts for 18.85J of the total energy dissipated for the 76.69m/s test whereas the next pre-ballistic limit test, at 92.42m/s (43.35J), only accounted for 10.58J and subsequent post-ballistic tests for approximately 11J. The percentage contribution of delamination energy relative to the impact energy decreases from 63% to 13% as impact energy increases.

Matrix cracking

Matrix cracking accounts for between 1% and 3% of the energy dissipated due to material failure, however a confidence level could not be established due to the small sample (Figure 45).

In relation to the total impact energy the contribution of matrix cracking to energy dissipation would appear to be insignificant of the order of 0.1 to 0.25J (Figure 44).

Shear fracture

Post-ballistic limit, i.e. once the shear cone is through the entire thickness, shear fracture accounts for approximately 9% of energy dissipated due to material damage (Figure 45), although with only 2 data points the level of confidence cannot be established.

The proportion of energy dissipated by shear fracture in relation to impact energy (Figure 44) lies between 3% and 6%, although with only 4 data points no firm conclusions can be drawn.

Strain energy

The strain energy at the ballistic limit can be estimated by applying the following assumptions;

- Ballistic limit is approximately 95m/s i.e. impact energy of 45.8J (see section 5.4.2 Ballistic limit of B laminate)
- Energy dissipated due to material failure is of similar magnitude as that of the 92.42m/s (43.35J) test (Figure 43), approximately 12.7J, as the value at the 111.61m/s (63.34J) test is not significantly different.
- Friction energy is approximately 1.37J

Impact energy (45.8J) - Material dissipation energy (12.7J) - friction energy (1.37J)

The strain energy is therefore approximately 31.73J, which is almost 2.5 times the total energy dissipated by material failure and friction.

Chapter 6. Finite element modelling

The finite element modelling has been based around implementing a model of the projectile impact event to the best of ABAQUS Explicit's abilities without producing a user material. The absence of a user material is a significant hindrance in using FEM as a tool to analyse the event satisfactorily. The modelling is therefore primarily an exercise in determining the usefulness of the standard ABAQUS features and their limits, however it does provide insights into the impact event.

ABAQUS Standard was used to compare the static compliance of the two laminates in order to illustrate its relevance to high velocity projectile kinetic energy dissipation.

6.1 Projectile impact

See APPENDIX C

A single impact velocity (72.57m/s) was simulated for both laminates as without a user material results suitable for comparing the effect of a variety of different impact velocities can not be obtained. First failure is highlighted by only plotting stress values that exceed the failure stress and stress waves are shown by plotting only positive or negative stresses.

The first lamina failure is due to normal out-of-plane compressive stresses, known as contact stresses, and occur before any laminate deflection takes place. The depth of lamina failure due to this contact stress reaches a maximum depth before the laminate deflects enough to cause other stresses of significance. The total simulation time was 70.5μs by which time the failure depth had reached its maximum depth without any other critical stresses or strains having been exceeded.

6.1.1 Geometry

The model geometry (Figure 46) is not fully representative of a full specimen as only the upper quarter of the tube (an eighth) is modelled, however, this was justified as the structural response is localised. The model behaviour and material properties are symmetrical about the 1,3 and 2,3 planes that pass through the impact point. The geometry being an eighth the full size should still be sufficient to highlight significant trends and features that differentiate the laminates' responses to projectile impact.

The projectile has been modelled as a revolved rigid surface and a mass element, which was assigned a value of 10.15grams like that used in the experimentation. The option TYPE=VELOCITY was used to specify the initial velocity of 72.57m/s, within the *INITIAL CONDITION command.

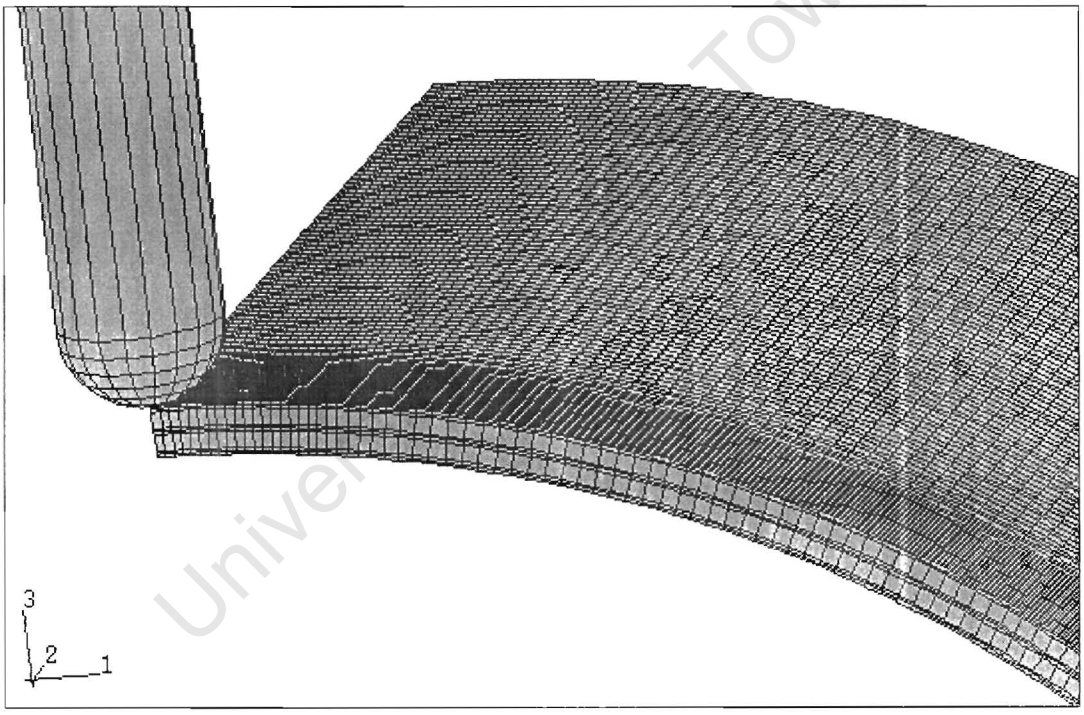

Figure 46 ABAQUS model geometry

6.1.2 Element selection

The C3D8R continuum element, an eight noded reduced integration continuum element, was chosen as it is less computationally expensive than other three dimensional continuum elements. The continuum element enables stresses and strains in all planes to

be considered unlike shell or plain stress or strain beam elements, which is important where the significant loading is normal to the plane.

Each +/-35° lamina and sets of three 90° laminae are modelled as a single layers of continuum elements (Figure 47) and the appropriate material properties and orientations assigned to them. The thickness of the elements are the same as the laminae they represent i.e. 0.15mm for each of the +/-35° laminae and 3x0.267mm for each set of 90° laminae.

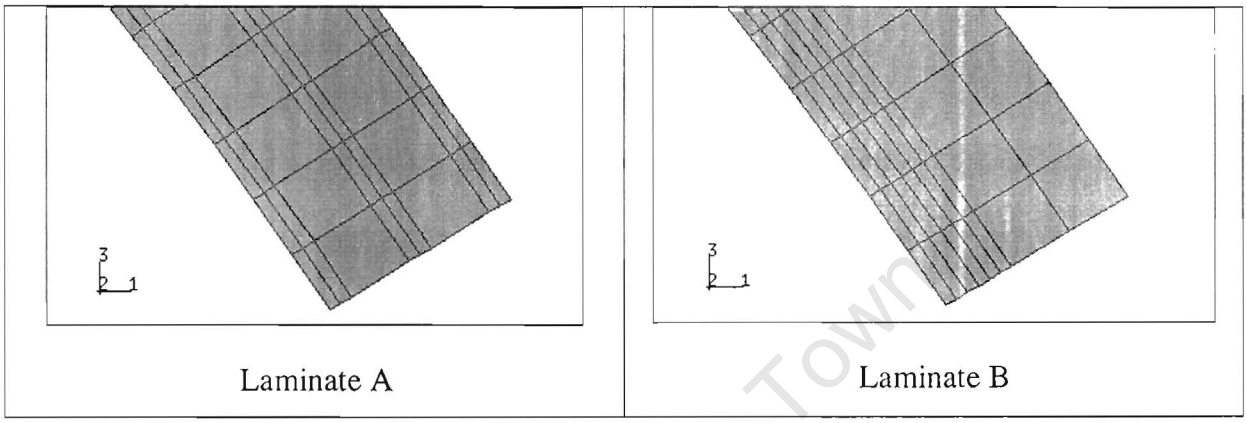

Figure 47 Laminate cross sections

An advantage of the continuum elements is that they provide a better approximation of the stresses and strains at the laminae surfaces. The reason for this being that the nodes lie on the interfaces and hence values at the interfaces can be obtained, whereas shell or beam elements require an integration point to lie at an interface in order to obtain values at the interface.

6.1.3 Material definition

The material properties of the continuum elements were defined using the ENGINEERING CONSTANTS option in the *ELASTIC command, as well as the *DENSITY command. The definition of a non-isotropic material in ABAQUS Explicit using this command precludes the use of the DEPENDENCIES option to define rate or other dependant material properties. The material properties can therefore only be altered during an analysis, in order to model failure, by means of a user defined material. The material properties in this analysis are strictly linear elastic as definition of plastic behaviour is also precluded.

The ENGINEERING CONSTANTS option enables the following material properties to be defined;

- Young's Moduli in all three planes
- In plane and transverse Shear Moduli
- In plane and shear Poisson's ratios

The orientation of the principle material directions, i.e. fibre orientation, were defined by defining an orientation using the *ORIENTATION command and assigning it to a material definition as an option within the *MATERIAL command. Orientations were specified using the cylindrical co-ordinate system which aligns the out-of-plane normal axis (normal to fibre direction) of the local laminate Cartesian system to the radius of the cylindrical system. The in-plane normal axis (transverse fibre direction) is aligned along the polar axis of the cylindrical system and the principle Cartesian axis (fibre direction) is normal to the radius of the cylindrical system. The orientation of the fibre is specified by a rotation about the normal axis of the laminate Cartesian system. See Figure 2 for a description of the axis system.

6.1.4 Boundary conditions

Boundary conditions were required to specify symmetric behaviour about the impact point and to account for clamping. The projectile also needed boundary conditions to prevent tumbling or rotations during contact.

Symmetric behaviour was specified about the 1,3 and 2,3 planes passing through the impact point in order to satisfy quarter symmetry. The symmetric boundary condition is specified using the XSYMM, YSYMM or ZSYMM statement on the subsequent *BOUNDARY data line.

Clamping was specified for the face of the geometry furthest from the impact point and in the 1,3 plane, by using the ENCASTRE statement, which prevents any rotation or displacement.

6.1.5 Contact definition

Contact between the projectile and specimen is specified using the *CONTACT PAIR command with PENALTY contact option. Penalty contact allows a small amount of over-closure to occur and was required in order to overcome noise during contact, which resulted in simulations failing.

6.2 Compliance test

See APPENDIX C.

A compliance test determines the overall quasi-static flexural response of a structure to a central displacement, which for beams is usually a 3 point bend test. The simulation does not attempt to reproduce a standard compliance test as this would require an overly complicated model. The test compares the response of the two laminates to a concentrated load at the impact site.

The simulation uses shell elements to model a quarter pipe and displaces the node at the impact point over a set distance (20mm) downwards in the 2 direction and over a fixed time (3 sec.). The reaction force in the 2 direction is then plotted against the displacement of that node to provide an indication of the compliance of the laminae. The strain energy of the two laminae are also plotted against displacement.

6.2.1 Geometry

(refer to Figure 48)

The model geometry represents a quarter tube as the behaviour is symmetrical about the 1,2 and 3,2 planes passing through the impact point[††]. The reduction in size was justified on the grounds that the problem is symmetric about the displaced node.

[††] Axes definition for shell model is different to continuum model, "vertical" axis is represented by 2 and not 3.

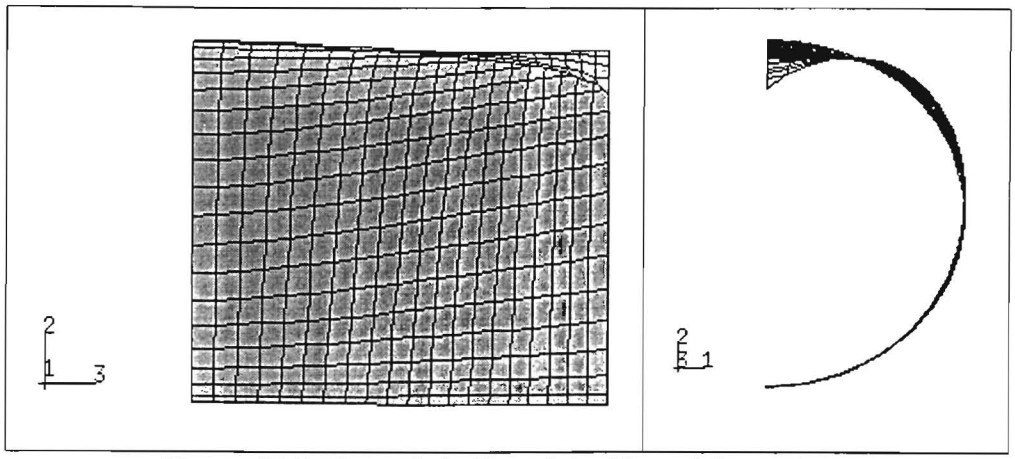

Figure 48 Deformed shell model, side and front views

6.2.2 Element selection

S4R 14 noded shell elements with reduced integration were used during the simulation as they are computationally efficient and are known to produce reliable results when modelling composites undergoing quasi-static loading. The rate of node displacement was sufficiently slow such that out of plane loads are negligible and only in plane stresses and strains are considered.

6.2.3 Material definition

The material properties of the shell elements were defined using the LAMINA option in the *ELASTIC command for the 90° and +/-35° laminae. A composite stress failure option was implemented using the *FAIL STRESS command, however this proved to be unnecessary as the laminate was not loaded to failure. The number of layers, layer thickness, material properties and their orientations were assigned to the shell elements using the *SHELL GENERAL SECTION command.

6.2.4 Boundary conditions

Boundary conditions were required to specify symmetric behaviour about the loading point and to account for clamping.

Symmetric behaviour was specified about the 1,2 and 3,2 planes passing through the loading point using the XSYMM, YSYMM or ZSYMM statement on the subsequent *BOUNDARY data line.

Clamping was specified for the face of the geometry furthest from the impact point and in the 1,2 plane, by using the ENCASTRE statement, which prevents any rotation or displacement.

Chapter 7. Finite Element Modelling Results

7.1 Projectile Impact

The following results are for simulations of an impact at 72.57m/s by a projectile with a hemispherical head and mass of 10.15grams upon laminates A and B.

Figure 49 and Figure 51 depict the stresses normal to the laminate approximately 70.5μs after impact. The figures show all stresses within the failure limits as a single colour (red) and all those exceeding the failure limit as varying shades. The through thickness compressive failure limit is –150Mpa and tensile limit is 930Mpa.

Laminate A

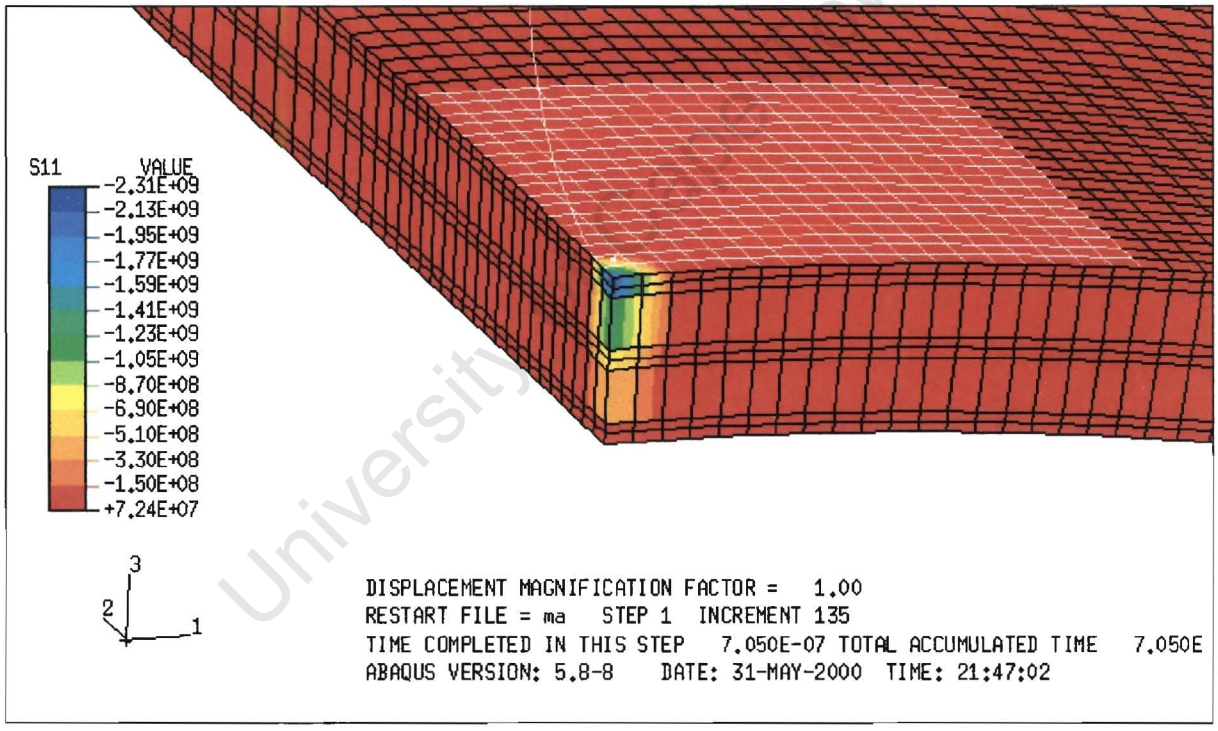

Figure 49 Laminate A: Normal laminate stresses

The maximum contact stress at the surface is -2.31GPa. Stresses exceeding the failure stress are largest and most prevalent in the upper half of the laminate where they range from -690MPa to -2.31GPa. The stresses extend into the lower half of the laminate where they range from -150MPa to -690MPa at the middle of the laminate, but are not as prevalent as in the upper half of the laminate. The simulation indicates that immediately

below the impact point the laminate fails in normal compression at least through the upper half and most likely into the lower half.

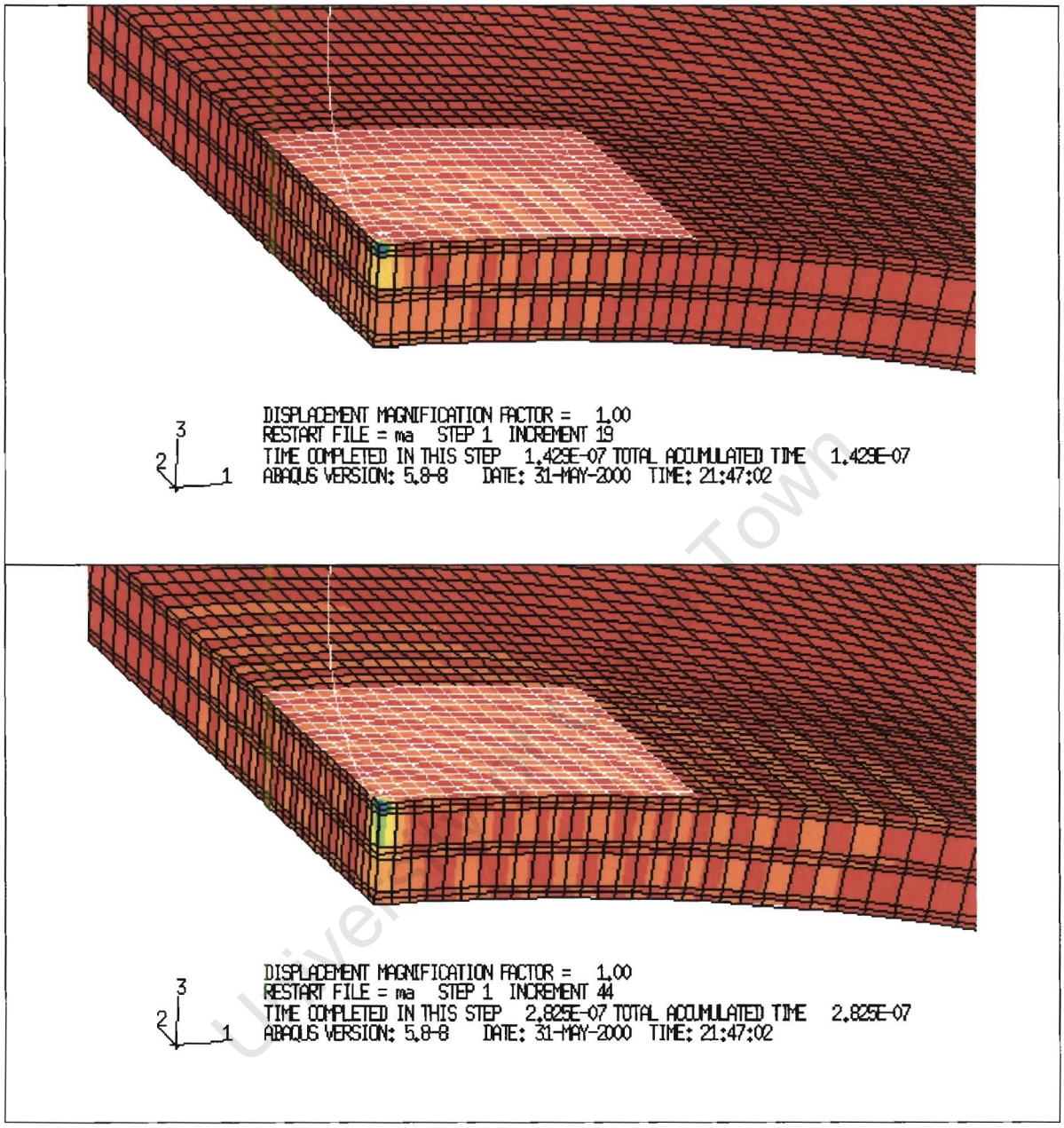

Figure 50 Laminate A: Stress waves

Figure 50 depicts the stress at subsequent time steps in the A laminate, showing ABAQUS Explicit's ability to account for stress waves as a result of contact.

Laminate B

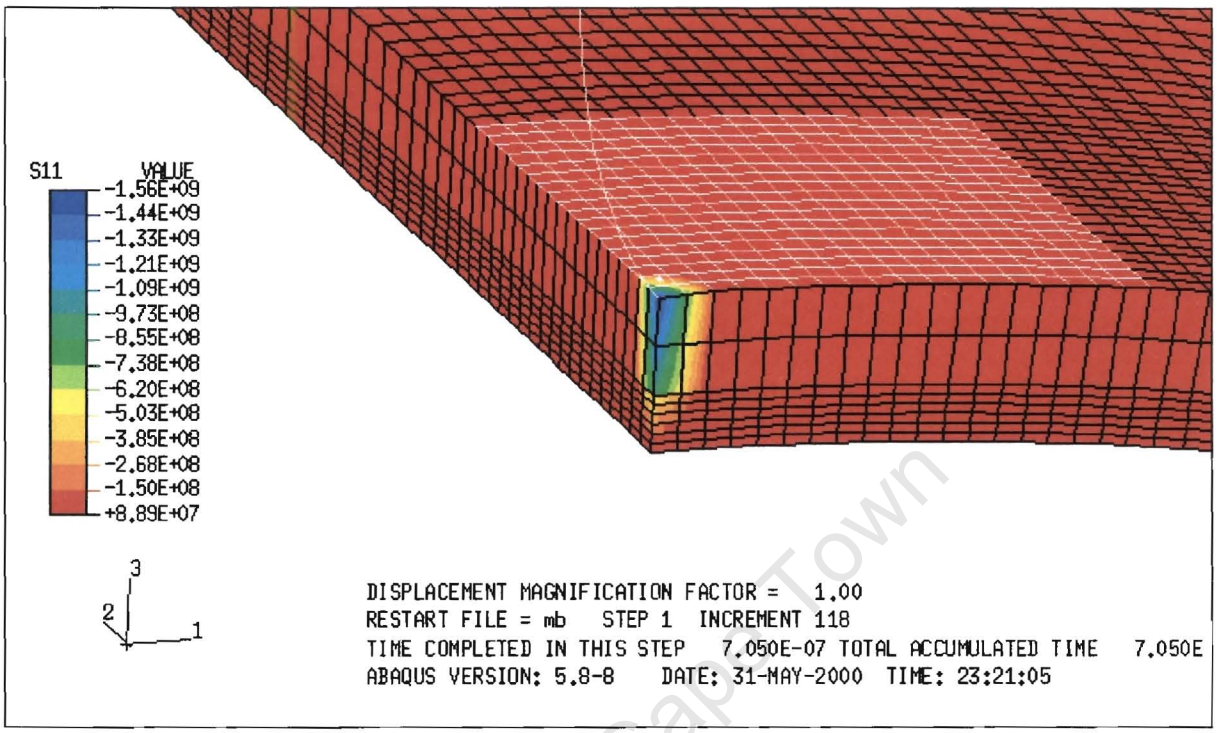

Figure 51 Laminate B: Normal laminate stresses

The maximum contact stress at the surface is -1.56GPa. Stresses exceeding the failure stress are largest and most prevalent in the upper 90° laminae where they range from -620MPa to -1.56GPa. The stresses extend into the +/-35° laminae where they range from -150MPa to -503MPa at the interface with the 90° laminae, but are not as prevalent as in the upper half of the laminate. The simulation indicates that immediately below the impact point the laminate fails in normal compression at least through most of the 90° laminae and most likely into some of the +/-35 degree laminae.

Figure 52 depicts the stress at subsequent time steps in the B laminate.

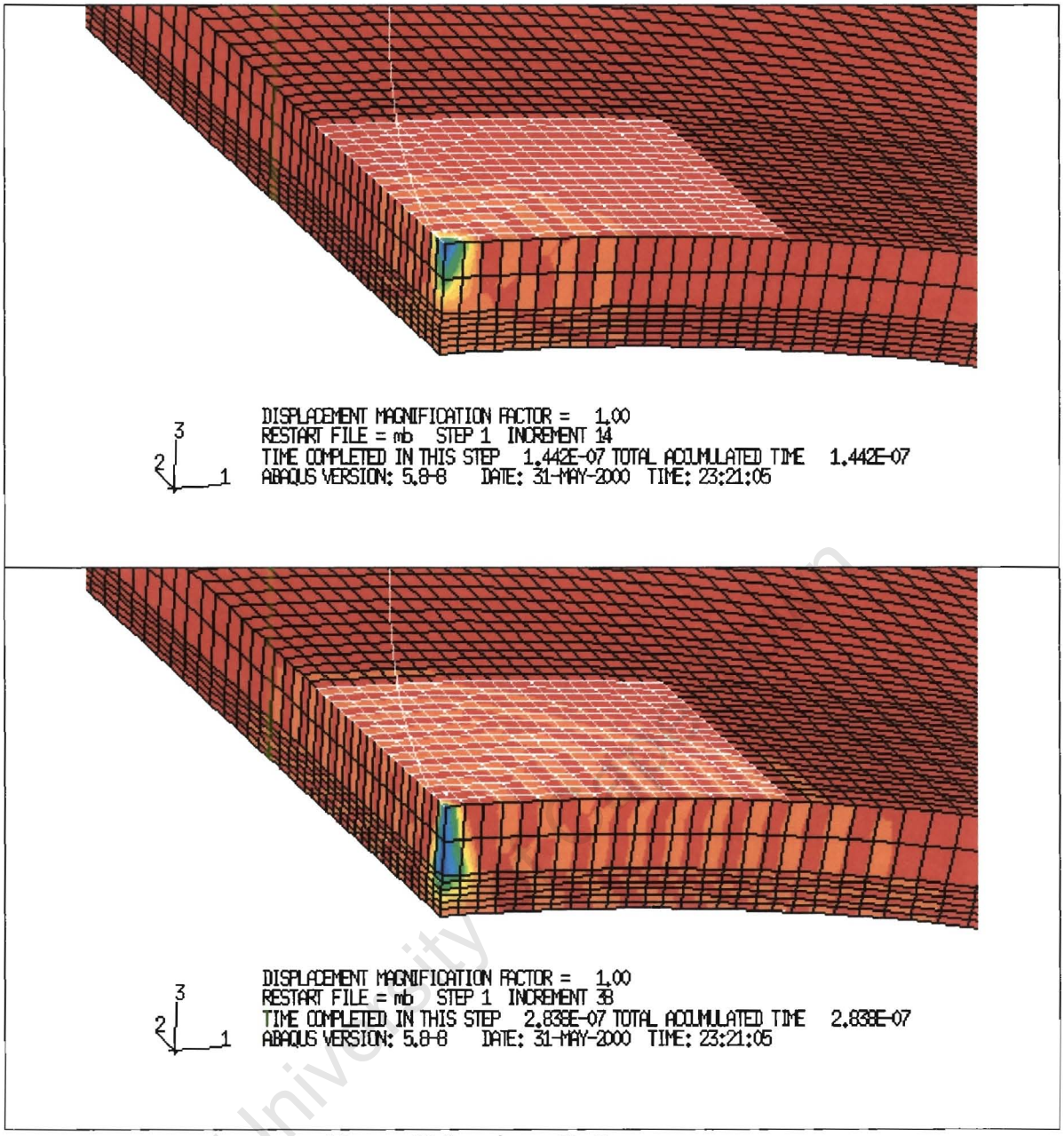

Figure 52 Laminate B: Stress waves

7.2 Compliance Testing

The finite element analysis performed to check the compliance due to static loading (see Figure 53) shows that Laminate A has the largest flexural modulus, i.e. smallest compliance, exhibiting the largest total strain energy (Figure 54). The applied load is due to deflection of the central node over an equal distance for both laminates within the an equal period of time (same rate of loading). The test provides a measure of overall compliance accounting for the differing compliance relative to laminate orientation and the geometry of the structure.

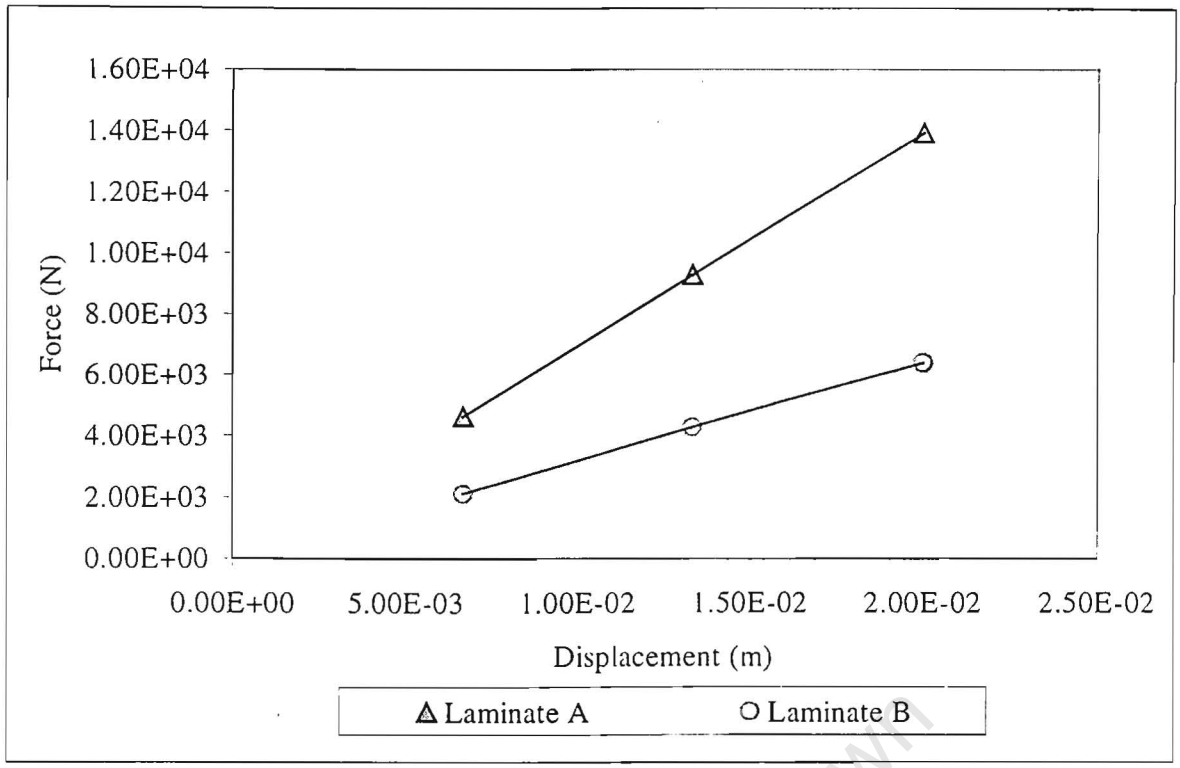

Figure 53 Vertical reaction force of central node versus displacement

The force versus displacement trend is perfectly linear indicating that no material failure has taken place. Plastic deformation or material failure would result in a non-linear relationship.

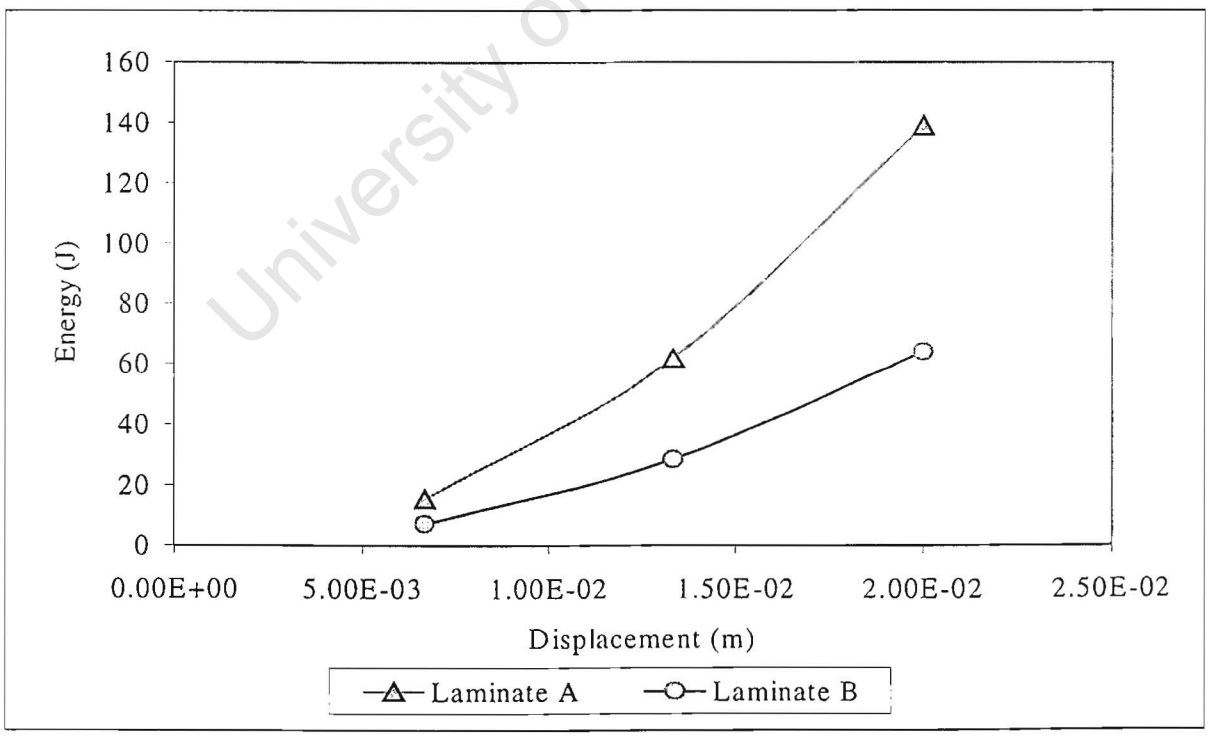

Figure 54 Strain energy versus displacement

Chapter 8. Discussion

The discussion is structured around the aims of the thesis, which are outlined in the introduction (section 1.2).

8.1 Projectile kinetic energy dissipation performance of the laminate

The ballistic limit of a laminate is a standard measure of a laminates performance when experiencing projectile impact. The B laminate has a ballistic limit almost 1.4 times higher than the A laminate in terms of velocity for a 10.15 gram projectile with a hemispherical head. The B laminate ballistic limit when considered in terms of energy, more significantly, is 1.8 times that of the A laminate. The B laminate therefore has the best energy dissipation performance for projectiles which penetrate the laminate, reducing the residual kinetic energy of the projectile after it has passed through.

Projectile impacts do not always exceed the ballistic limit and in thin laminates in particular pre-ballistic limit impact results in the projectile rebounding off the laminate. The reduction in rebound kinetic energy of the projectile therefore also needs to be considered as it can also be of concern.

The projectile upon impact is brought to rest when the laminate has achieved its maximum deflection and material damage, upon which it is propelled in the opposite direction as the laminate returns to its original position. The projectile regains kinetic energy, in a normal incidence, impact event as a result of recoverable energy from the target, which is the elastic strain energy of the target. The elastic strain energy of a laminate is a function of the material properties, which are degraded as a result of material damage. In order to reduce the available elastic strain energy, and hence the rebound velocity, the material properties, i.e. elasticity, of the laminate need to be degraded by increasing the extent of material failure. An alternative way of considering this is from the fracture mechanics stand point (the approach taken in this thesis) that views material damage as dissipating energy as it is "consumed" in initiating and propagating fractures/cracks. The energy dissipated is assumed, in Linear Elastic Fracture Mechanics, to be directly proportional to fracture area.

The laminate that exhibits the most fracture as a result of pre-ballistic limit impact will likely retain the least elastic strain energy. The extent of fracture is therefore an important

measure of a laminates ability to dissipate projectile kinetic energy in pre-ballistic impact events. Fracture in CFRP laminates, as described previously, consists of a number of fracture modes with different energy release rates. The physical size of damage is not sufficient a measure of the importance of the various fracture modes as it also depends on the magnitude of their energy release rates. Determining the laminate which performs best, in terms of projectile kinetic energy dissipation, first requires careful assessment of the extent of the significant damage modes and then application of the relevant energy release rates to them.

Section 8.2.2 discusses the energy dissipated by material failure in the B laminate and concludes that it is only slightly higher or of similar magnitude to that of the A laminate post-ballistic limit. The implication being that both laminates have the same energy dissipation performance prior to the A laminate ballistic limit. The A laminate will have the best performance between the A and B laminate ballistic limits as additional energy is dissipated by friction. The B laminate has the best performance at impact velocities grater than the B laminate ballistic limit

The A laminate therefore only performs better for a narrow range of impact velocities (Figure 55) while for all other impact velocities the B laminate performs as well or better than the A laminate. The B laminate is therefore the best laminate, in general, for dissipating projectile kinetic energy. The A laminate should be considered for use only if the impact velocity (energy) is known to be between the A ballistic limit of 70m/s (24.8J) and the B ballistic limit of 95m/s (45.8J) for a projectile of similar mass and geometry.

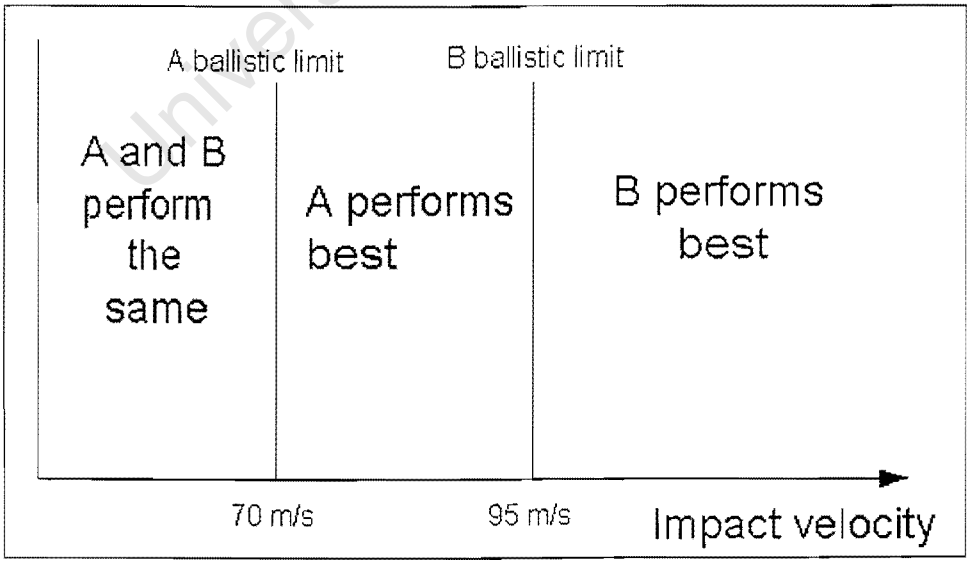

Figure 55 Laminates A and B projectile kinetic energy dissipation performance

8.2 Energy dissipation mechanisms

The following discussion utilises energy release rates quoted in the literature and obtained from the single drop test (Figure 30). The analysis performed in this thesis is considered valid as the same trends and conclusions are reproduced whether using the maximum or minimum values quoted.

The analysis neglects one energy dissipation mechanism that some analysts consider to be of importance, that is fibre pull-out. The reason for doing so is that it is difficult to quantify and it does not appear, in the current tests, to be prevalent. Some fibre pull out will occur along the shear fracture cone and immediately below the impact point where the fibres break, however it is not evident in the X-rays or to the naked eye. The lack of plug separated material was an indication that although severe fracture did occur very little fibre pull out occurred. If fibre pull out did occur but was not detected the contribution to energy absorption would be of a similar value for both laminates as the total surface area along which it would occur is significantly different.

8.2.1 Laminate A

Material failure

The total energy dissipated due to material failure (Figure 39) increases steadily with impact energy up until the ballistic limit after which it appears to level out at about 11J to 12J (Table 5), having a mean of 11.4J. The proportion of impact energy it dissipates (Figure 40) is seen to grow from 20% of an impact energy of 5.79J to 35% of an impact energy of 26.73J (just post-ballistic limit) after which the proportion it accounts for decreases steadily with impact energy.

The major material failure mechanism contributing to energy dissipation is delamination, which accounts for approximately 97% of the energy dissipated by material failure (Figure 41) prior to the onset of shear fracture. Delamination apparently reaches a threshold at the ballistic limit at which point the size either levels off or the rate at which it grows is much diminished. The energy dissipated due to delamination post-ballistic limit lies in a band between 5.7J and 9J.

Table 5 Laminate A: Materal failure energy dissipation

Impact velocity	**Impact energy**	**Shear Fracture**	**Friction**	**Matrix cracking**	**Delamination**	**Total**
m/s	J	J	J	J	J	J
33.78	5.79	0.00	0.00	0.023	1.13	1.15
36.93	6.92	0.00	0.00	0.043	1.45	1.50
41.77	8.86	0.00	0.00	0.054	3.09	3.15
55.62	15.70	0.00	0.00	0.105	3.57	3.67
56.63	16.27	0.00	0.00	0.085	3.99	4.08
59.03	17.69	1.36	0.00	0.11	4.51	5.98
62.11	19.62	1.40	0.00	0.12	5.86	7.38
72.57	26.73	3.46	9.89	0.24	9.05	12.75
78.74	31.47	3.46	14.84	0.25	5.70	9.40
86.66	37.92	3.46	14.84	0.34	8.22	12.02

Shear fracture (Table 5) is first observed in the test at 59.03m/s (17.69J) impact velocity at which point it is responsible for approximately 20% of the energy dissipated due to material failure (Figure 41). Shear fracture is seen to be the next most important energy dissipating mechanism. Shear fracture reaches a threshold once the laminate has been fully perforated, dissipating 3.46J of energy.

Prior to shear fracture the only other failure mechanism than delamination observed is matrix cracking which consistently accounts for about 3% of the energy dissipated due to material failure pre-shear fracture and 2% post shear fracture. The correlation of 0.94 (Figure 35) shows cracking to be strongly linearly dependent on impact energy up to and beyond the ballistic limit.

The ballistic limit is a threshold in the development of material damage and hence energy dissipated by this means. The reason for this being the constant shear fracture once the projectile has passed through and the apparent threshold in delamination growth at the ballistic limit. The lack of data post-ballistic limit prevents any conclusions from being drawn as to the development of material damage post-ballistic limit, however it would be reasonable to expect further damage propagation at higher impact energies albeit at a reduced rate.

Friction

Friction accounts for about 6% of dissipated energy at the ballistic limit and increases as more of the projectile length passes through the laminate such that when it has passed through entirely it dissipates about 14.84J (Table 5). At 72.57m/s (26.73J) slightly over half the projectile (15.5mm) has passed through the laminate and at 78.74m/s (31.47J) it has passed through entirely such that between those two tests lies the point when the projectile just passes through. The 72.57m/s test is about 2J greater than the ballistic limit, i.e. just perforated, case so assuming a linear relationship would imply an impact energy of about 29J, or velocity of 75.6m/s, is required for a projectile to just pass through the laminate. The projectile can be expected to have a minimal, i.e. negligible, residual kinetic energy at this impact velocity of 75.6m/s.

Strain

The energy dissipated due to strain at the ballistic limit is determined to be in the region of 11J or 40% of the impact energy (approx. 24.87J).

Strain energy in pre-ballistic impact events is returned to the projectile as kinetic energy and dissipated through vibrations, however in post-ballistic limit events the projectile passes through the laminate just prior to or at its maximum deflection. The laminate therefore cannot impart the strain energy, at that point, to the projectile and it is subsequently dissipated through vibrations and by propagating material failure. The strain energy pre-ballistic limit was not measured and cannot be readily determined analytically, however it would have a magnitude similar to the kinetic energy of the rebounded projectile, assuming minimal subsequent loss due to vibration and damage propagation.

The strain energy responsible for dissipating projectile kinetic energy can be estimated by considering that at approximately 75.6m/s (29J);

- Energy dissipated due to material failure has reached a threshold of about 11.4J
- Friction energy reaches a maximum of approximately 14.84JJ
- Projectile residual kinetic energy is almost zero.
- Once the projectile passes through the laminate the strain energy used in retarding its velocity cannot be recovered as kinetic energy by the projectile.

The strain energy responsible for dissipating projectile kinetic energy at this point is equal to approximately 29J-(14.84J+11.4J)=2.76J. Considering that the ballistic limit essentially remains constant [19] and that the material damage has reached a threshold, it is reasonable to assume that the projectile kinetic energy dissipated due to straining may remain fairly constant.

Projectile residual velocity

The test at 86.66m/s (37.92J) resulted in a residual energy of approximately 11J (Figure 39) so that the residual projectile kinetic energy, assuming strain energy of approximately 2J, is 9J. The projectile residual velocity is therefore about 42m/s. The evidence supporting this velocity is the mark and small delamination left on the inside of the tube opposite the penetration hole. The mark left did not deviate significantly from the initial flight path and did not penetrate the tube. The delamination length is about 5.5cm long and 4cm wide, which compares well to the delamination length (5.3cm) and width (4.3cm) of the test at 41.77m/s (8.86J). The mark and small delamination are therefore consistent with an impact velocity of 42m/s on a concave surface. It cannot be assumed that a concave and convex surface will produce the same results, especially as the largest delamination in the convex scenario appears to lie on the impacted side. The size of the delamination does, however, suggest an impact velocity in the region of 42m/s.

8.2.2 Laminate B

The lack of B laminate specimens combined with its higher ballistic limit has precluded extensive testing over the range of impact velocities performed on A laminate specimens, and only consisted of 2 tests pre- and post-ballistic limit. The low number of tests means that robust conclusions cannot be drawn from them especially as the test at 76.69m/s (29.76J) is in doubt. The reason for querying this test is due to the extent of material failure being larger than tests at higher impact velocities when results from laminate A tests indicate it should be lower. The low t test value for this test is also an indication that the experimental results may not be valid. The remaining three B laminate tests are then all that is left upon which to base a discussion.

Material failure

The total energy dissipated due to material failure ranges from 12.5J to 15.2J (Figure 43 and Table 6) and the mean energy dissipated (13.5J) is slightly higher (approx. 2J) than the mean post-ballistic limit value (11.4J) for the A laminate (Table 5). The values are of a similar level and are an indication that energy dissipation due to material failure may not differ significantly at lower impact energies/velocities.

Delamination is the significant failure mechanism accounting for approximately 80% to 90% of the energy dissipated by material failure prior to the onset of shear fracture (Figure 45). The post ballistic limit results indicate that delamination accounts for 35% to 40% of the material failure dissipation energy. The absolute value of energy dissipated due to delamination appears to lie in a band between 10J and 12.7J (Table 6), although this excludes the 76.69m/s test result due to questions about its validity. The mean value for laminate B (11J) is only 44% higher than that of the A laminate post-ballistic limit mean value (7.6J) despite the mean B laminate impact energy being 112% greater than that of the A laminate post-ballistic limit tests. The slight increase in delamination area over that of Laminate A is due to the increased number of dissimilar interfaces in the lower half of the laminate. Laminate B has 5 interfaces with a 70° degree difference in laminae orientations while A laminate has 2 interfaces with a 70° difference and 2 with a 55° difference (see section 4.1.1).

Table 6 Laminate B: Material failure energy dissipation

Impact velocity	**Impact energy**	**Shear Fracture**	**Friction**	**Matrix cracking**	**Delamination**	**Total**
m/s	J	J	J	J	J	J
76.69‡‡	29.76	1.64	0.00	0.32	18.85	20.81
92.42	43.35	1.76	0.00	0.37	10.58	12.71
111.61	63.34	2.44	14.84	0.25	9.84	12.54
138.89	97.90	2.44	14.84	0.29	12.53	15.26

Shear fracture is first observed in the test at 76.69m/s (29.76J) impact. Shear fracture is seen to be the next most important material failure energy dissipating mechanism after

‡‡ Values from this test are not used in the analysis due to doubt as to their validity

delamination, responsible for 8% to 9%. Shear fracture reaches a threshold once the laminate has been fully perforated, dissipating 2.44J of energy (Table 6). The level of energy dissipated is less than that for A laminate as the area of the shear cone is smaller due to the smaller shear cone angle.

Matrix cracking accounts for about 1% to 2% of energy dissipated due to material failure at all tests and in relation to impact energy is almost negligible.

Friction

Friction accounts for about 3% (1.37J) of dissipated impact energy at the ballistic limit and increases as more of the projectile shank passes through the laminate such that when it has passed through entirely it dissipates about 14.84J.

Strain

The energy dissipated due to strain energy at the ballistic limit is determined to be in the region of 31.4J or approximately 70% of the impact energy (approx. 45.8J) and almost 3 times the A laminate strain energy at its ballistic limit. The strain energy is therefore the primary reason for the difference in ballistic limits. The strain energy cannot be used simplistically as section 8.3 shows that the overall structural compliance can be different to the effective local compliance during a projectile impact event.

The inclusion of fibre pull-out energy would not affect these observations as its contribution to energy absorption is assumed to be about the same for both laminates.

8.3 Strain energy

The reason for the increased projectile kinetic energy dissipation performance of B laminate over A as a result of the change in stacking sequence has been shown to be due to an almost 3 fold increase in strain energy. Cantwell and Morton [5] indicate that laminate quasi-static compliance, should not play a significant role in absorbing the impact energy as laminate response is localised, which implies that localised straining is responsible for the strain energy. The manner in which the local response differs between the two laminates is not self-evident and so to address the possibility of overall laminate compliance being of significance was investigated.

8.3.1 *Quasi-static laminate compliance*

The compliance of the laminates to a deflection at the impact point was assessed by a simple finite element model (see section 6.2). The FEM simulated a point load and a standard compliance test such as a three point bend test. The FEM better represents loading applied by a tup or projectile and therefore better represents the contribution of quasi-static compliance. The test provides insight into the quasi-static compliance such that geometry and orientation dependent flexural moduli are accounted for.

The force versus displacement graphs (see Figure 53) are representative of the compliance of the structure, as are the plots of whole body strain energy versus displacement (see Figure 54). The plots show that A laminate clearly has the highest flexural modulus for a point load. The strain energy plot confirms this as A exhibits the greatest strain energy for the same displacement and as is therefore the better laminate for absorbing energy due to static/quasi-static point loading. The experimental impact results clearly indicate that B laminate absorbs the greatest amount of energy by straining, which implies that either the experimental results are wrong or confirms that the overall compliance of the structure plays no significant role in high velocity projectile impact energy dissipation.

The experimental results conform favourably to previous work (see section 8.4) and the possible sources of error have been addressed (see section 4.11) such that the results are considered valid. Any error in the experimental results is not considered to affect the main conclusion that strain energy is the mechanism which differentiates the performance of the two laminates.

The strain energy difference, since it is not due to the overall compliance of the laminates, must then be due to the localised response of the laminates.

8.3.2 *Local compliance*

The overall compliance of the tubes have been shown not to contribute significantly to the difference in strain energy. The difference in strain energy must therefore be a result of localised effects implying that the laminate compliance can differ from the overall compliance, however, this cannot literally be so. The difference in the local compliance to overall structural compliance is likely a result of the localised damage affecting the ability of the laminates to strain. Assessing the reasons for this difference requires identifying the

differences in damage and its development. The following discussion attempts to identify such reasons, however it is only a presumption as no numerical or conclusive experimental evidence is available.

The significant differences in damage between the two laminates are the delamination locations and shear fracture surfaces.

The total extent of delaminations appears to be of a similar magnitude for both laminate A and B, however the distribution of the delaminations is different. The delaminations in the B laminate are located at all the interfaces in the lower half of the laminate. In the A laminate not all the interfaces in the lower half of the laminate exhibit delaminations. Shear fracture in the A laminate, at its ballistic limit, has occurred through the entire laminate while in the B laminate it has not. The closest test on the B laminate to the A laminate's ballistic limit occurred at 76.69m/s at which point the shear fracture cone extends through 75% of the laminate. The A laminate is completely perforated at its ballistic limit (approx. 70m/s) while it would be reasonable to expect the B laminate to still have about 30% of the laminae intact immediately below the projectile. Since the B laminate has intact laminae able to carry load it is in a position to dissipate more energy due to straining. However, the difference in intact laminae is only local and so it can only expect to contribute a significant difference in strain energy if the laminate response is localised. Laminate response due to projectile impact is localised as shown in the discussion on laminate static compliance. The FE models (see Figure 49 and Figure 51) using continuum elements are able to illustrate the effect of contact (Hertzian) stresses, showing that laminate normal compressive failure occurs locally before any laminate deflection occurs. The suggests that failure will be slightly more extensive in the A laminate, although to a similar depth.

The projectile causes straining due to whole laminate deflection, stress waves and as it penetrates the laminate by pulling the delaminated portions of the laminae down with it (Figure 56). The greater number of delaminations in the lower half of the B laminate than the A laminate mean more laminae are able to deflect resulting in greater strain energy. The localised behaviour also reduces the effect of structural geometry on compliance, which combined with damage being localised may explain the lack of influence of overall compliance on strain energy.

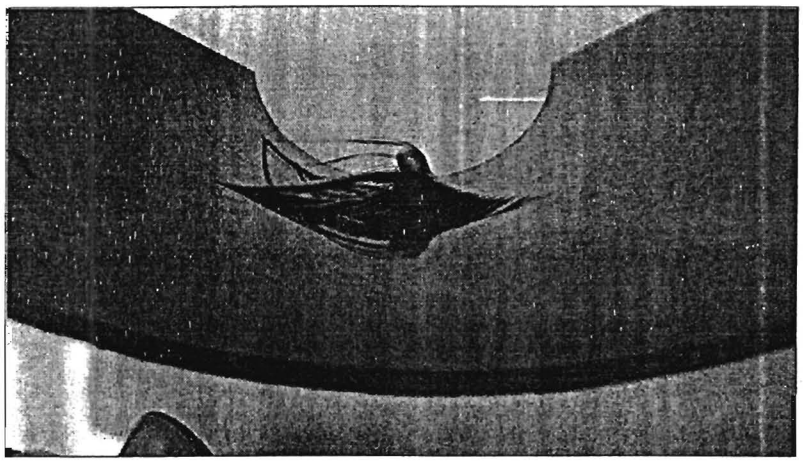

Figure 56 Local laminate straining

The possible reasons outlined for the difference in strain energies are by no means conclusive, however they are reasonable. It is recommended that this effect is best investigated using finite element analysis and implementing a comprehensive user material.

8.4 Comparisons to previous work

The application of previous research performed on flat panels cannot be applied directly to tubes as the geometry is different. Cantwell and Morton [5] clearly state that geometry is a fundamental parameter in determining the impact response of a composite component, although it is less important at high strain rates. The question remains whether some of the basic conclusions regarding damage development and distribution can be applied rigorously.

A comparison to previous work is another method of checking whether the methods employed in this investigation have produced valid results.

8.4.1 Delamination development

The delamination length distribution through the thickness of the laminate has been shown to be non-linear (Figure 29) which compares favourably to the work performed by Kitchen and Hemp [17] (Figure 11). The largest delamination always occurs at the distal interface as described by Hull and Shi [18].

The damage zone progresses from a wide base on the distal surface to a pinnacle at the impact point and as such conforms to the "fir tree" shape described in the theory.

The delamination distribution determined by applying the non-linear trends is seen to be almost linear. The t test values of 0.71 to 0.81 indicate that the extrapolated areas compare well to experimental values indicating that the method of extrapolation is valid. The delamination distribution is non-linear, however a linear interpolation between 2 delaminations of known area would appear to be an acceptable method as used by Mines et al. [21].

The total delamination area for the A laminate tests shows a linear relationship to impact energy pre-ballistic limit (Figure 33), which agrees well with work presented by Cantwell and Morton [5] (Figure 10). Hull and Shi [18] also conclude that total delamination area of impacted laminates shows a near linear correlation with the impact energy over the energy range investigated.

The delamination shapes observed correspond well to those described by Hitchen and Kemp [17]. The prevalence of "peanut" and cross-shaped delaminations in specimens impacted at higher velocities and oval shaped delaminations in those at lower velocities also corresponds well to previous work [17] Previous suggestions [17] that "peanut" shaped delaminations are a result of stress relief at the impact site due to fibre fracture appear to be confirmed. Shear fracture, which incorporates fibre fracture, is only prevalent at higher velocities as are the "peanut" shaped delaminations (Figure 31), the shear fracture may be relieving stress at the impact site causing the necking in the delaminations.

The shapes of the delaminations also correspond well to the previous literature [5], [9] which describes the influence of bounding laminae. The orientations of a delamination shape are influenced heavily by the orientation of the laminate furthest from the impact point bounding the delamination. The cross shaped delaminations lie at interfaces bound by $+35^{\circ}$ and -35° laminae and the cross arms are oriented in these directions. The oblong delaminations at interfaces 2 and 7 in the A laminates have a lower 90° lamina and upper 35° lamina and are oriented in the 90° direction.

The occurrence of delaminations also concurs well with theory such that the delaminations occur at interfaces with laminae of dissimilar orientations.

8.4.2 Intralamina matrix cracking and shear fracture

The development of intralamina matrix cracks through the thickness of the laminate has not been observed other than in the region immediately below the impact point. The cracks are not considered to play a significant role in the dissipation of impact energy, however, they do play a role in the formation of the shear fracture cone. The cone is likely to form along existing fault lines, which in the laminates under investigation are the intralamina cracks formed prior to perforation. The angle at which an intralamina matrix crack propagates has been observed [8],[18] to be dependent on the configuration of the laminate i.e. stacking sequence. The cone angle is seen to consistently differ between the A and B laminates and so agrees with the previous observations in flat panel impact.

The energy release rate for the shear fracture cone was determined from the single drop test to be between 21 and 25kJ/m^2, which compares favourably to values ascertained from literature of between 20 and 40kJ/m^2 (see section 3.6.2).

The significant energy dissipation mechanism, due to material failure has been shown in this investigation to be delamination, which agrees with the conclusion of Hull and Shi [18] that it dissipates the majority of the energy imparted to the laminate. Mines et al. [21], however, observed in a study on GFRP laminates that delamination dominated when the number of plies was greater than 12 and for 6 plies shear fracture/perforation energy dominated. A possible reason for their findings may well be that the ability of the 6 ply laminate to dissipate more energy is limited by the reduced number of interfaces available for delamination.

8.5 Suitability of FEM (ABAQUS)

The use of FEM to determine which of two stacking sequences results in the best projectile kinetic energy dissipater is, as has been shown, an exercise in impact damage analysis and local laminate behaviour. If, as is suggested in section 8.3.2, the difference in energy dissipated by straining is a result of the damage affecting the local behaviour/compliance then a FE analysis requires a comprehensive material model. ABAQUS provides the capability of a user defined material model and has been used before to model composite material failure. Defining a composite material model and validating it is a complex and tedious task not suited to a general engineering analysis. How suited then is ABAQUS to aiding such an analysis with its standard features?

A model suited to analysing impact damage requires continuum elements for more accurate values of laminate normal stress and stresses at the interfaces. A separate layer of elements, at least, is required for every successive lamina with a change in orientation. Laminates being extremely thin relative to their width and length, result in an extremely large numbers of elements in order to satisfy element aspect ratios and distortion requirements. Modelling a whole structure, even if it is as simple as a tube, results in extremely large models with impracticably long computational times. ABAQUS is therefore best suited to investigating the localised behaviour of a structure due to impact. The behaviour of a laminate due impact is, however, very localised and much of the damage is initiated before any significant structural response occurs. The current continuum model is an example of this as it is able to show the significant contact stresses (Figure 49 and Figure 51) and stress waves (Figure 11 and Figure 50) that occur before the structure deflects significantly. It is also able to show differences of stress distribution as a result of laminate changes as evidenced by the slightly lower level of failed B laminate compared to A at a 72.57m/s impact. ABAQUS Explicit could therefore provide useful insight, in conjunction with a valid user material, into the initiation of damage and the early stages of its propagation. The insights combined with a greater understanding of the affect of damage on localised response of laminates to impact would aid an engineer in making judgements as to the best performing laminates.

Modelling projectile impact events with shell elements in ABAQUS Explicit is also feasible with a user defined material, however, it would not take into account stresses and strains normal to the laminate. The ability of shell elements to illustrate the stress distribution through the laminate is more limited than the continuum element model. Shell elements are therefore not suited for a comprehensive material failure model or for gaining insight into the localised behaviour. Obtaining qualitative results as opposed to quantitatively accurate results for the benefit of better computational times is therefore the only practical reason for using shell elements. The process of defining a user material, as well as the user material model, would also require extensive validation before being able to be used.

ABAQUS Standard is only suited to static and quasi-static loading and is suitable for qualitative and occasionally quantitative analyses. The current study used it to show the overall compliance played no role in projectile energy impact dissipation. ABAQUS

standard is definitely suited to such an analysis as well as low velocity quasi-static impact loading.

The judicious use of ABAQUS in its standard format can aid an analysis, however, without a proven user material it will not reduce the need for experimentation. In the current study it served to eliminate analytical analysis of the tubes flexural modulus as well as the physical compliance testing. It also provided some insight into failure due to contact stresses. The use of ABAQUS did not, however, affect the main conclusions of the analysis which were based almost solely on the experimental data and it served only to reinforce the conclusions.

Chapter 9. Conclusions

The difference in laminate stacking sequence results in one laminate being a better projectile kinetic energy dissipater as a result of an increase in local strain energy.

General

The investigation of the effect of a filament wound laminate's ability to dissipate the kinetic energy of an impacting projectile, having a mass of 10.15 grams and hemispherical head, was successful. It fulfilled its primary aims of determining the best of two stacking sequences and the identifying the main reasons for the difference in performance. The thesis also addresses the secondary aims of; describing the various energy dissipation mechanisms, their roles in the dissipation of projectile energy, and the agreement of observations to previous work.

The experimental set-up used is shown to be reasonable and any error shown not to affect the observations and conclusions of the analysis. The effect of systematic error on the analysis and its conclusions is discounted as it was determined to be at worst a consistent over-estimate of features measured from the X-rays. The systematic error implies that energy dissipated by material failure may be less than has been determined, which would serve only to emphasise the role of strain energy.

The main experimental results relating to damage distribution and damage size in relation to impact energy have been shown to be consistent with previous work on flat panels, further enhancing confidence in the experimental results.

The role and suitability of using finite element modelling, namely ABAQUS, in such an investigation is also discussed and recommendations made, satisfying another aim of this investigation.

Primary aims

The laminate with the stacking sequence $[90^{\circ}_6,(+35^{\circ},-35^{\circ})_3]$ (B laminate) is the better overall projectile kinetic energy dissipater than the laminate with the stacking sequence of $[+35^{\circ}, -35^{\circ},90^{\circ}_3, +35^{\circ},-35^{\circ},90^{\circ}_3, +35^{\circ}, -35^{\circ}]$ (A laminate). The A laminate is found to be a better projectile kinetic energy dissipater only for impact velocities that fall in the range between the A laminate ballistic limit and the B laminate ballistic limit.

The ballistic limit for the A laminate is determined to be approximately 70m/s while for the B laminate it is approximately 95m/s, for the projectile used in this investigation. The difference in ballistic limit being a basic indication that the B laminate is the better projectile kinetic energy dissipater.

The difference in energy dissipation between the A laminate and the B laminate is accounted for by a single energy dissipation mechanism, strain energy. The strain energy difference is shown not to be a result of overall structural compliance but due to a localised strain effect. The cause of the difference in localised straining cannot be concluded, however, it is hypothesised that it is a result of the differences in local damage.

Material Damage

The significant energy dissipating damage mechanism is shown to be delamination followed by laminate shear fracture. Matrix cracking accounts for a small yet consistent proportion of the energy dissipated by material fracture.

The total energy dissipated by material fracture for A laminate is linearly dependent on the impact energy up to the ballistic limit, however it does not exhibit any dependence beyond the limit. The ballistic limit is a threshold in the development of material damage, which is strongly dependent on impact energy up to that limit.

The threshold in damage development is a result of delamination size increasing with impact energy up to the ballistic limit and the extent of shear fracture being constant post-ballistic limit.

The laminate stacking sequence influences the total delamination area, delamination locations and the shear fracture area. The total energy dissipated by material failure for impacts beyond A laminate's ballistic limit is, however, similar in both A and B laminates.

ABAQUS FEM

The use of FEM in the analysis has been useful, although not critical, in obtaining the significant observations and conclusions.

The use of ABAQUS Explicit to model the entire volume of a laminate structure that responds to projectile impact is computationally very expensive.

ABAQUS Explicit, with its standard features, is not suited to modelling projectile impact damage. The development of a process for composite user material development as well as a validated CFRP material model is required in order to effectively model projectile impact damage in fibre reinforced laminates.

In order to analyse a laminate's ability to dissipate projectile kinetic energy the failure model must not only predict failure but also account for the energy dissipated as a result of failure.

Chapter 10. Recommendations

Further work

The difference in projectile kinetic energy dissipation between the two laminates investigated has been identified as due to a difference in local straining. Possible reasons for this difference in local straining have been suggested, however, additional work is required to adequately ascertain the cause of the difference in local strain energy.

The rate of increase of damage with impact energy appears to reduce post-ballistic limit, however to what level has not been ascertained. Further testing post-ballistic limit would do much to determine the relationship of damage to projectile impact energy. A greater number of tests over the whole range of impact velocities investigated would enhance the statistical validity of the investigation.

It is suggested that the total energy absorbed by material damage in both the A and B laminates reaches a similar threshold. The implication being that although the stacking sequence affects the strain energy it has no significant effect on the total energy absorbed by material failure. Further work is needed to investigate whether a material failure energy threshold exists for a given volume of material irrespective of stacking sequence

Experimental set-up

The ballistic testing of curved laminates has no apparent standard for ensuring consistent boundary conditions as some studies utilise fully clamped specimens or leave them free-standing on a flat surface or in a cradle. The development of standard clamping conditions and procedures would enhance the validity of comparisons made between various studies and simplify the testing process.

The ability to measure the residual velocity of a projectile is essential for accurate assessment of the total projectile kinetic energy dissipated by a laminate at impact velocities below and beyond the ballistic limit. The accurate assessment of ballistic limit also requires the measurement of residual velocity post ballistic limit. The development of procedures and sensors to reliably measure the projectile residual velocity would prove a worthwhile project.

In order to validate any numerical models experimental values of stress, strain, damage extent, and laminate displacement are required. The development and implementation of

some form of measurement of some or all of these aspects is required for development of a validated user material for finite element modelling. High velocity instrumented impact test rigs are in use, however, they are not common mainly as a result of the expense of the load cell used. A cost-effective approach to this problem may be to focus on a single measurable feature, such as the maximum deflection of a laminate or the displacement profile through the impact point. The validation of a user material would not be comprehensive yet would still lend confidence to its use in an investigation.

Non-destructive testing and evaluation

The most practical means of assessing impact damage throughout a laminate are non-destructive techniques such as ultrasound C-scanning and X-raying, yet such facilities are not readily available. The time cost of relying on industrial sponsors to conduct the necessary X-ray imaging added significantly to the project schedule. The lack of experience in interpreting the results of such non-destructive testing has resulted in increased evaluation time. It has also resulted in a systematic error such that damage extent may have been overestimated.

The acquisition of both ultrasound and X-ray imaging facilities or access to such facilities by the University of Cape Town would do much to aid the process of investigating damage. The regular use of such tools would help develop the necessary experience in interpreting their results and so reduce error and analysis times.

The investigation and implementation of a variety of X-ray techniques, such as stereoscopy, would further aid analyses of damage through the laminate.

Finite element modelling

The development of a user fibre reinforced composite material for ABAQUS is required in order to use it to investigate impact damage and its effects. The development of such a complex user material requires great care and testing before it can be used with assurance. The process of developing a user material as well as the user material needs to be developed, as a proven and documented process would be of benefit in developing other user materials, whether simple or complex. The development of such a process would be a useful project and as part of such a project, the development of a user material could serve as a case study.

References (In alphabetical order)

[1] *ABAQUS Explicit and Standard Operating and Theory Manuals*, Stichting Mathematisch Centrum,1995

[2] Abrate, S., *Impact on Composite Structures*, Cambridge University Press

[3] Ashbee.K, *Fundamental Principles of Fiber Reinforced Composites*, Technomic,

[4] Belingardi, G., Gugliotta, A., Vadori, R., *Numerical Simulation of Fragmentation of Composite Material Plates Due to Impact*, Int. J. Impact Engng,1998, 21(5), 335-347

[5] Cantwell, W.J., Morton, J., *The impact resistance of composite materials - a review*, Composites, 1991, 22(5)

[6] Cantwell, W.J., *The influence of fibre stacking sequence on the high velocity impact response of CFRP*, Jnl of Materials Science Letters, 1988, 7, 756-758

[7] Chamis, C.C., Hanson, M.P., Serafini, T.T., *Impact resistance of unidirectional fibre composites*, Composite Materials: Testing and Design (2nd conf.), 324-349

[8] Choi, H.Y., Wang, H.S., Chang, F., *Effect of Laminate Configuration and Impactor's Mass on the Initial Impact Damage of Graphite/Epoxy Composite Plates Due to Line-Loading Impact*, Jnl Composite Materials, 1992, 26(6), 804 – 827

[9] Choi, H.Y., Chang, F.K., *Impact Damage Resistance of Graphite/Epoxy Laminated Composites*, Polymer Engng and Science, 1991, 31(18), 1294-1300

[10] Davies, G.A.O, Zhang, X., Zhou, G., Watson, S., *Numerical modelling of impact damage*, Composites, 1994, 25(5), 342-350

[11] Dee, A.T., Vinson, J.R., Leon, G., *High strain-rate mechanical properties of a torospherical shell composed of IM7/E7T1-2 graphite epoxy composite*, www.ud.ac,

[12] Evans, K.E., Alderson, K.L., *Low velocity transverse impact of filament-wound pipes: Part 2. Residual properties and correlations with impact damage*, Composite Structures, 1992, 20, 47-52

[13] Franz, T., *CERECAM AMU508Z course notes*, University of Cape Town,1999

[14] Goldsmith, W.,*REVIEW Non-ideal projectile impact on targets*, Int. J. Impact Engng, 1999, 22(2-3), 95-395

[15] Hearn, E.J., *Mechanics of Materials 2*,Butterworth/Heineman, 1999

[16] Highsmith, A.L, Ledbetter, F.E., Nettles, A., Russel, S.S., *Low Velocity Impact Damage in Filament-Wound Composite Pressure Bottles*, Jnl of Comp. Tech. & Research, 1996, 18(2), 109-117

[17] Hitchen, S.A., Kemp, R.M.J., *The effect of stacking sequence on impact damage in a carbon fibre/epoxy composite, Composites*, 1995, 26, 207-214

[18] Hull, D., Shi, Y.B., *Damage mechanism characterisation in composite damage tolerance investigations*, Composites Structures, 1993, 23, 99-120

[19] Jenq, S.T., Jing, H.-S., Chung, C., *Predicting the ballistic limit for plain woven glass/epoxy composite laminate*, Int. J. Impact Engng, 1994, 15, 451-464

[20] Jones, N, *Structural Impact*, Cambridge University Press, 1989

[21] Mines, R.A.W., Roach, A.M., Jones, N., *High velocity perforation behaviour of polymer composite laminates*, Int. J. Impact Engng, 1999, 22, 561-688

[22] Phillips, D.C., Harris, B., *Strength, Toughness and Fatigue Properties*, Polymer Engineering Composites, Applied Science Publishers, 1977, 45-154

[23] Parsons, A., Somchem / Denel, private communication

[24] Qian, Y.,Swanson, S.R., *Experimental Measurement of Impact Response in Carbon/Epoxy Plates*, AIAA Jnl, 1990, 28(6), 1069-1074

[25] www.toray.com

[26] Franz, T., CERECAM, University of Cape Town, private communication

APPENDIX A: Experimental results

Key	
S-O	Slightly Off
O-T	On Target
OK	Satisfactory i.e. not noticeably off target
A-O-T	Apparently On Target
*	velocity of between 135 & 140 m/s
GAS	Gas gun test, Laminate A, Seam impact
GAOS	Gas gun test, Laminate A, Off Seam impact
GBS	Gas gun test, Laminate B, Seam impact

Table 7 Test results

Test No.	Time	Distance	Velocity	Mass	E_i	Tag
	msec	m	m/s	kg	J	
A1	1.480	0.050	33.78	0.01015	5.79	GAS
A2	1.354	0.050	36.93	0.01015	6.92	GAOS
A3	1.197	0.050	41.77	0.01016	8.86	GAS
A4	0.899	0.050	55.62	0.01015	15.70	GAS
A5	0.883	0.050	56.63	0.01015	16.27	GAOS
A6	0.847	0.050	59.03	0.01015	17.69	GAOS
A7	0.805	0.050	62.11	0.01017	19.62	GAS
A8	0.689	0.050	72.57	0.01015	26.73	GAOS
A9	0.635	0.050	78.74	0.01015	31.47	GAS
A10	0.577	0.050	86.66	0.01010	37.92	GAS
B1	0.652	0.050	76.69	0.01012	29.76	GBS
B2	0.541	0.050	92.42	0.01015	43.35	GBS
B3	0.448	0.050	111.61	0.01017	63.34	GBS
B4	0.360	0.050	138.89	0.01015	97.90	GBS

Table 7 lists the mass of each test projectile and the time taken to travel between the sensors of the velocity sensor. Impact energy and velocity are also listed as is the impact location.

Table 8 Laminate A: Tangential X-ray length measurements

Velocity	Depth	Interface	Length
m/s	mm		cm
33.78	0.22	10	1.75
33.78	0.13	6	0.88
33.78	0.03	2	0.38
36.93	0.22	10	1.76
36.93	0.11	5	1.55
41.77	0.22	10	2.02
41.77	0.12	6	1.95
41.77	0.10	5	1.14
41.77	0.04	3	0.51
55.62	0.22	10	2.96
55.62	0.12	6	2.68
55.62	0.11	5	0.77
55.62	0.08	4	0.50
56.63	0.23	11	3.03
56.63	0.12	5	2.77
59.03	0.12	6	2.82
59.03	0.24	11	2.89
59.03	0.11	5	1.01
62.11	0.22	10	3.80
62.11	0.13	7	2.77
62.11	0.12	6	0.87
62.11	0.11	5	0.65
72.57	0.23	11	6.14
72.57	0.13	6	2.81
72.57	0.12	5	1.59
78.74	0.23	11	4.60
78.74	0.13	7	1.99
78.74	0.12	6	0.60
78.74	0.07	4	0.62
86.66	0.23	11	5.15
86.66	0.13	7	2.01
86.66	0.11	5	1.35

Table 8 lists the laminate A measurements from the tangential x-rays, giving the depth and length of delaminations, and the probable interface location.

Table 9 Laminate B: Tangential X-ray length measurements

Velocity	Depth	Interface	Length
m/s	mm		cm
76.69	0.22	10	7.28
76.69	0.17	8	2.46
76.69	0.14	7	1.12
92.42	0.24	11	9.11
92.42	0.20	9	2.49
92.42	0.16	7	1.67
111.61	0.23	11	7.73
111.61	0.19	9	2.02
111.61	0.15	7	1.73
138.89	0.23	11	7.85
138.89	0.19	9	2.14
138.89	0.15	7	1.13

Table 9 lists the laminate B measurements from the tangential x-rays, giving the depth and length of delaminations, and the probable interface location.

Table 10 Axial image length measurements

Velocity	Interface	length
m/s		cm
59.03	2	0.13
59.03	3	0.14
59.03	7	0.26
59.03	8	0.18
78.74	2	0.27
78.74	3	0.24
78.74	7	0.50
78.74	8	0.37
76.68	2	0.14
76.68	3	0.18
76.68	4	0.24
76.68	5	0.42

Table 10 laminae separation measurements and interfacial locations from axial images.

Table 11 Laminate A: Interface delamination areas

Velocity	Interface	Trend Ratio	Trend Areas	Measured Areas
m/s			cm^2	cm^2
33.78	11.00	1.00	9.23	9.25
33.78	6.00	0.57	5.28	6.01
33.78	5.00	0.48	4.46	
		Total	18.97	
36.93	11.00	1.00	11.82	11.85
36.93	6.00	0.57	6.76	6.94
36.93	5.00	0.48	5.72	
		Total	24.30	
41.77	11.00	1.61	29.65	18.46
41.77	6.00	0.78	14.43	15.96
41.77	5.00	0.63	11.62	
		Total	55.71	
55.62	11.00	1.54	40.30	26.15
55.62	6.00	0.46	12.15	14.40
55.62	5.00	0.32	8.47	
		Total	60.92	
56.63	11.00	1.54	45.82	29.73
56.63	6.00	0.46	13.81	15.37
56.63	5.00	0.32	9.63	
		Total	69.26	
59.03	11.00	1.54	51.56	33.45
59.03	6.00	0.46	15.54	14.83
59.03	5.00	0.32	10.83	
		Total	77.92	
62.11	11.00	2.02	76.54	37.94
62.11	6.00	0.39	14.86	13.37
62.11	5.00	0.24	9.08	
		Total	100.48	
72.57	11.00	1.04	92.71	89.44
72.57	6.00	0.39	35.03	21.76

Table 11 continued ..				
72.57	5.00	0.29	26.14	
		Total	153.89	
78.74	11.00	0.89	64.22	72.20
78.74	6.00	0.24	17.57	19.32
78.74	5.00	0.16	11.90	
		Total	93.69	
86.66	11.00	0.95	87.613	92.040
86.66	6.00	0.34	30.935	
86.66	5.00	0.25	22.618	
		Total	141.166	

Table 11 lists the delamination area determined for various interfaces.

Table 12 Laminate B: Delamination areas and t test probability value

Velocity	Interface	Trend Ratio	Trend Areas	Measured Areas
m/s			cm^2	cm^2
76.69	11.00	1.34	120.40	89.90
76.69	10.00	1.05	94.20	88.80
76.69	9.00	0.80	71.82	27.94
76.69	8.00	0.59	53.03	6.95
76.69	7.00	0.42	37.60	
		Total	377.05	
			T test	0.27
92.42	11.00	0.73	67.19	92.12
92.42	10.00	0.57	52.75	92.32
92.42	9.00	0.44	40.37	30.68
92.42	8.00	0.33	29.94	11.10
92.42	7.00	0.23	21.33	
		Total	211.60	
			T test	0.71
111.61	11.00	0.84	62.11	73.94
111.61	10.00	0.66	48.95	71.00
111.61	9.00	0.51	37.63	16.60
111.61	8.00	0.38	28.04	7.60
111.61	7.00	0.27	20.09	2.90
		Total	196.82	
			T test	0.79
138.89	11.00	0.91	87.82	96.50
138.89	10.00	0.67	64.64	80.10
138.89	9.00	0.48	46.06	20.94
138.89	8.00	0.33	31.54	7.34
138.89	7.00	0.21	20.53	
		Total	250.59	
			T test	0.81

Table 12 lists the delamination area determined for various interfaces

Table 13 Laminate A: Matrix cracking area

Velocity	E_i	Area	Correlation
m/s	J	m^2	
33.78	5.79	4.53E-05	
36.93	6.92	8.56E-05	
41.77	8.86	1.07E-04	
55.62	15.70	2.10E-04	
56.63	16.27	1.69E-04	
59.03	17.69	2.23E-04	
62.11	19.62	2.43E-04	
72.57	26.73	4.82E-04	
78.74	31.47	4.89E-04	
86.66	37.92	6.88E-04	0.98

Table 13 lists the approximated matrix cracking area for each laminate A test and the correlation (0.98) of the areas with impact energy.

Table 14 Laminate B: Matrix cracking area

Velocity	E_i	Area	Correlation
m/s	J	m^2	
76.69	29.76	6.33E-04	
92.42	43.35	7.44E-04	
111.61	63.34	5.06E-04	
138.89	97.90	5.80E-04	-0.49

Table 14 lists the approximated matrix cracking area for each laminate B test and the correlation (-0.49) of the areas with impact energy.

Table 15 Laminate A: Shear cone angle

Velocity	E_i	**Angle**	**Standard deviation**	**Confidence**
m/s	J	degrees		
59.03	17.69	74.86		
62.11	19.62	73.37		
72.57	26.73	73.26		
78.74	31.47	72.24		
86.66	37.92	72.86		
	Average	73.32	0.97	0.85

Table 15 lists the shear cone angle measured for each laminate test which exhibited shear fracture, as well as the standard deviation and confidence o the measurements.

Table 16 Laminate B: Shear cone angle

Velocity	E_i	**Angle**	**Standard deviation**	**Confidence**
m/s	J	degrees		
76.69	29.76	51.09		
92.42	43.35	51.70		
111.61	63.34	48.22		
138.89	97.90	56.06		
		51.77	3.24	3.17

Table 16 lists the shear cone angle measured for each laminate test which exhibited shear fracture, as well as the standard deviation and confidence o the measurements.

Laminate A: Trend figures

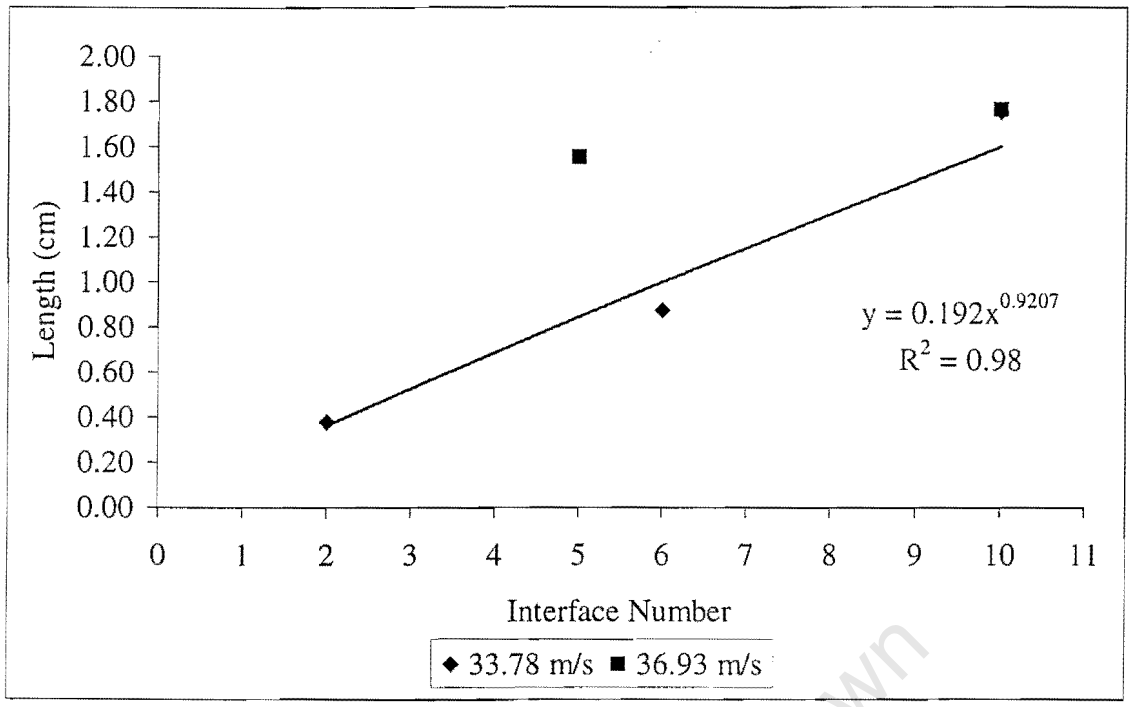

Figure 57 33.78 m/s test trend and correlation

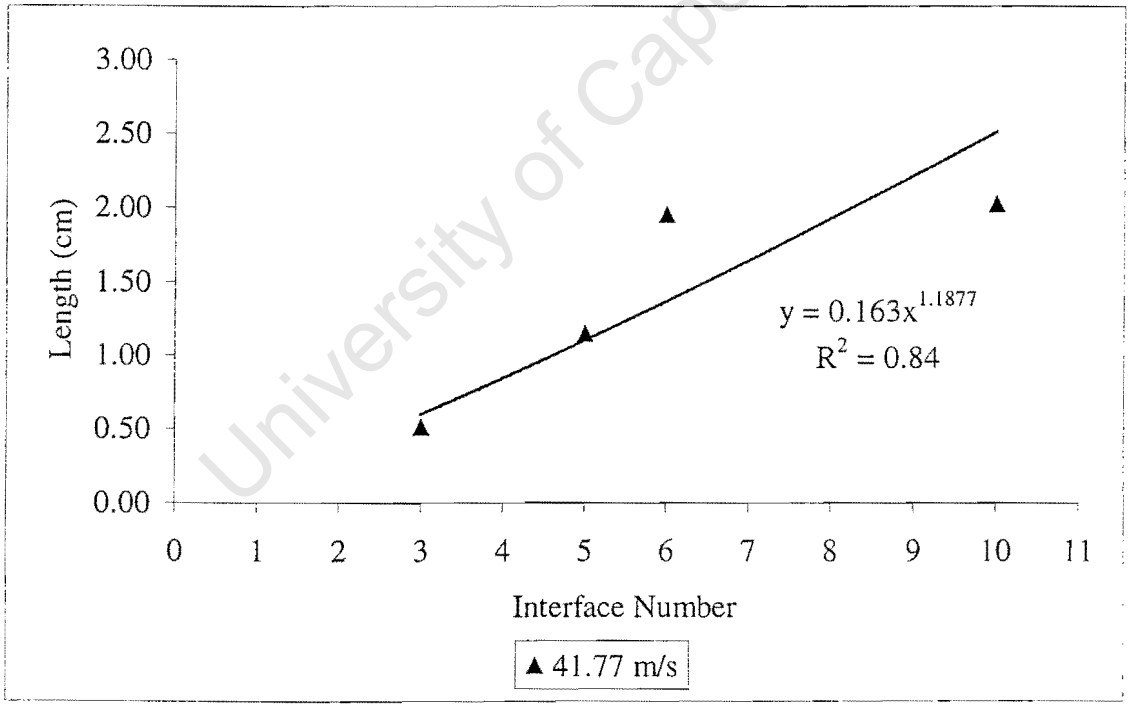

Figure 58 41.77 m/s test trend and correlation

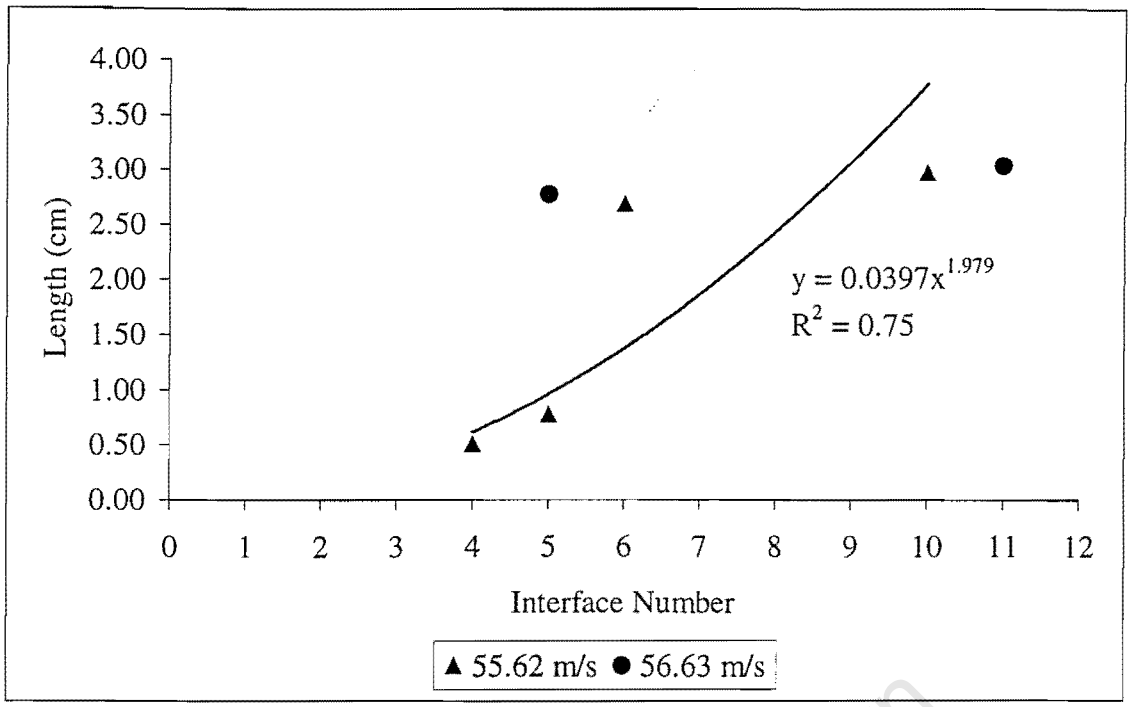

Figure 59 55.62 m/s test trend and correlation

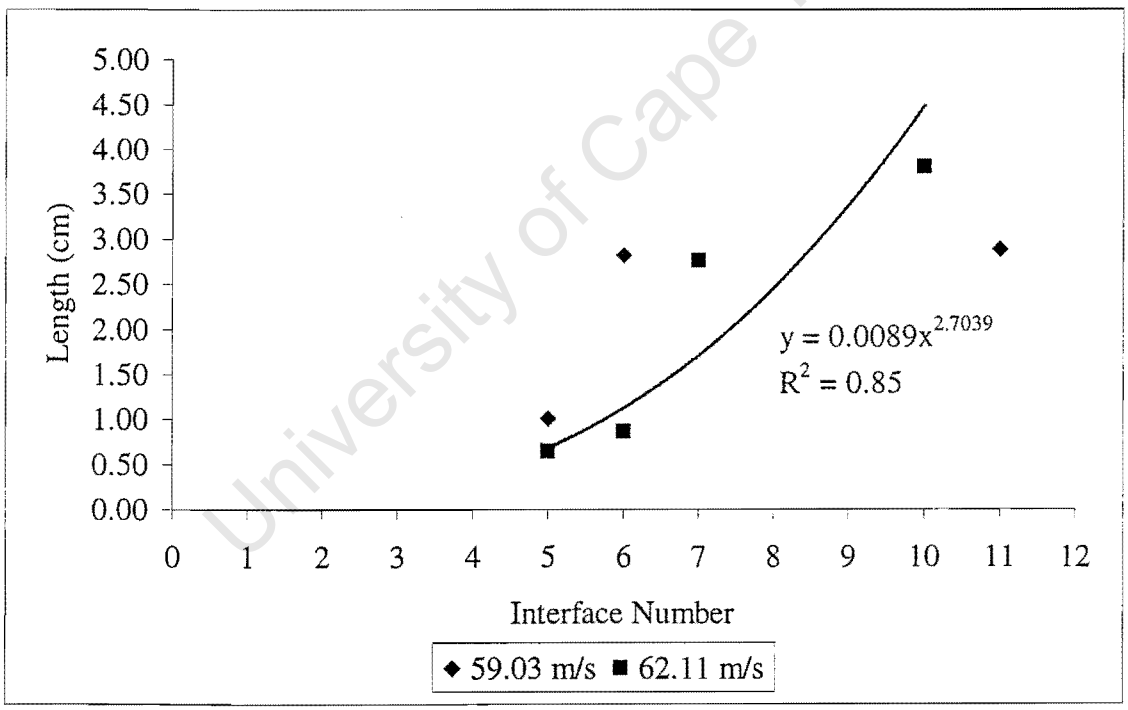

Figure 60 62.11 m/s test trend and correlation

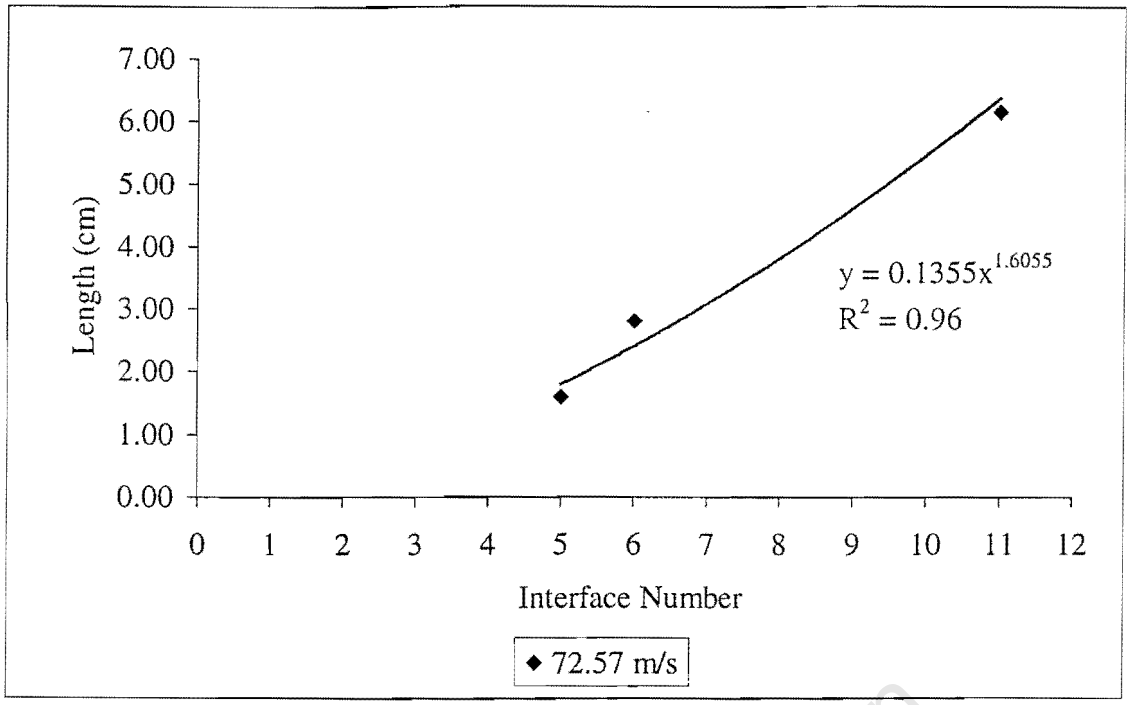

Figure 61 72.57 m/s test trend and correlation

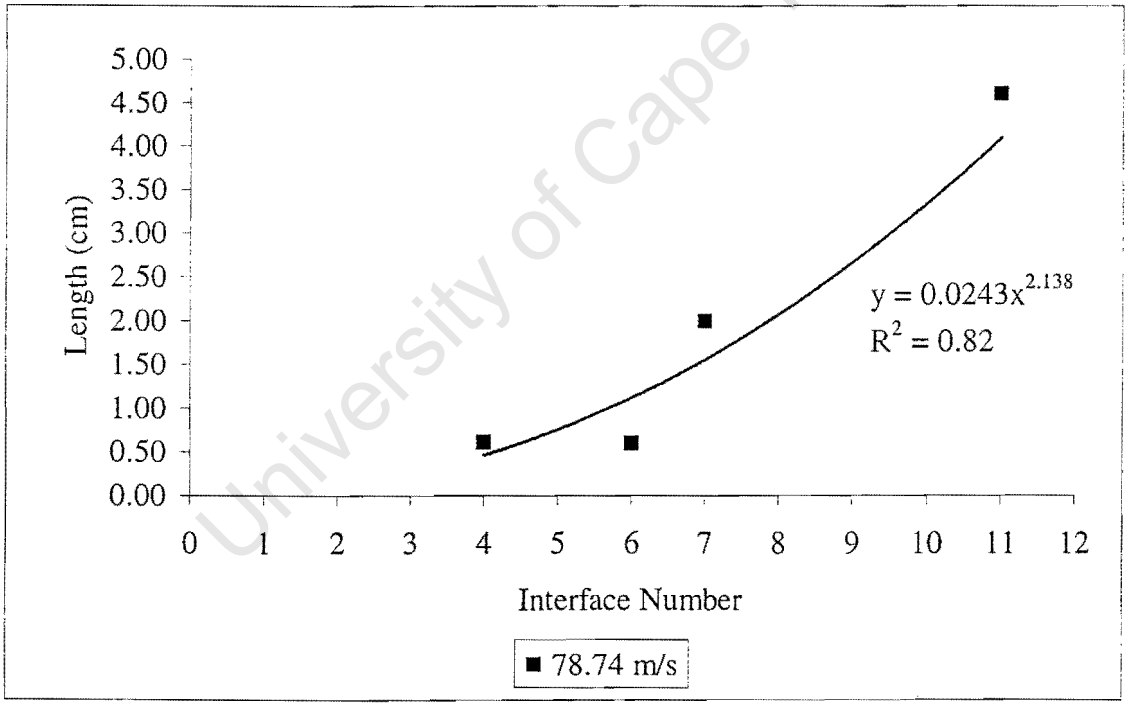

Figure 62 78.74 m/s test trend and correlation

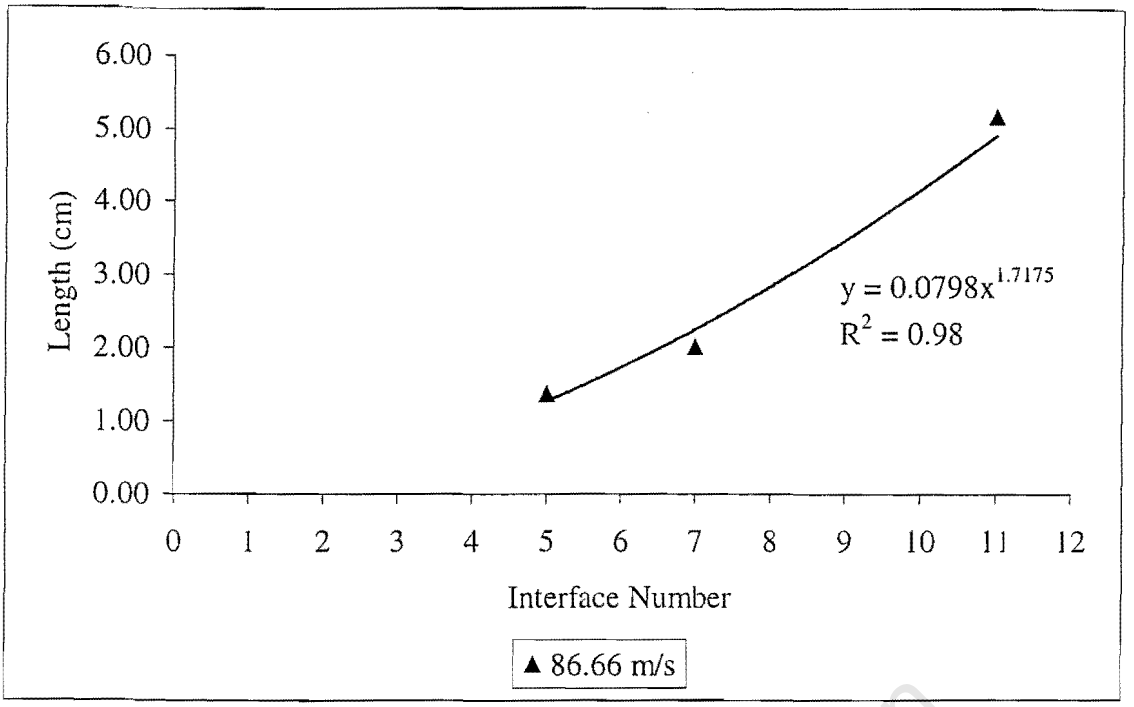

Figure 63 86.66 m/s test trend and correlation

Laminate B: Trend figures

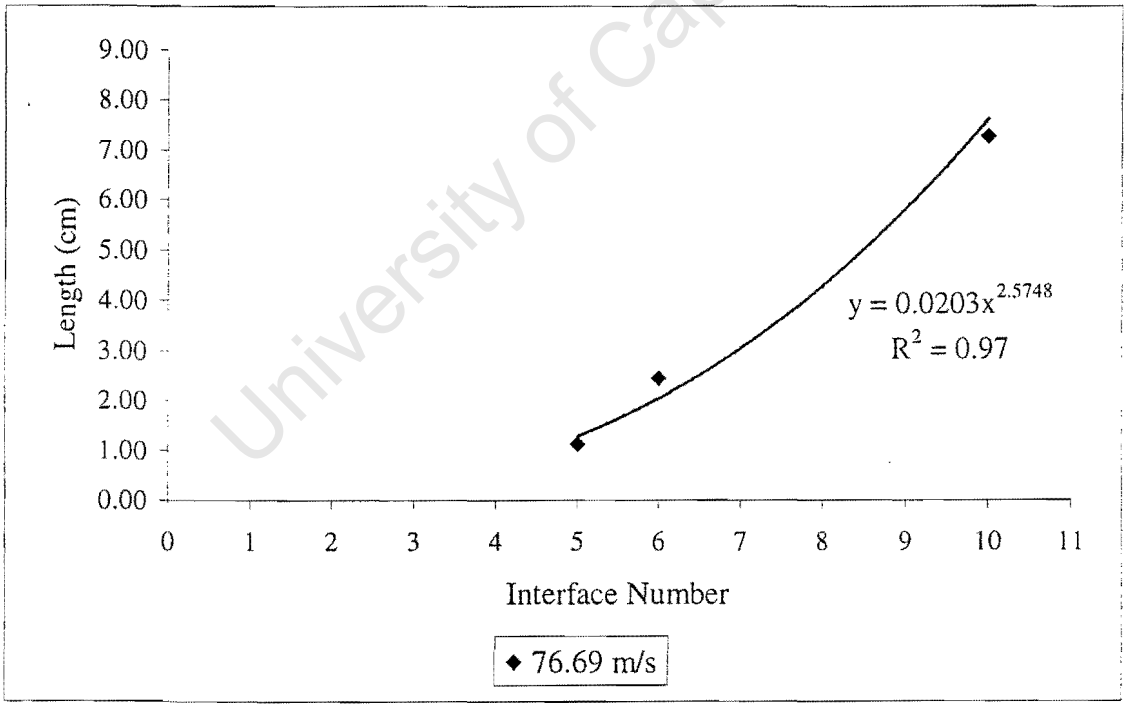

Figure 64 76.69 m/s test trend and correlation

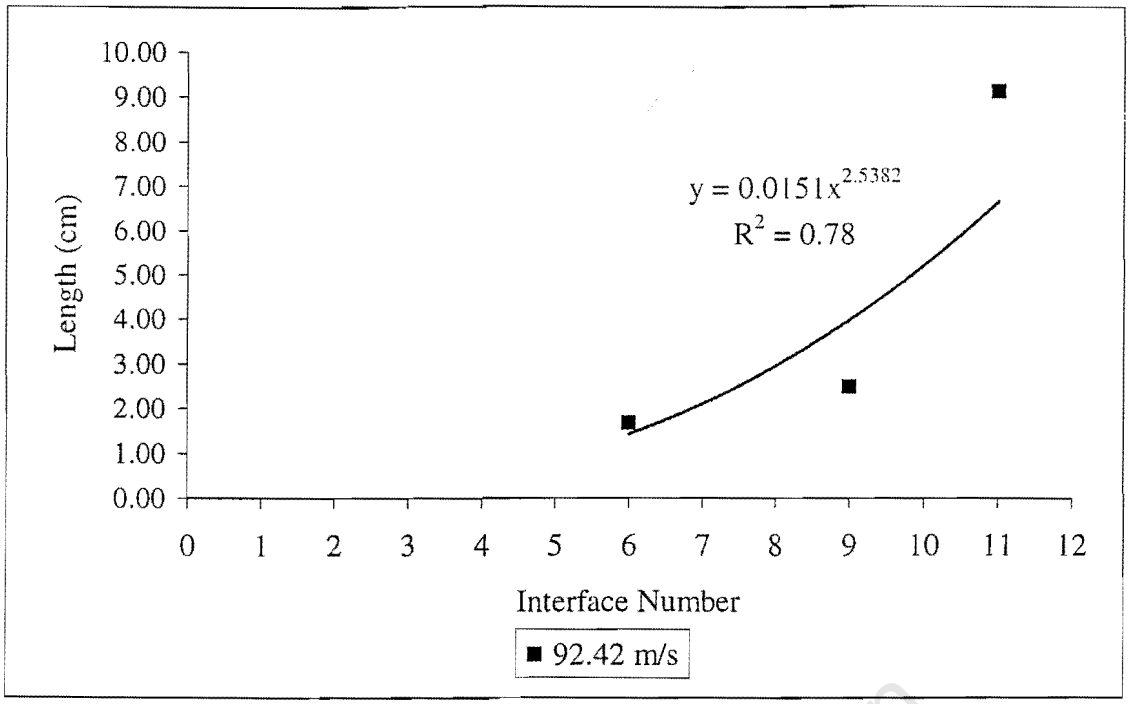

Figure 65 92.42 m/s test trend and correlation

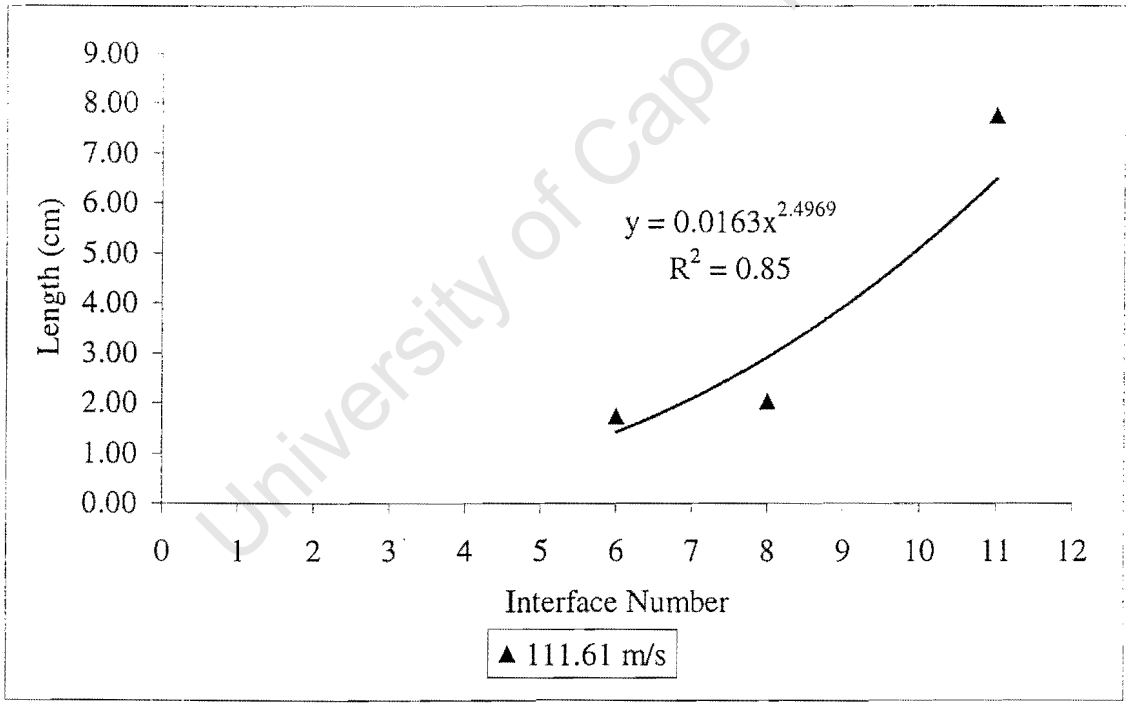

Figure 66 111.61 m/s test trend and correlation

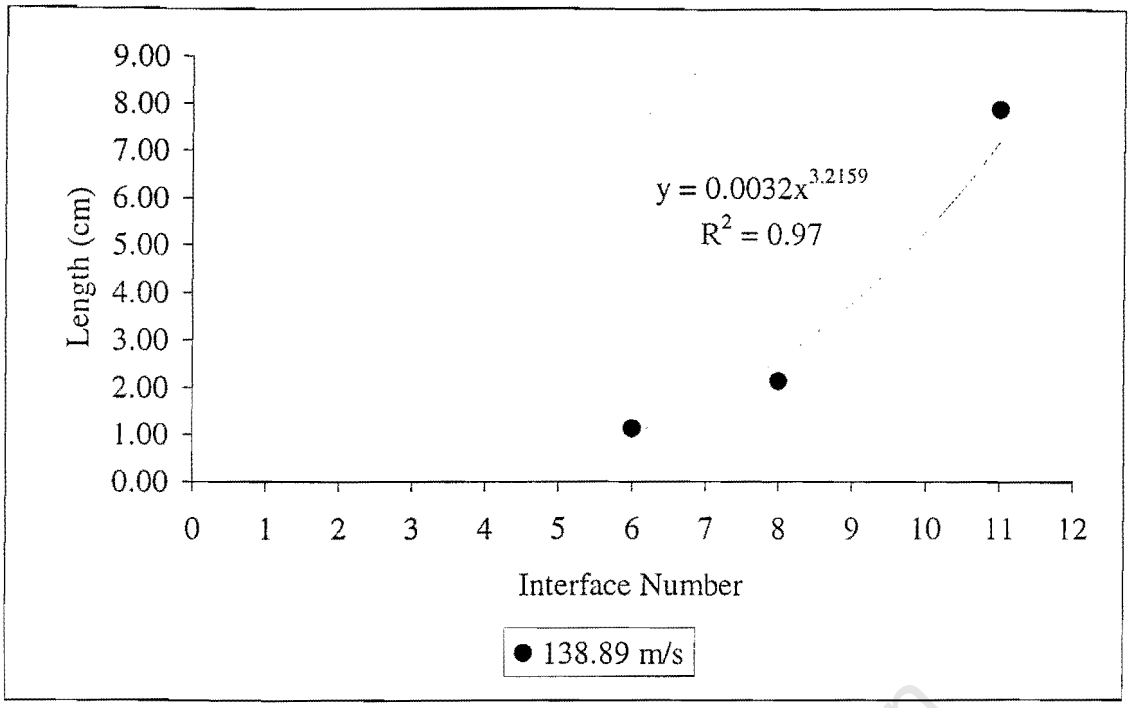

Figure 67 138.89 m/s test trend and correlation

APPENDIX B: Specimen images

Laminate A Specimens

Specimen Impacted at 33.78m/s or 5.79J

Inverted Radial X-ray Image

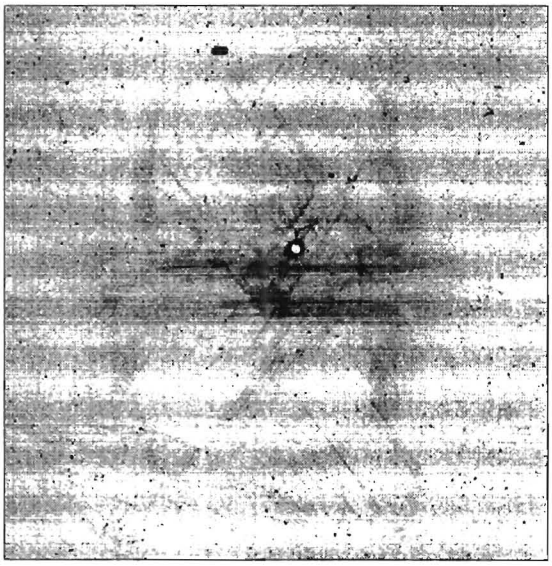

AutoCAD Measurement Radial X-ray

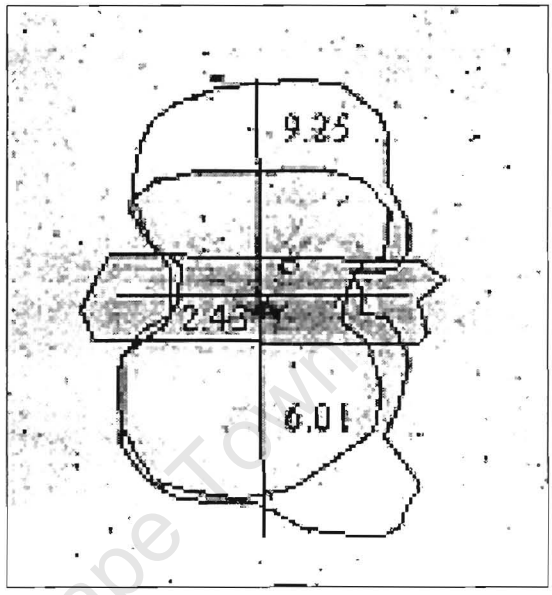

Tangential X-ray Image

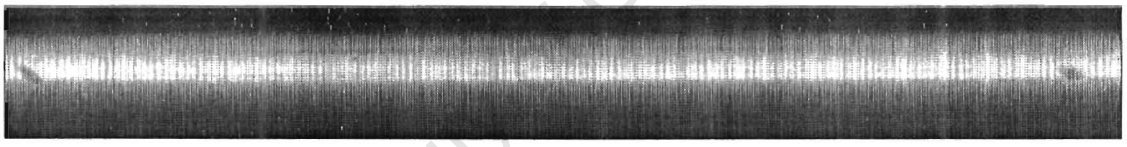

AutoCAD Measurement of Tangential X-ray

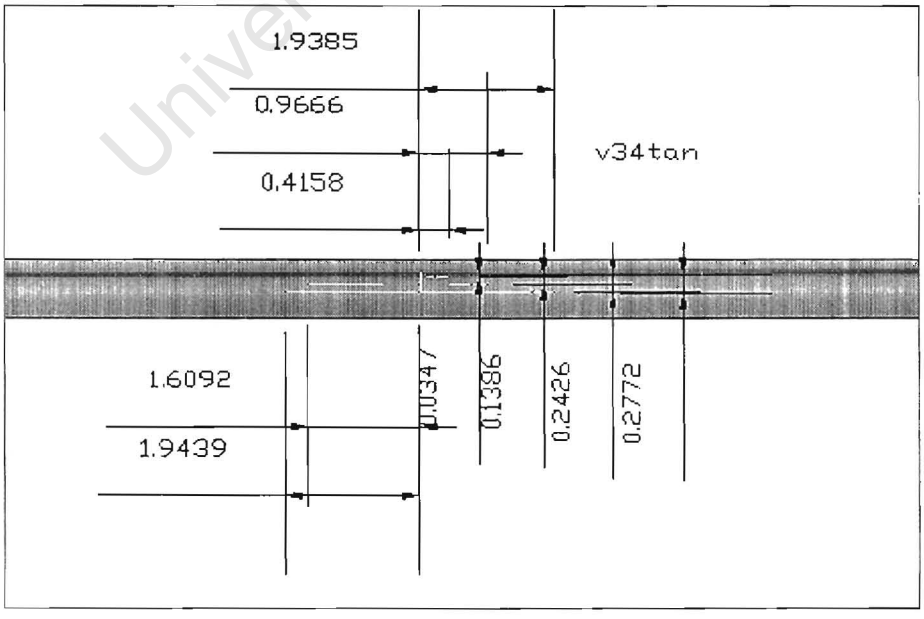

Specimen Impacted at 36.93m/s or 6.92J

Inverted Radial X-ray Image

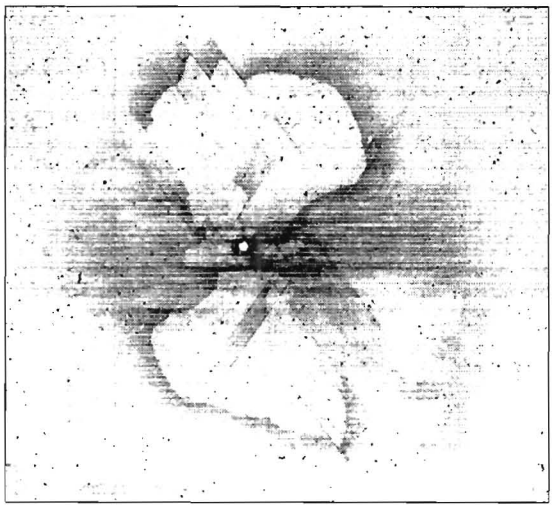

AutoCAD Measurement Radial X-ray

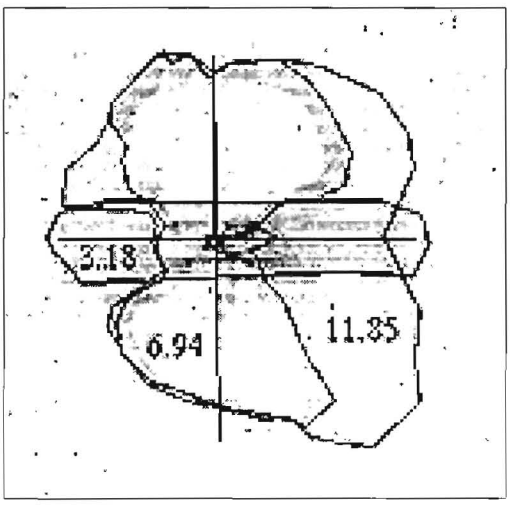

Tangential X-ray Image

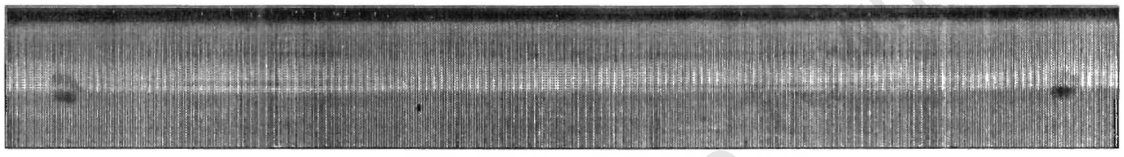

AutoCAD Measurement of Tangential X-ray

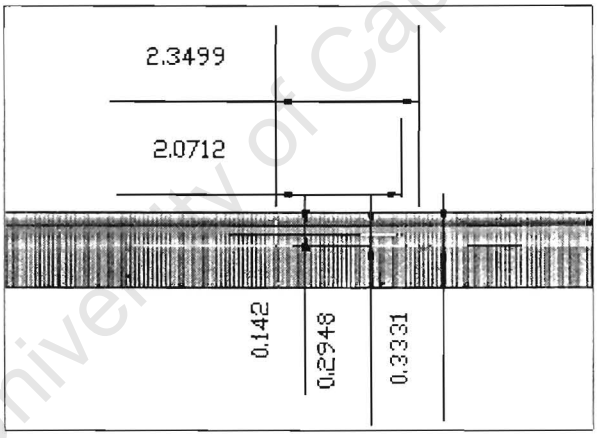

Specimen Impacted at 41.77m/s or 8.86J

Inverted Radial X-ray Image

AutoCAD Measurement Radial X-ray

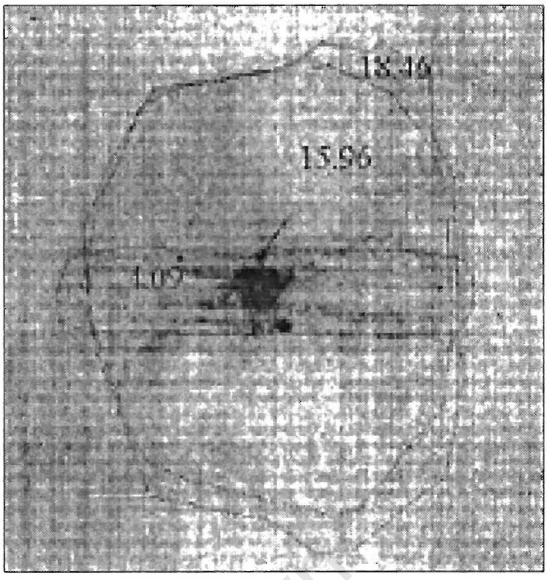

Tangential X-ray Image

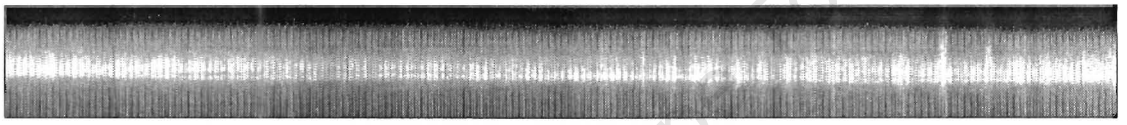

AutoCAD Measurement of Tangential X-ray

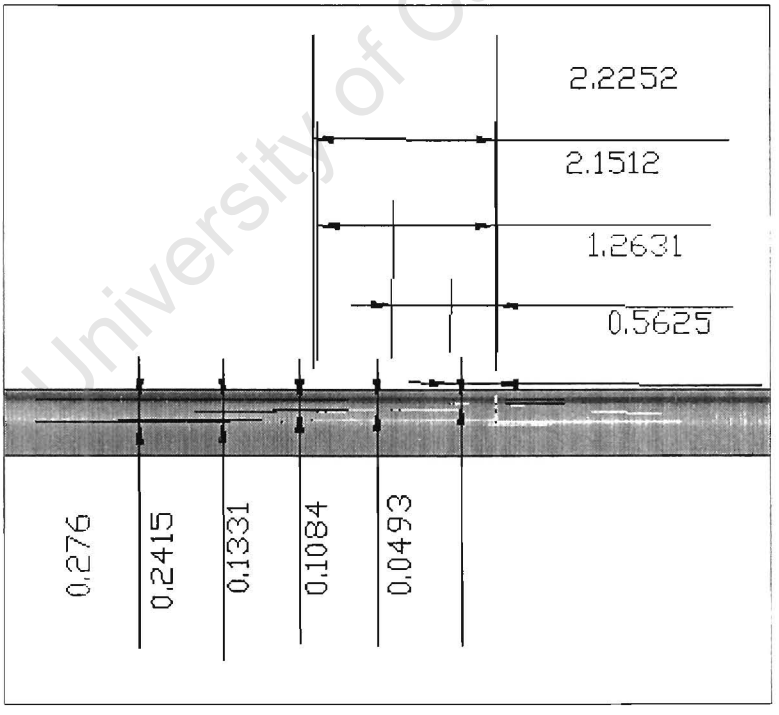

Specimen Impacted at 55.62m/s or 15.7J

Inverted Radial X-ray Image

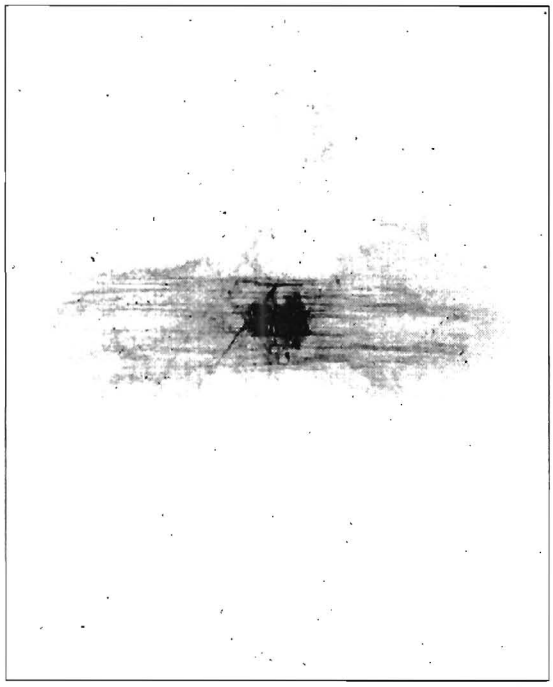

AutoCAD Measurement Radial X-ray

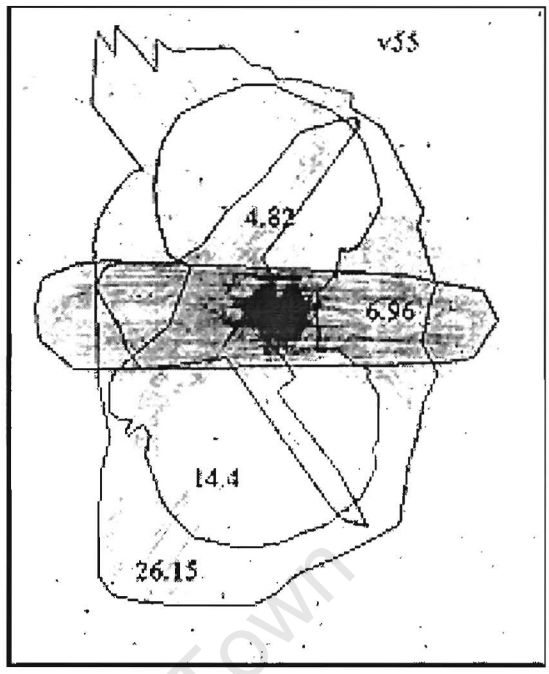

Tangential X-ray Image

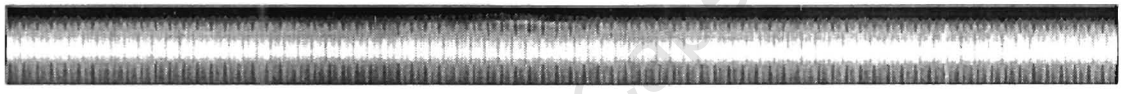

AutoCAD Measurement of Tangential X-ray

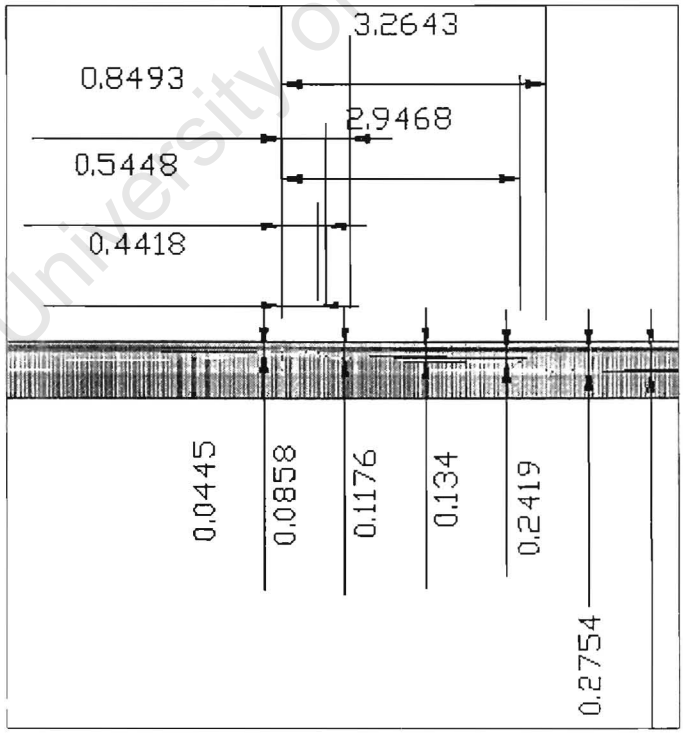

Specimen Impacted at 56.63m/s or 16.27J

Inverted Radial X-ray Image

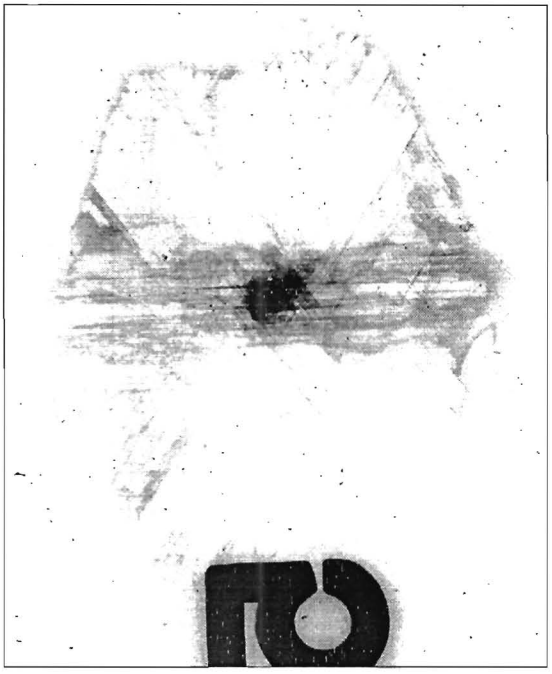

AutoCAD Measurement Radial X-ray

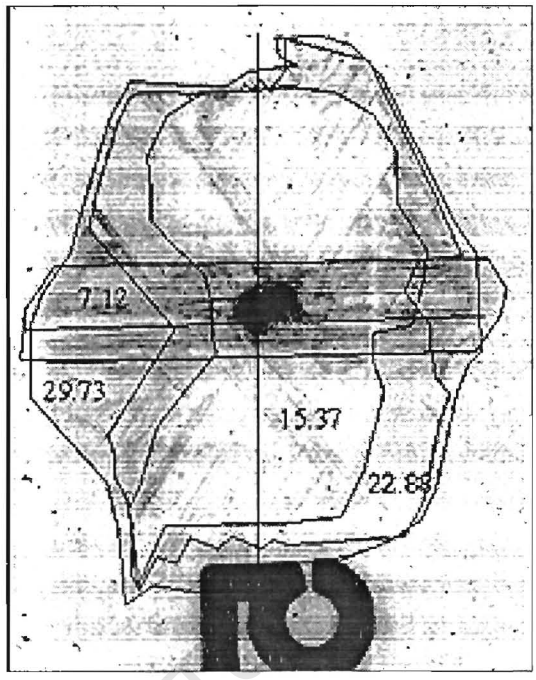

Tangential X-ray Image

AutoCAD Measurement of Tangential X-ray

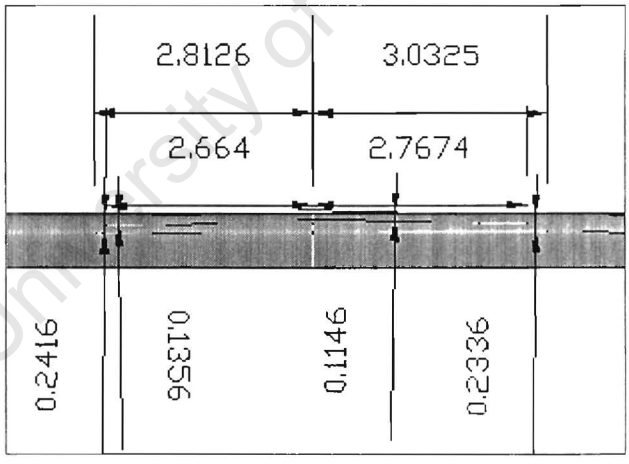

Specimen Impacted at 59.03m/s or 17.69J

Inverted Radial X-ray Image

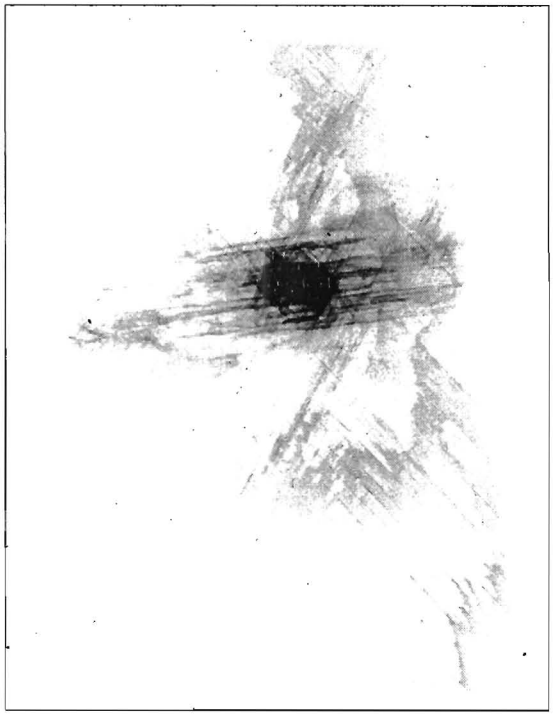

AutoCAD Measurement Radial X-ray

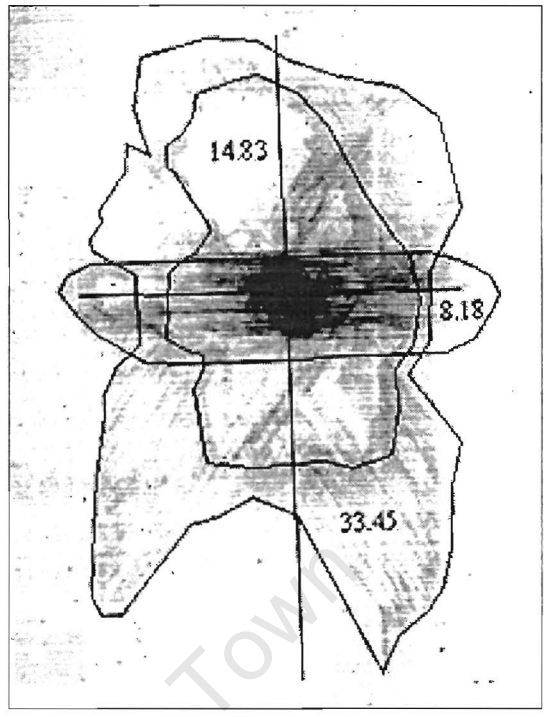

Tangential X-ray Image

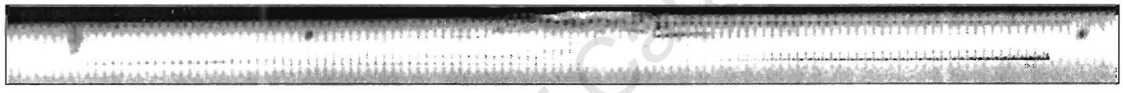

AutoCAD Measurement of Tangential X-ray

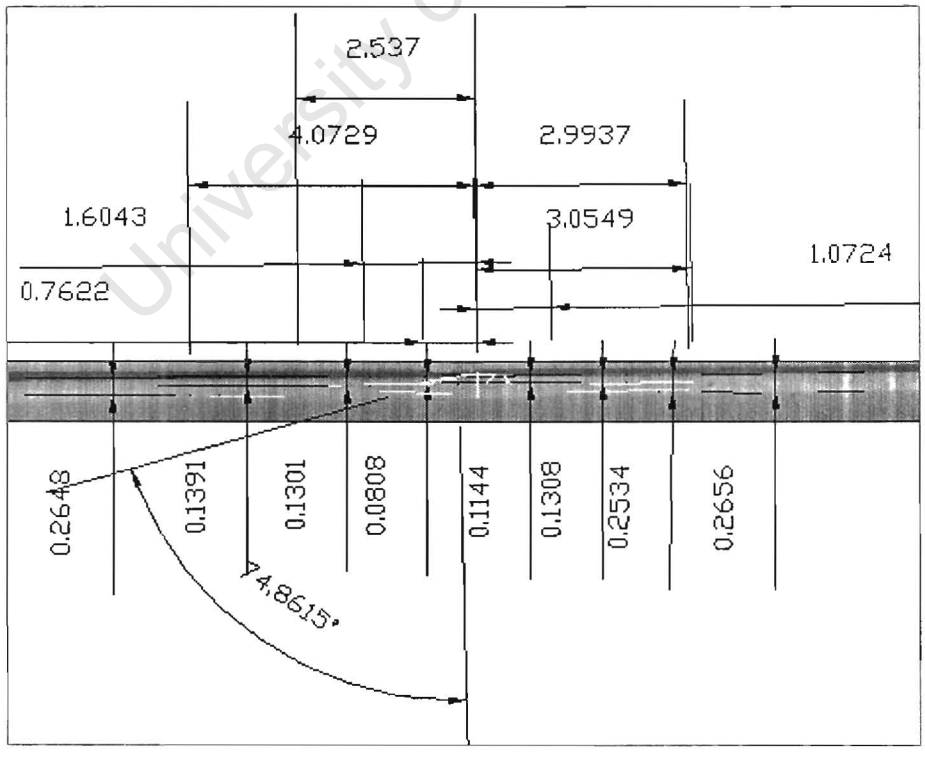

Specimen Impacted at 62.11m/s or 19.62J

Inverted Radial X-ray Image

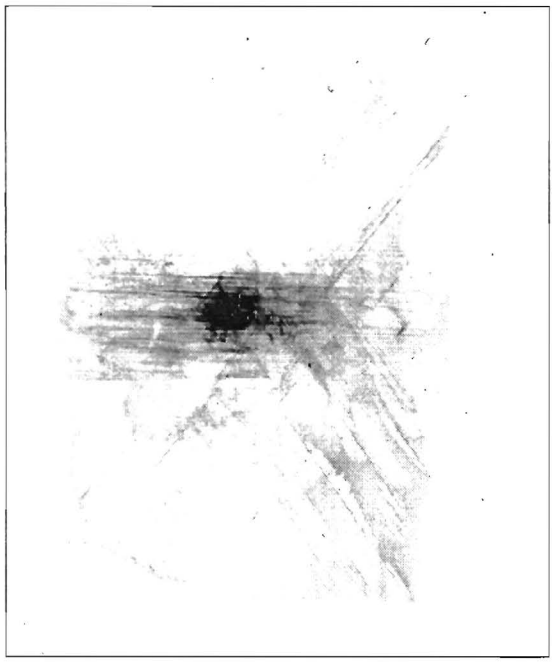

AutoCAD Measurement Radial X-ray

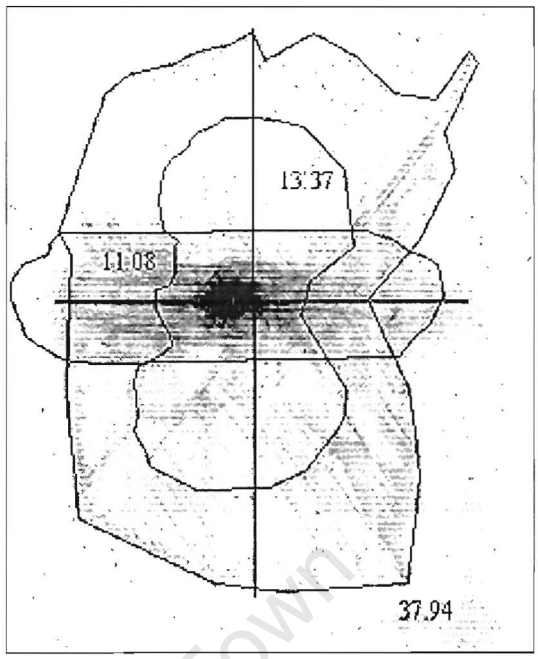

Tangential X-ray Image

AutoCAD Measurement of Tangential X-ray

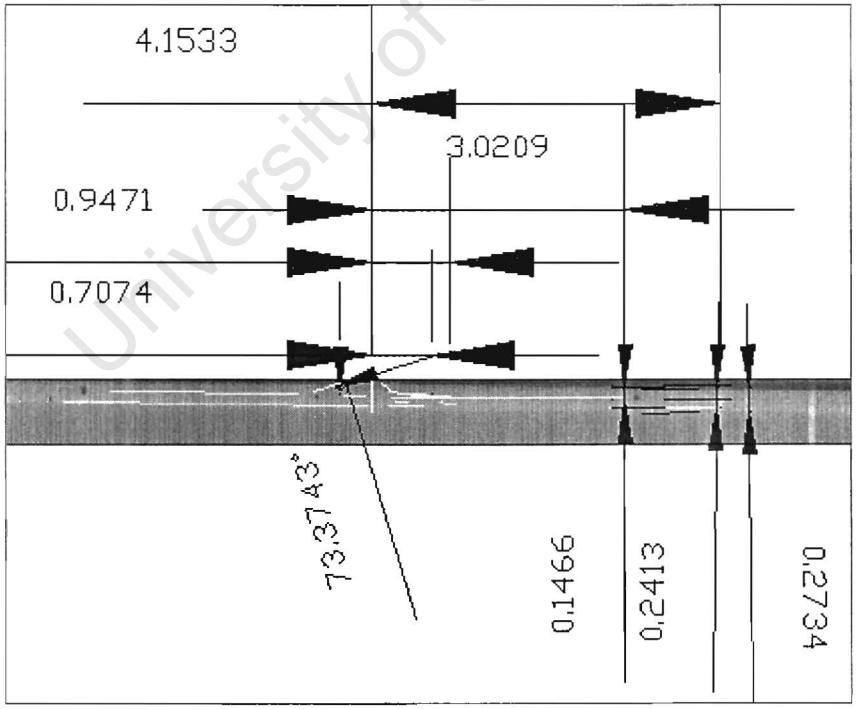

Specimen Impacted at 72.57m/s or 26.73J

Inverted Radial X-ray Image

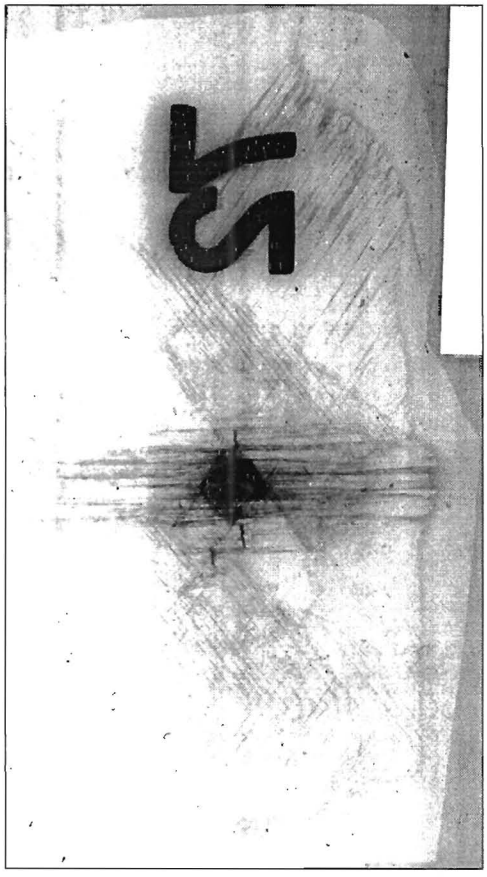

AutoCAD Measurement Radial X-ray

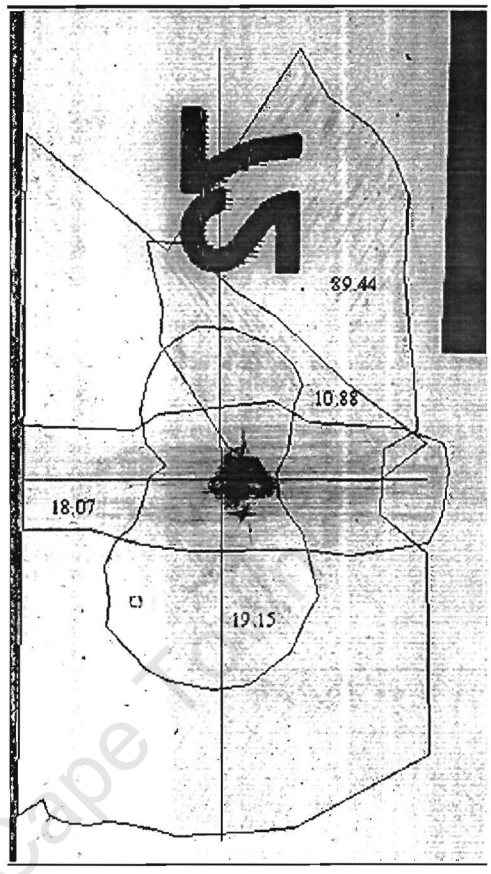

Tangential X-ray Image

AutoCAD Measurement of Tangential X-ray

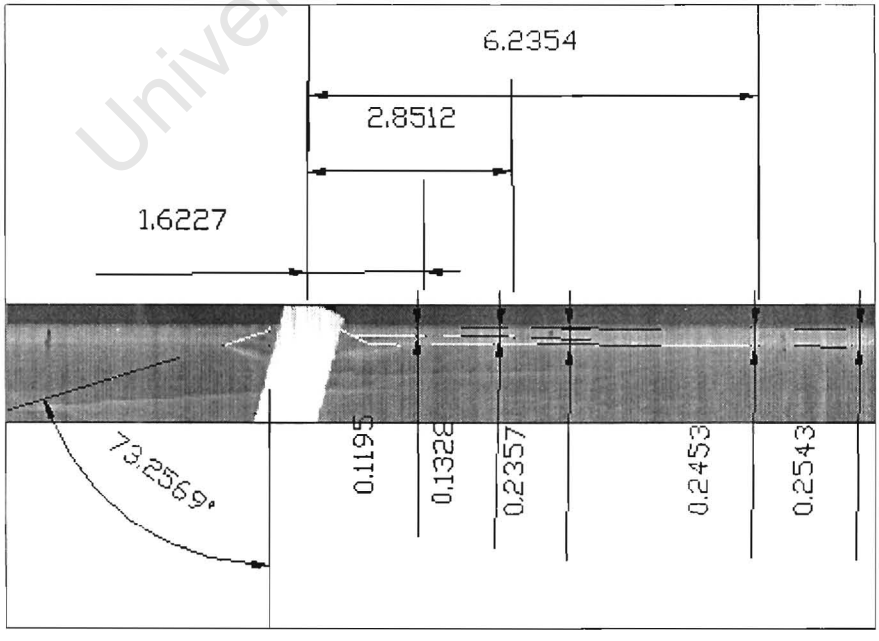

Specimen Impacted at 78.74m/s or 31.47J

Inverted Radial X-ray Image

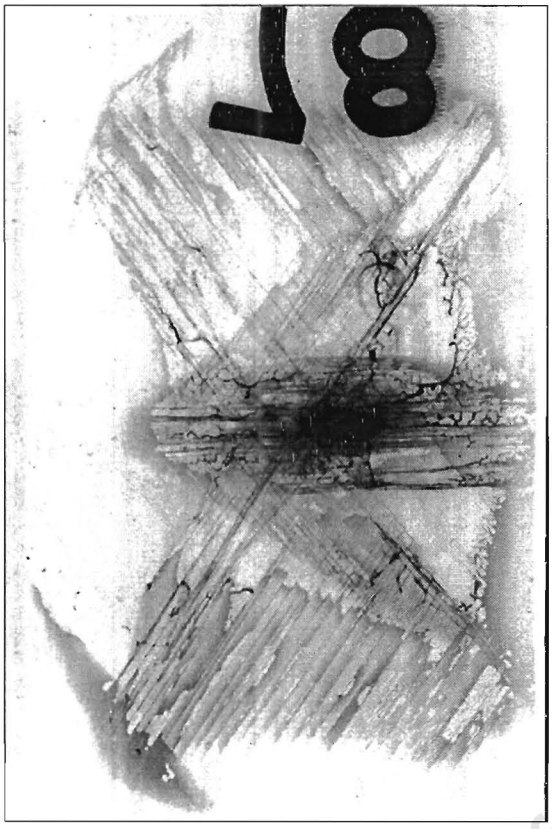

AutoCAD Measurement Radial X-ray

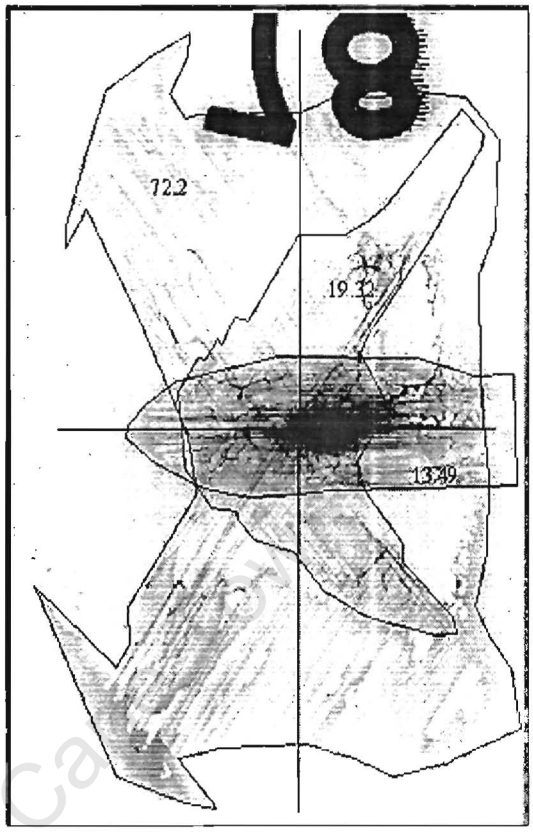

Tangential X-ray Image

AutoCAD Measurement of Tangential X-ray

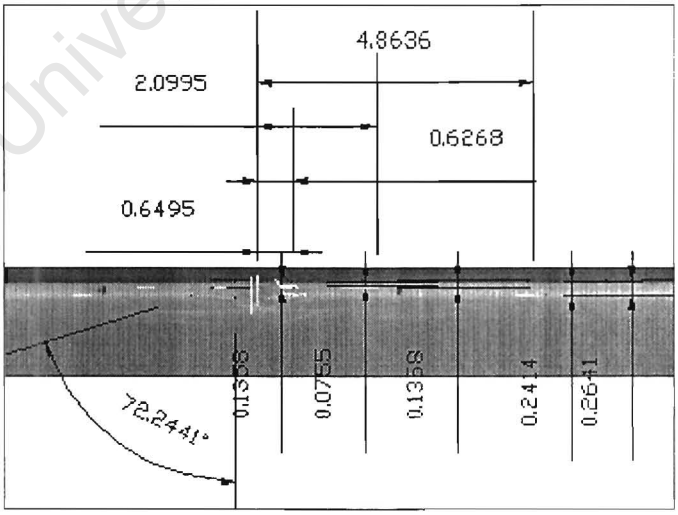

Specimen Impacted at 86.66m/s or 37.92J

AutoCAD Measurement Radial X-ray

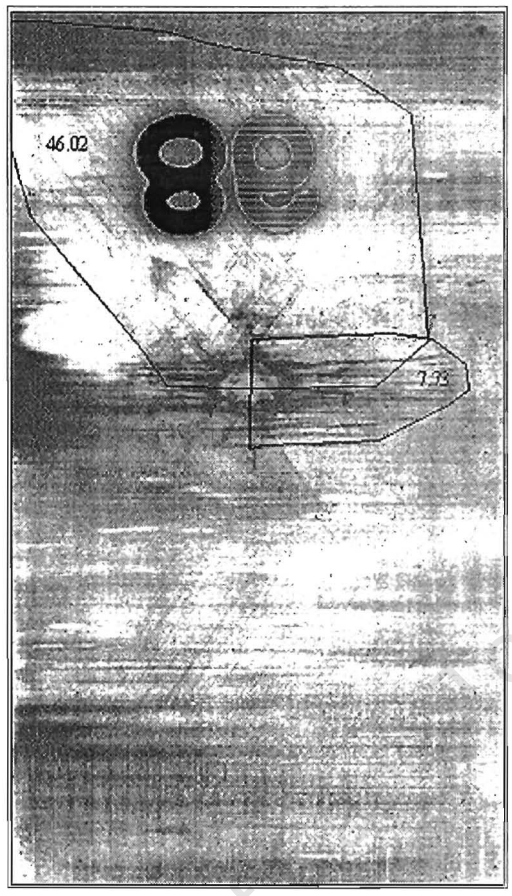

Tangential X-ray Image

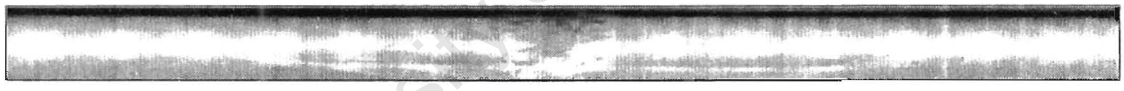

AutoCAD Measurement of Tangential X-ray

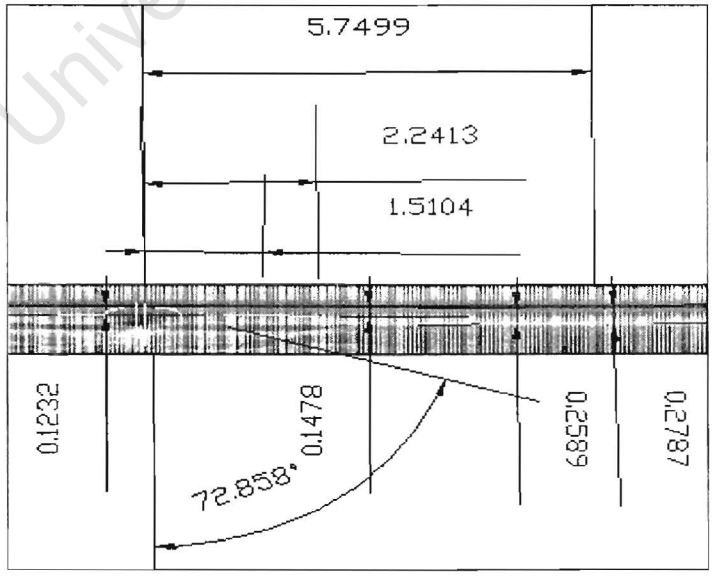

Laminate B Specimens

Specimen Impacted at 76.69m/s or 29.76J

Inverted Radial X-ray Image

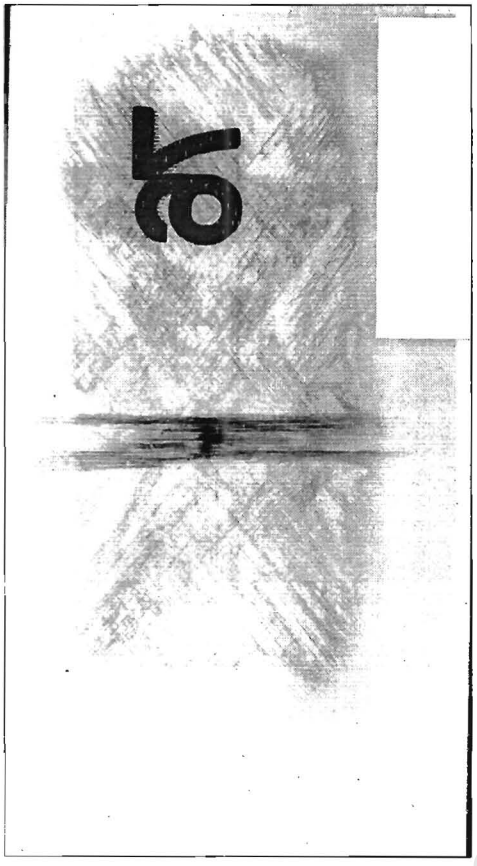

AutoCAD Measurement Radial X-ray

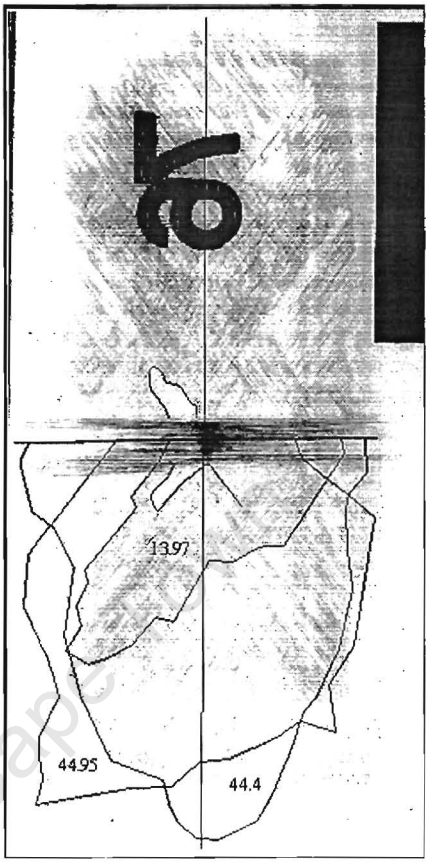

Tangential X-ray Image

AutoCAD Measurement of Tangential X-ray

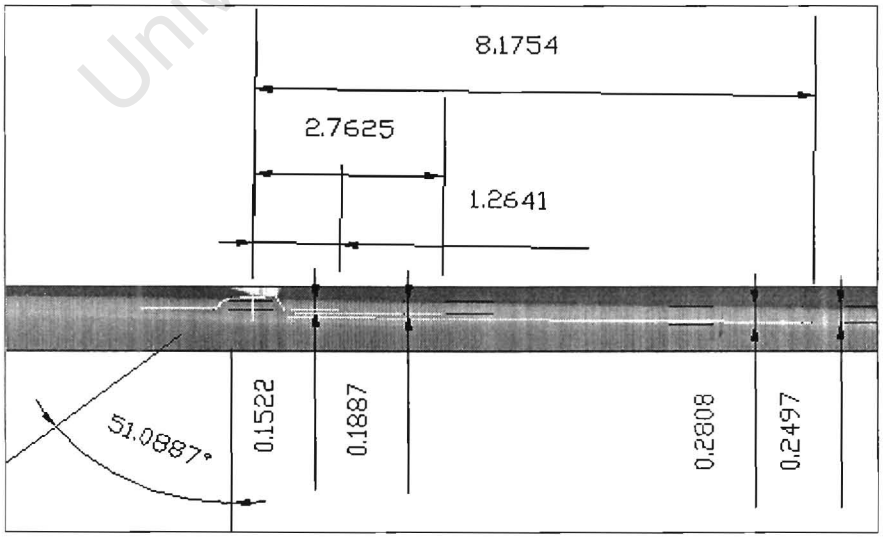

Specimen Impacted at 92.42m/s or 43.35J

Inverted Radial X-ray Image

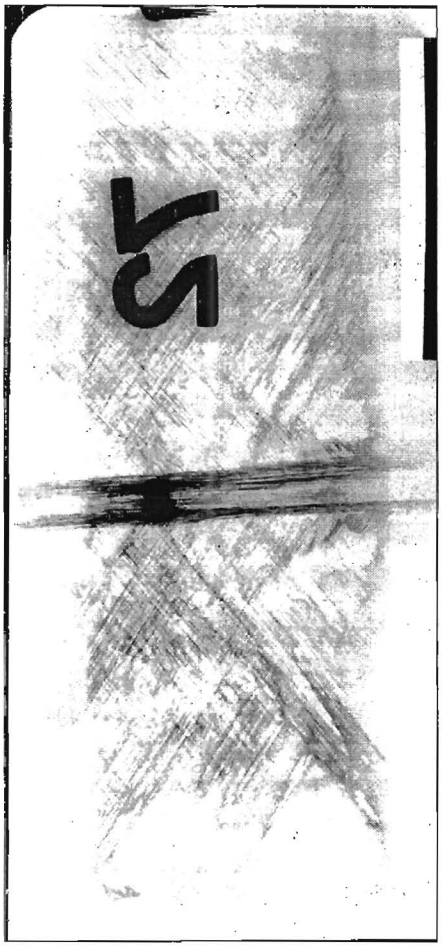

AutoCAD Measurement Radial X-ray

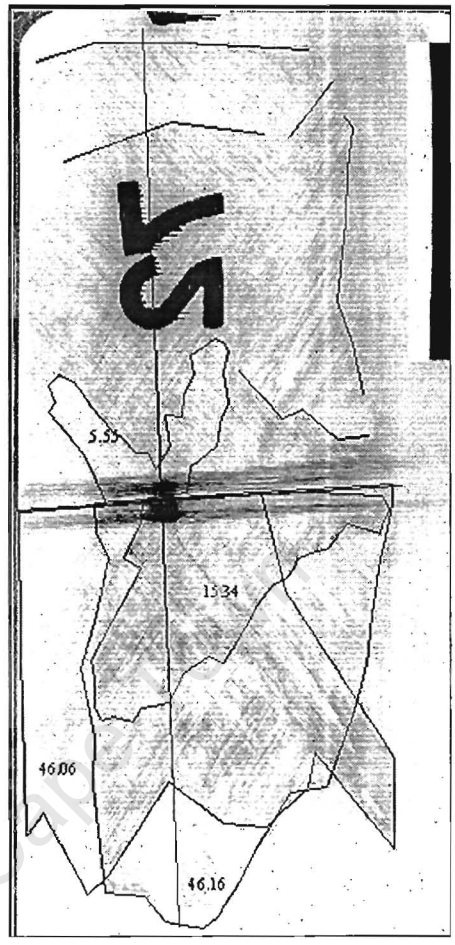

Tangential X-ray Image

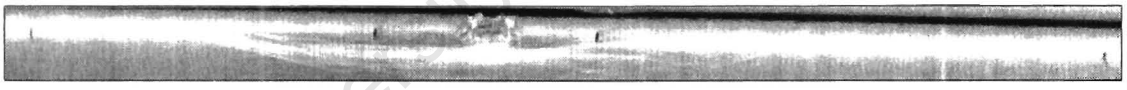

AutoCAD Measurement of Tangential X-ray

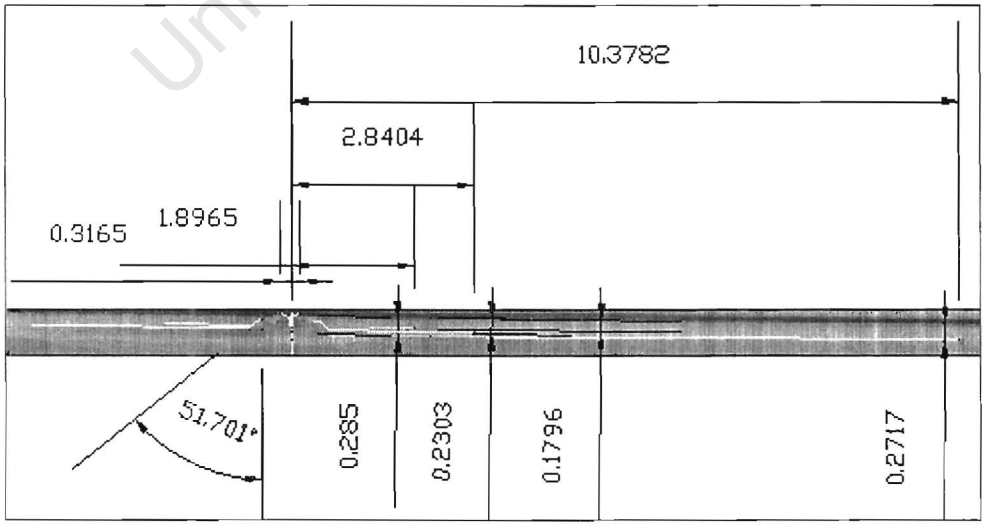

Specimen Impacted at 111.61m/s or 63.34J

Inverted Radial X-ray Image

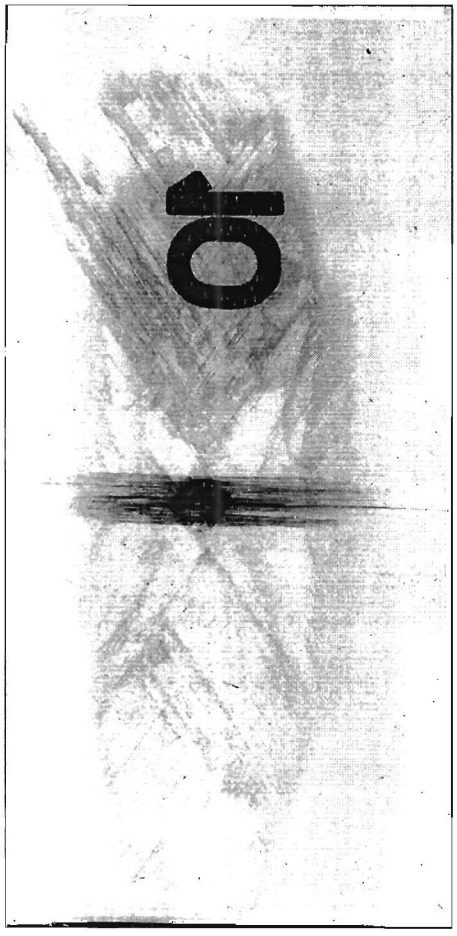

AutoCAD Measurement Radial X-ray

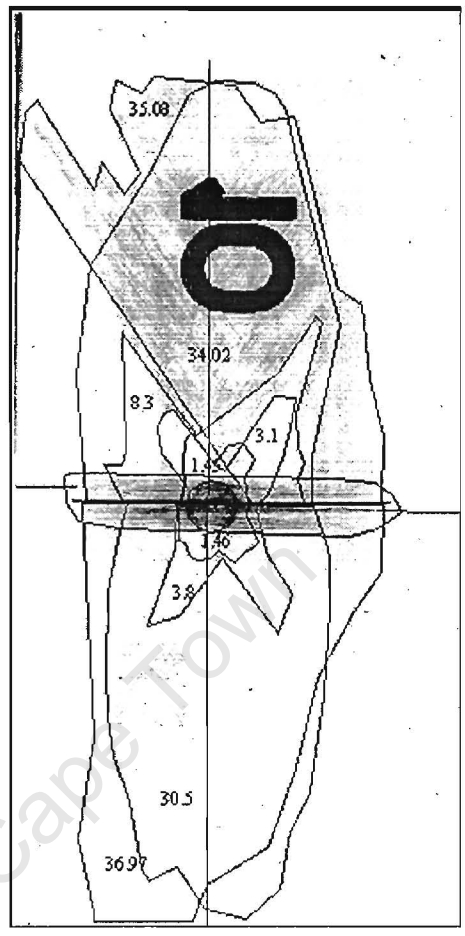

Tangential X-ray Image

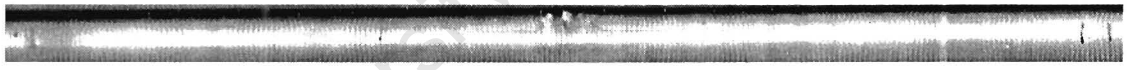

AutoCAD Measurement of Tangential X-ray

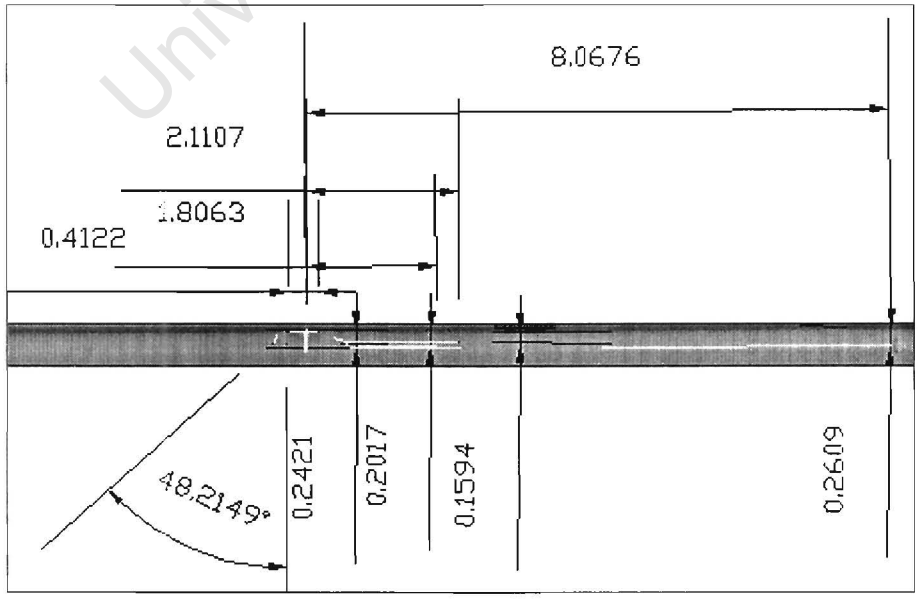

Specimen Impacted at 138.89m/s or 97.9J

AutoCAD Measurement Radial X-ray

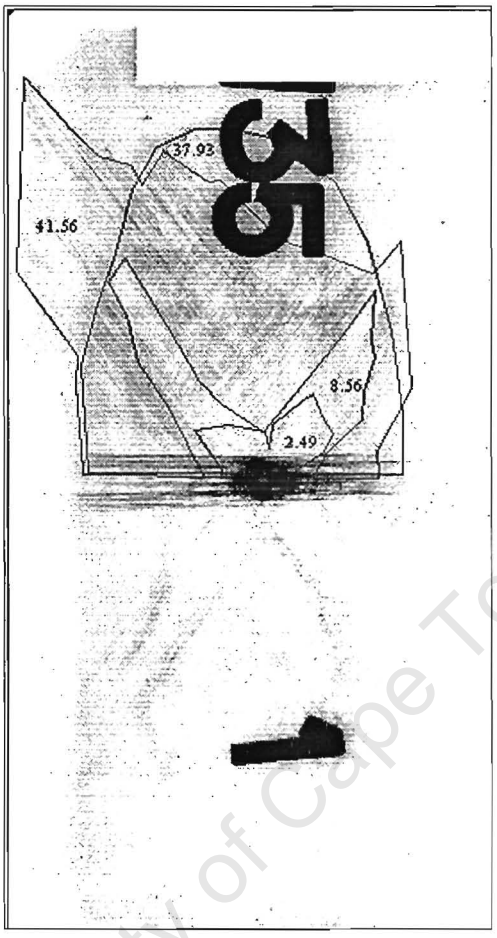

Tangential X-ray Image

AutoCAD Measurement of Tangential X-ray

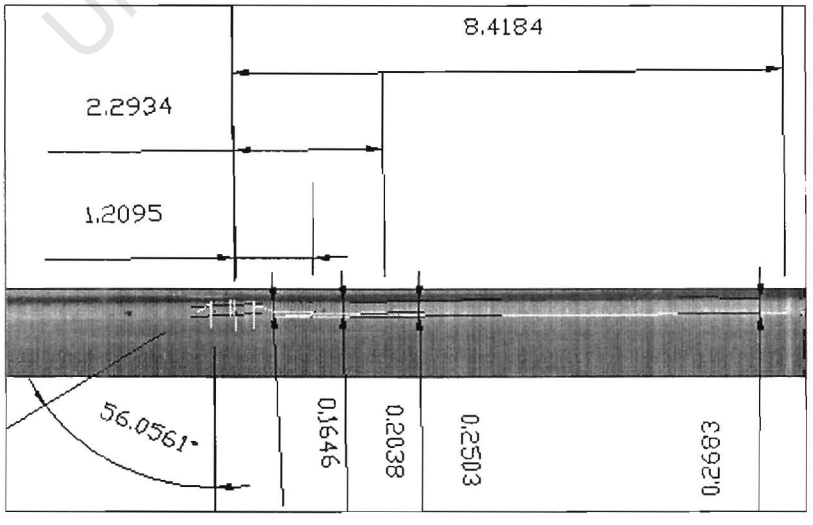

Axial Images

Laminate A

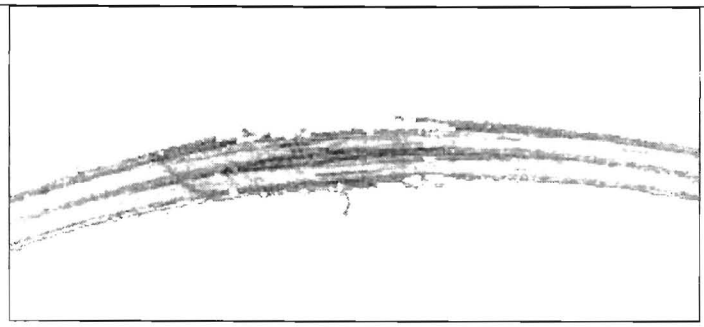

Specimen impacted at 59.03m/s

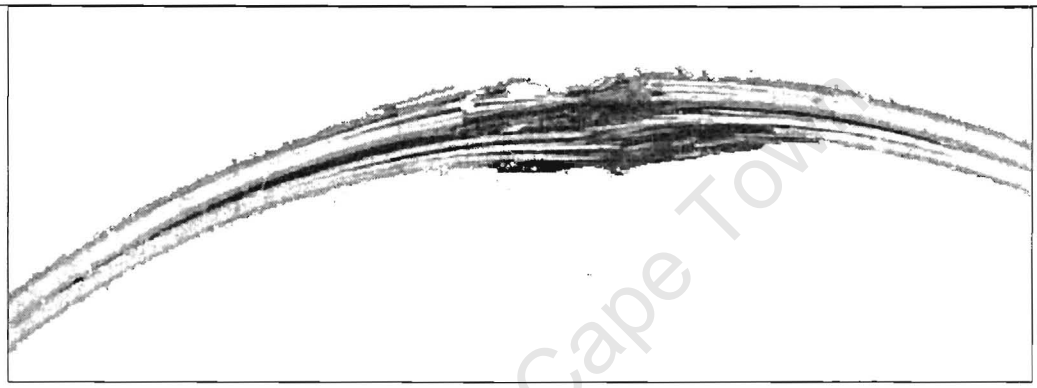

Specimen impacted at 78.74m/s

Laminate B

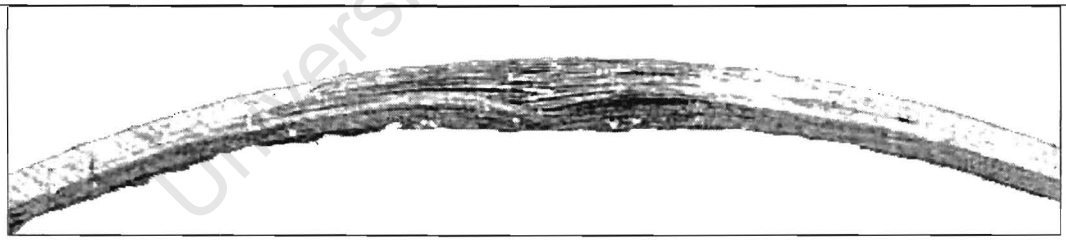

Specimen impacted at 76.69m/s

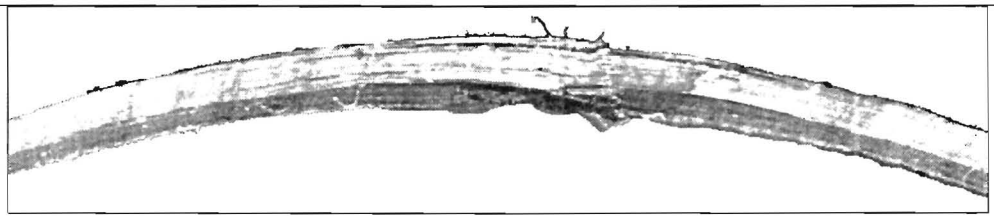

Specimen impacted at 111.61m/s

APPENDIX C: Finite element input decks

A laminate Finite Element Model of test at impact velocity of 72.57m/s

```
**************************************
*HEADING
**************************************
* Node and Element definition is not
* displayed due to the number of nodes
* and elements.
**************************************
**************************************
** Edges of nodes
**************************************
*NSET,NSET=TCLOSE,GENERATE
90101,99601,100
*NSET,NSET=BCLOSE,GENERATE
10101,19601,100
*NSET,NSET=TFAR,GENERATE
90196,99696,100
*NSET,NSET=BFAR,GENERATE
10196,19696,100
*NSET,NSET=TLEFT,GENERATE
90101,90196,1
*NSET,NSET=BLEFT,GENERATE
10101,10196,1
*NSET,NSET=TRIGHT,GENERATE
99601,99696,1
*NSET,NSET=BRIGHT,GENERATE
19601,19696,1
**************************************
** Edge Surfaces of nodes
**************************************
*NSET,NSET=CLOSE,GENERATE
90101,99601,100
80101,89601,100
70101,79601,100
60101,69601,100
50101,59601,100
40101,49601,100
30101,39601,100
20101,29601,100
10101,19601,100
*NSET,NSET=FAR,GENERATE
90196,99696,100
80196,89696,100
70196,79696,100
60196,69696,100
50196,59696,100
40196,49696,100
30196,39696,100
20196,29696,100
10196,19696,100
*NSET,NSET=LEFT,GENERATE
90101,90196,1
80101,80196,1
70101,70196,1
60101,60196,1
```

```
50101,50196,1
40101,40196,1
30101,30196,1
20101,20196,1
10101,10196,1
*NSET,NSET=RIGHT,GENERATE
99601,99696,1
89601,89696,1
79601,79696,1
69601,69696,1
59601,59696,1
49601,49696,1
39601,39696,1
29601,29696,1
19601,19696,1
**********************************
** Generating the elements
**********************************
*ELEMENT, TYPE=C3D8R
10101,10101,10201,10202,10102,20101,20201,20202,20102
*ELGEN,ELSET=PLATE
10101,95,100,100,95,1,1,8,10000,10000
*Element, type=MASS, elset=mass
90000, 90000
**********************************
* element sets defining layers
**********************************
*ELSET,ELSET=L1,GENERATE
80101,89900,1
*ELSET,ELSET=L2,GENERATE
70101,79900,1
*ELSET,ELSET=L3,GENERATE
60101,69900,1
*ELSET,ELSET=L4,GENERATE
50101,59900,1
*ELSET,ELSET=L5,GENERATE
40101,49900,1
*ELSET,ELSET=L6,GENERATE
30101,39900,1
*ELSET,ELSET=L7,GENERATE
20101,29900,1
*ELSET,ELSET=L8,GENERATE
10101,19900,1
**********************************
* element sets defining element sets
* with common material and orinetation
* definitions
**********************************
*ELSET,ELSET=HOOP
L1,L2
*ELSET,ELSET=POS
L3,L5,L7
*ELSET,ELSET=NEG
L4,L6,L8
**********************************
** Generating the Contact element set
** specify contact on Face 2
**********************************
*ELSET,ELSET=PCONTACT,GENERATE
80101,80118,1
80201,80218,1
```

```
80301,80318,1
80401,80418,1
80501,80518,1
80601,80618,1
80701,80718,1
80801,80818,1
80901,80918,1
81001,81018,1
81101,81118,1
81201,81218,1
81301,81318,1
81401,81418,1
81501,81518,1
81601,81618,1
81701,81718,1
81801,81818,1
**********
** Assigning Material definitions and Orientations
**********
*
**********
* layers with +35 degree orientations
**********
** Section: Section-1
*Orientation, Name=npos, System=CYLINDRICAL
0.,0.,0., 0.,0.14,0.
1,55.
*Solid Section, elset=POS, material=Material-a, Orientation=npos
**********
* layers with -35 degree orientations
**********
** Section: Section-2
*Orientation, Name=nneg, System=CYLINDRICAL
0.,0.,0., 0.,0.14,0.
1,-55.
*Solid Section, elset=NEG, material=Material-a, Orientation=nneg
**********
* layers with 90 degree orientations
**********
** Section: Section-3
*Orientation, Name=hoop, System=CYLINDRICAL
0.,0.,0., 0.,0.14,0.
1,0.
*Solid Section, elset=HOOP, material=Material-b, Orientation=hoop
**********
* Material definitions
**********
*Material, name=Material-a
*Density
1614.,
**E1,E2,E3,N12,N13,N23,G12,G13
**G23,
*Elastic, Type=ENGINEERING CONSTANTS
192.1e+9, 2.843e+09,2.843e+09, 0.272,0.272,0.527, 5.088e+09, 5.088e+09
3.003e+09,
*Material, name=Material-b
*Density
1586.,
**E1,E2,E3,N12,N13,N23,G12,G13
**G23,
*Elastic, Type=ENGINEERING CONSTANTS
```

```
1.776e+11, 2.845e+09,2.845e+09, 0.278,0.278,0.528, 4.438e+09, 4.438e+09
3.012e+09,
** Section: Section-4
*Mass, elset=mass
0.01015,
*Nset, nset=BULLET
 90000,
*Rigid Body, ref node=BULLET
*********************************
** Boundary conditions
** See edge surface nodes to apply conditions on
*********************************
*BOUNDARY
FAR,ENCASTRE
*Boundary
CLOSE, XSYMM
*Boundary
LEFT, YSYMM
*BOUNDARY
90000,1,1
90000,2,2
90000,4,4
90000,5,5
90000,6,6
** Initial Condition: IC-1
*Initial Conditions, type=VELOCITY
90000, 1, 0.
90000, 2, 0.
90000, 3, -72.57
*********************************
** Step Control
*********************************
*Restart,Write,Number Interval=5,Time Marks=No
*Step
Step-1: Composite Tube Impact
*Dynamic, Explicit
,7.05E-07
*Bulk Viscosity
0.06, 1.2
*Surface Definition, name=_G56
PCONTACT, S2
*Rigid Surface, type=REVOLUTION, name=_G55, ref node=BULLET
0., 0., 0.0702538, 0., 0., 100.071
START,        0.004,        0.027
 LINE,        0.004,        0.004
CIRCL,          0.,           0.,           0.,        0.004
**
** INTERACTION PROPERTIES
**
*Surface Interaction, name=IntProp-1
** Interaction: Int-1
*Contact Pair, interaction=IntProp-1,penalty
_G56, _G55
**
** OUTPUT REQUESTS
**
*End Step
```

B laminate Finite Element Model of test at impact velocity of 72.57m/s

```
************************************
* B laminate input deck
************************************
* The only difference to the A laminate
* input deck is the node co-ordinate definitions,
* which are not shown due to space considerations,
* and the definition of layer element sets.
* The layer element sets are shown below for
* comparison to the A laminate.
************************************
*ELSET,ELSET=L1,GENERATE
80101,89900,1
*ELSET,ELSET=L2,GENERATE
70101,79900,1
*ELSET,ELSET=L3,GENERATE
60101,69900,1
*ELSET,ELSET=L4,GENERATE
50101,59900,1
*ELSET,ELSET=L5,GENERATE
40101,49900,1
*ELSET,ELSET=L6,GENERATE
30101,39900,1
*ELSET,ELSET=L7,GENERATE
20101,29900,1
*ELSET,ELSET=L8,GENERATE
10101,19900,1
*ELSET,ELSET=HOOP
L1,L2
*ELSET,ELSET=POS
L3,L5,L7
*ELSET,ELSET=NEG
L4,L6,L8
```

A laminate compliance test input deck

```
*Heading
 complya
** Job name: comply3 Model name: Model-4
** ----------------------------------------------------------------
**
** Compliance test A laminate input deck
**
************************************************************
** Node and element definition is included
** due to space considerations.
************************************************************
**
** Defining shell section by defining each layer by
** asssigning a material definition and orientation
************************************************************
**
** Section: Section-1
*SHELL GENERAL SECTION,ELSET=Part-5-1._G5,COMPOSITE
0.00015,,Material-a,35.0
0.00015,,Material-a,-35.0
0.000267,,Material-b,90.0
0.000267,,Material-b,90.0
```

```
0.000267,,Material-b,90.0
0.00015,,Material-a,35.0
0.00015,,Material-a,-35.0
0.000267,,Material-b,90.0
0.000267,,Material-b,90.0
0.000267,,Material-b,90.0
0.00015,,Material-a,35.0
0.00015,,Material-a,-35.0
*System
*Nset, nset=_G4
   1,  21,  22,  42,  43,  63,  64,  84,  85, 105, 106, 126, 127, 147,
148, 168
 169, 189, 190, 210, 211, 231, 232, 252, 253, 273, 274, 294, 295, 315,
316, 336
 337, 357, 358, 378, 379, 399, 400, 420, 421, 441
*Elset, elset=_G4
   1,  20,  21,  40,  41,  60,  61,  80,  81, 100, 101, 120, 121, 140,
141, 160
 161, 180, 181, 200, 201, 220, 221, 240, 241, 260, 261, 280, 281, 300,
301, 320
 321, 340, 341, 360, 361, 380, 381, 400
*Nset, nset=_G5, generate
 421,  441,    1
*Elset, elset=_G5, generate
 381,  400,    1
*Nset, nset=_G6, generate
  1,  21,   1
*Elset, elset=_G6, generate
  1,  20,   1
*Nset, nset=_G15
 441,
**********************************************************************
** Material definition
** ********************************************************************
*Material, name=Material-b
*Elastic, type=LAMINA
 1.776e+11, 2.845e+09, 0.278, 4.438e+09, 4.438e+09, 3.003e+09
*Fail Stress
 3.294E09,0.93E09,80.35E06,150.6E06, 20.01e+06, 5e-18, ,
*Density
1586
*Material, name=Material-a
*Elastic, type=LAMINA
 1.921e+11, 2.843e+09, 0.272, 5.088e+09, 5.088e+09, 3.027e+09
*Fail Stress
 3.569E09,1.008E09,80.31E06,150.6E06, 20.43e+06, 5e-18, ,
*Density
1614
**
** BOUNDARY CONDITIONS
**
** BC: BC-1 Type: Typed
*Boundary
_G4, XSYMM
** BC: BC-2 Type: Typed
*Boundary
_G5, ZSYMM
** BC: BC-3 Type: Typed
*Boundary
_G6, ENCASTRE
** ----------------------------------------------------------------
```

```
**
** STEP: Step-1
**
*Restart, write, frequency=1
*Step
Step-1: comply3
*Static
1., 3., 1e-05, 1.
**
** BOUNDARY CONDITIONS
**
** BC: BC-4 Type: Displacement
*Boundary
_G15, 1, 1
_G15, 2, 2, -0.02
_G15, 3, 3
**
*End Step
```

B laminate compliance test input deck

```
*****************************************************
** The only difference between the B laminate input
** deck for the compliance tests is the element
** material property and orientation definition. It is
** included for comparison.
*****************************************************
** Section: Section-1
*SHELL GENERAL SECTION,ELSET=Part-3-1._G9,COMPOSITE
0.000267,,Material-b,90.0
0.000267,,Material-b,90.0
0.000267,,Material-b,90.0
0.000267,,Material-b,90.0
0.000267,,Material-b,90.0
0.000267,,Material-b,90.0
0.00015,,Material-a,35.0
0.00015,,Material-a,-35.0
0.00015,,Material-a,35.0
0.00015,,Material-a,-35.0
0.00015,,Material-a,35.0
0.00015,,Material-a,-35.0
```